Polymer-Based MEMS Calorimetric Devices for Characterization of Biomolecular Interactions

Yuan Jia

Submitted in partial fulfillment of the
requirements for the degree of
Doctor of Philosophy
in the Graduate School of Arts and Sciences

Columbia University

2017

ABSTRACT

Polymer-Based MEMS Calorimetric Devices for Characterization of Biomolecular Interactions

Yuan Jia

Biomolecular interactions are central to all biological functions as the execution of biological function usually depends on the concerted action of biomolecules existing in protein complexes, metabolic or signaling pathways or networks. Therefore, understanding biomolecular interactions, and the temperature dependence of biomolecular interactions is of critical importance for the study of fundamental science, therapeutic drug development, and biomolecule manipulation. Biocalorimetry, a process of measuring the heat involved in biomolecular interactions, has distinct advantages over other biomoelcualr interactions characterization methods as it is solution based, label free, universally applicable, and allows for determination of thermodynamic propoerties. However, the utility of available commercial instruments is limited by complex design, rather large sample consumption, and slow responses. Micro-electro-mechanical systems (MEMS) technology, as an alternative approach, potentially offers solutions to such limitations as it can potentially be fabricated at low cost, operated at high throughput with minimum sample consumption, and available for integration with various functional units. However, existing MEMS calorimeters either do not yet allow proper control of reaction conditions for thermodynamic characterization of biomolecular reaction systems or is not yet suitable for practical applications because of a lack of sensitivity, reliability, and high operating cost. This thesis will build upon our existing knowledge of the MEMS technology in biocalorimetry and develop new generation of

polymer MEMS calorimetric devices that are economical, sensitive, and robust for studying biomolecular characterization in practical settings.

The development of such devices requires innovations in the fabrication process as the conventional photolithography process is largely incompatible with polymer substrates. To address that, this thesis first presents a novel method of fabricating polymer-based MEMS thermoelectric sensors using a thermally assisted lift-off approach, by which, thick metal or semiconductor films experience controlled breakup due to thermal reflow of the underlying lithographically defined patterns. The thick film MEMS thermoelectric sensors exhibit electric and thermoelectric performances comparable to those made from bulk materials. This allows the sensors to be useful in low-noise, high-efficiency thermoelectric measurements.

The polymer-based MEMS sensors fabrication approach is then implemented in making MEMS calorimetric devices for solution-based, quantitative thermodynamic characterization of biomolecular interactions. This thesis presents both polymer-based MEMS differential scanning calorimetry (DSC) and isothermal titration calorimetry (ITC) devices that are more robust, and cost lower. The polymer-based MEMS calorimeters eliminate the need for complex, fragile silicon freestanding structures and offer real-time, in-situ temperature control to biomolecules with well-defined miniature volume. Combining with the improved sensitivity, the polymer-based devices also reduce consumption of material and leads to substantially reduced thermal mass of the measurement system for a rapid response time and improved throughput. The interpretation of the DSC, ITC measurement results yielded complete thermodynamic information of several biomolecular interactions of critical scientific and therapeutic interest that include the characterization of the unfolding of protein (lysozyme)

for the determination of its thermodynamic properties, and the binding parameters of interactions of 18-Crown-6 and barium chloride in practically applicable reagent concentrations.

In addition, PDMS-based microfluidic structures that are used in molecular biological analysis platforms, including MEMS calorimeters are known to be problematic due to its surface adsorption effects and high permeability. To address this, this thesis eliminates the use of PDMS microfluidic structures in MEMS calorimeters entirely by presenting the first demonstration of a miniaturized 3D-printed Lab-on-a-chip (LOC) platform that integrates the polymer-based MEMS calorimeter for quantitative ITC characterization of biomolecular interactions. Exploiting topographical flexibility offered by 3D printing, the platform design features fully isolated cantilever-like calorimetric measurement structures in a differential setup. This design layout improves thermal isolation and reduces overall platform thermal mass, thereby enhancing the measurement sensitivity and reducing the platform response time. The utility of the platform is demonstrated with ITC measurements of the binding of 18-Crown-6 with barium chloride and the binding of ribonuclease A with cytidine 2'-monophosphate in a reusable manner, and with practically relevant reagent concentrations.

Finally, some perspectives of how far away the devices are from commercializing are summarized, and future works in suggesting the strategies to achieve this goal are proposed.

Table of Contents

List of Charts

List of Symbols

k_{on}……Association rate constant

k_{off}……Dissociation rate constant

K_d……Equilibrium dissociation constant

u……Flow rate for sample introduction

h……Chamber height

R……Resistance of a temperature sensor

T……Temperature

h……Natural convection heat transfer coefficient

T_s……Average surface temperature

T_∞……Temperature at an infinite distance

L……Characteristic dimension

k……Thermal conductivity

β……Thermal expansion coefficient

v……Kinetic viscosity

α……Thermal diffusivity

g……Gravitational constant

ΔP……Differential thermal power

P_s……Thermal power generated in the sample material

P_r……Thermal power generated in the reference material

ΔC_p……Differential heat capacity

C_{ps}……Heat capacity of the sample material

C_{pr}……Heat capacity of the reference material

$\dot{T}$ .....Time rate of the controlled temperature of sample and reference materials

ΔU……Output from the thermoelectric sensor

S……Thermoelectric sensitivity

c……Partial specific heat capacity of biomolecules

ΔH……Total change of molar enthalpy

T_m……Melting temperature

τ……Thermal time constant

C……Total heat capacity of the sample and its containing chamber

C_{solv}……Partial specific heat capacity of reference solvent

Δc……Difference in the specific heat capacity of biomolecules

m……Mass of biomolecules in sample chamber

v……Partial specific volume of biomolecules

v_{solv}.....Partial specific volume of reference solvent

[M]……Equilibrium concentration of a binding reagent

[MX]……Equilibrium concentration of the binding product

N……Stoichiometry

Q……Biomolecular reaction heat

r……Molar ratio of reactants

V_0……Active volume for reaction

M_t……Total concentration of sample molecule

X_t……Total concentration of binding reagent

K_B……Equilibrium binding constant

List of Abbreviations

MEMS……Micro-Electro-Mechanical Systems

DNA……deoxyribonucleic acid

RNA……ribonucleic acid

SPR……surface plasmon resonance

QCM……quartz crystal microbalance

MALDI-MS……matrix-assisted laser desorption/ionization mass spectrometry

DSC……differential scanning calorimetry

ITC……isothermal titration calorimetry

CMOS……complementary metal-oxide-semiconductor

Sb-Bi……antimony-bismuth

PDMS……poly(dimethylsiloxane)

Cr/Au……chromium/gold

CVD……chemical vapor deposition

RIE……reactive ionic etching

PID……proportional-integral-derivative

TCR……temperature coefficient of resistivity

mRNA……messenger RNA

Cryo-EM……cryogenic electron microscopy

TMAH……tetramethylammonium hydroxide

RMA……root-mean-square

18-C-6……18-Crown-6

$BaCl_2$……barium chloride

RNase A……ribonuclease A

2'CMP……cytidine 2'-monophosphate

PECVD……plasma-enhanced chemical vapor deposition

Acknowledgements

Undertaking my Ph.D. and completing this thesis have been a truly life-changing and rewarding journey for me and it would not have been possible to do without the support, love, and guidance that I received from all my family, friends, colleagues throughout all these years.

Foremost, I would like to express my sincerest gratitude to my advisor, Professor Qiao Lin for all the support, encouragement, and guidance he gave me, both in aspects of academic research, and in ethics of conducting them. His help, for provide me insights whenever I experienced research difficulties, sometimes even at the cost of his own time is invaluable, and indispensable to the completion of this thesis.

I also want to extend my appreciation to Professor James Li at University of Rochester who introduced me to academic research and convinced me during our many discussions that I should pursue a doctoral degree and who made it possible for me through his recommendations. In addition, I want to thank Professors Joachim Frank, Dr. Rick Brown, Anthony Maletta, and Bill Buote for their advice and support through our collaboration on multiply research projects. I am also grateful to other members of my thesis committee, Professors Arvind Narayanaswamy, Michael Burke, Sinisa Vukelic and Yuan Yang, for their insightful comments and suggestions on my thesis.

I gratefully acknowledge the funding received towards my PhD from the National Science Foundation, and Netzsch North America. My thanks also go

out to my colleagues, Bin Wang, Jing Zhu, Hao Sun, Bing Song, Tim Olsen, Haogang Cai, Zhixing Zhang, Cheng Wang, Junyi Shang, Yibo Zhu, Zhuang Hao, Xuejun Wang, Chao Su, Jinho Kim, Jaeyoung Yang and the rest of the BioMEMS lab members. Their valuable help and input has made a vital contribution towards my Ph.D, More importantly, working with you all has made research fun and a whole lot easier. I would also like to thank the CEPSR clean room and the nanofabrication facility at CUNY for their support through my research.

I would also like to say a heartfelt thank you to girlfriend, Yu Zhao, for being by my side every minute throughout the completion of this thesis. Your support, encouragement, and patience help me completed what I started, and I can't wait for us to embark on a journal together.

Finally, my parents Annian Jia and Yanjun Li, to whom this thesis is dedicated. Although I am 8000 miles away from home, both of you have always been there for me, with endless patience and unconditionally trust during the best of worst of my times, Thank you!

Dedication

This thesis is dedicated to my parents.

Chapter 1 Introduction

1.1 Biomolecular Interactions

Biomolecules very rarely act in isolation, and the execution of biological function usually depends on the concerted action of biomolecules existing in protein complexes, metabolic or signaling pathways or networks. Therefore, biomolecular interactions are central to all biological functions [1], and understanding biomolecular interactions is hence critical to a range of fundamental sciences, new treatments for disease, and a wide range of highly functional products. Specifically, the ability to accurately determine kinetic rate constants and thermodynamic parameters for biomolecular interactions provides the possibility of new insights for study the fundamental science of molecular recognition and computational methods for data interpretation [2]. Also, pharmaceutical industry relies on biomolecular interaction studies to help understand the mechanism of the binding reactions, and this information can be directly used to improve binding properties of a drug candidate [3].

Temperature dependence is a very important effect of biomolecular interactions as almost all the biomolecular interactions are thermally active and temperature may change the physiology of the biomolecules due to thermoregulation [4]. Therefore, understanding the mechanisms governing temperature-dependent biomolecular interactions is important for developing potential applications in biosensing, and thermally controlled biomolecule manipulation [5]. For instance, biomolecules of different kinds can bind to the sample probe molecule and create a nonspecific signal interference. Therefore, temperature dependence of biomolecular interaction can be used to assist in identifying therapeutic targets and

differentiate binding between two similar biomolecules to their target and potentially eliminate non-specific signal interference [6]. In addition, once fully characterized, the temperature dependence of the biomolecular interactions can be used to control active release of analytes from the conformational changes in the receptor structure [7]. Therefore, there has been a strong need for developing techniques that can reliably characterize the temperature dependence of biomolecular interactions.

1.2 Methods for Characterization of Biomolecular Interactions

Upon occurrence, biomolecular interactions can induce changes in physical or chemical properties of biomolecules, resulting in a detectable signal (e.g. heat, light intensity) that can be resolved to characterize biomolecular interactions. Using this, many technical methods have been developed. Such methods include but not limited to fluorescence spectroscopy [8], surface plasmon resonance (SPR) [9], ultra violet-visible (UV-Vis) spectroscopy [10], mass spectroscopy [11], affinity chromatography [12], and capillary electrophoresis [13], and biocalorimetry [14, 15].

The most common approach is fluorescence microscopy and spectrometry, which is based on the use of fluorescent labels, via measuring the fluorescence emitted by the label either attached to the analyte or to a molecule that binds to the analyte [16]. Thus, the increase in the polarization of the fluorescence upon binding of the labeled molecule to its receptor can be used to characterize the interaction. Surface plasmon resonance on the other hand is the most commonly used label-free measurement technique. It measures a change in refractive index of the medium in close vicinity of a substrate surface that can be used to monitor the binding of analyte molecules to receptor molecules immobilised on the substrate [17]. Therefore, SPR

offers label-free meaurements of real-time quantification of binding affinities and kinetics with relatively small amount of matertial consumption. The methods also include ultra violet-visible (UV-Vis) spectroscopy which measures the reflectivity and scattering of light from the substrate surface as a function of wavelength [18], and mass spectroscopy, which is an analytical technique that ionizes chemical species and sorts the ions based on their mass to charge ratio that can be used to characterization and sequencing proteins by ionization of whole proteins.

Biocalorimetry is a method that directly measures the heat involved in biomolecular interactions. Biocalorimetry has distinctive advantages over others methods. First, it is a solution based method, as calorimetric measurements can be performed in solutions so that the biomolecules are free from having to be immobilized to a solid surface as others generally require. Therefore, biomolecule can retain their full conformational strength during interactions. Also, calorimetry directly measures heat involved in biomolecular activities and allows for determination of their thermodynamic propoerties. Moreover, calorimetry is a universally applicable method, as almost all of the biomolecular interactions are thermally active. At last, calorimetry is a label-free method, which means it generates biologically relevant data that enable understanding of molecular interactions without using artificial probes or labels [19].

There are two major biocalorimetry techniques, the first is **differential scanning calorimetry (DSC)**, which is a thermal analysis technique that determines the temperature and heat flow associated with material transitions within a specified temperature range [20]. It works by measuring the heat release in the temperature induced biomolecular activities,

either endothermic or exothermic, between a sample and a reference. The sample and reference are located in two idential calorimetric measurement cells whose temperatures are scanned at a specific rate in a chosen range. The measured heat release can then be used to calculate the temperature dependent thermodynamic properties of the sample molecules. Therefore, DSC is often used to observe fusion and crystallization events as well as heat induced protein confomational changes. The second technique **isothermal titration calorimetry (ITC)** on the other hand, measures heat either released or absorbed in biochemical reactions as a function of the molar ratio of the reactants. For example, a ligand solution in known concentration and volume is tritrated into a receptor solution of interest under isothermal conditions. The measured reaction heat is then recorded and used to calculate the binding parameters associated with the reactions. ITC is known to be the only technique that can simultaneously determine all binding parameters in a single experiment, and is label-free and solution-based, requiring no molecular labeling or surface immobilization. ITC is widely used in basic biochemical studies, as well as practical applications such as drug discovery and biotherapeutics development.

1.3 MEMS Technology as Applied to Characterization of Biomolecular Interactions

1.3.1 MEMS Technology

MEMS technology is defined as miniaturized (from millimeters to submicrometers) mechanical and electro-mechanical elements such as sensor, actuators. The elements are made using the techniques of microfabrication as those used to create integrated circuits, which is usually achieved by repeating sequences of photolithography, etching, and

deposition steps to produce the desired configuration of features [21]. MEMS systems can potentially be fabricated at low cost and operated at high throughput due to batch fabrication and parallelized sample processing. In addition, due to the size scale advantage, MEMS technology also enables minimized sample consumption and the ability to respond on short time scales. Furthermore, It also allows for the integration of different functional units such hermetically sealed microfluidic structures for fluidic handling, manipulation, and well-controlled micro and nano environments in which biomolecules can be manipulated and studied [22]. Therefore, the development of MEMS devices for biomolecular analysis holds promise to overcome the disadvantages of the conventional technique for biological experiments and acts as a powerful strategy in molecular biology [23].

Silicon is generally considered the material of choice in MEMS devices as the ability to incorporate electronic functionality make silicon attractive for a wide variety of MEMS applications. However, for the application of biomolecular characterization, flexible polymeric materials include polydimethylsiloxane (PDMS), poly (methyl methacrylate) (PMMA), polypropylene (PP), polyimide (PI), hydrogel, and polystyrene (PS) have exceled recently because of their enhanced and adjustable physiochemical properties such as robustness, transparency, low heat conductivity or electrochemical resistance. More importantly, polymer-based MEMS devices can be engineered thin and bendable, potentially allowing for the integration of sensors within textiles so as to achieve conformal contact to the curvilinear or uneven surfaces [24].

However, the development of the polymer-based MEMS devices demands innovations in the fabrication process as the conventional photolithography process is largely incompatible

with polymer substrates. Therefore, functional printing techniques such as screen printing, ink-jet printing, etc., have become the most prevalent manufacturing method [25]. Nevertheless, the functional printing methods still is limited by the feature resolution as well as lacks the material available for processing so that it is still a pressing need to develop a suitable photolithographical process for polymer substrates.

In addition, biomolecules are generally most stable and active in liquid form in a well-conditioned buffer. Therefore, MEMS devices used in biomolecular characterization generally are integrated with microfluidic structures for reagent handling and manipulation. Soft-lithography are the most commonly used process for manufacturing microfluidic structures, and PDMS is commonly used as a stamp resin material. PDMS based microfluidics, however, have three inherent limitations. First, PDMS can both absorb small hydrophobic molecules and adsorb larger biomolecules such as proteins on its surface. This has been identified as a significance problem for molecular biological analysis, as the use of PDMS can significantly bias the result of experiments with inconsistent reagent concentration information and impact the device reusability. In addition, since PDMS is a gas permeable material, water vapor permeation through PDMS can lead to inaccurate reagent volume information and change in reagents molarity, especially at elevated temperature, which may affect the accuracy of the experiment. Most importantly, PDMS based microfluidics made by soft-lithography techniques only allows the fabrication of two-dimensional (2D) topographical profile per step, so that any attempt to enable a high operating efficiency of a 3D microfluidic functional structure (e.g. for efficient micromixing) would require manual, and complicated multi-step process integration, thus reducing the fabrication yield, increasing

the device cost, and affecting the device reliability.

Alternatively, 3D printing, a technology that was widely believed by many to have the potential to change the field of microfluidics has emerged as preferred method for manufacturing microfluidic devices. 3D printing excels in many areas. First, it has the capability to fabricate a complete microfluidic device in a single step with a feature resolution as small as tenth of microns; second, it enables fabrication in three dimensions, thus enabling the construction of 3D microfluidic structures that are not achievable using conventional photolithography technique; finally, it also enables rapid prototyping, thereby significantly shortening the design turnaround time. Thus, in recent years, the use of 3D printing technology in the field of microfluidics had flourished. However, a collection of microfluidic structures alone cannot enable all the lab-on-a-chip operations, as they also require integrated electronics such as sensors and transducers to become complete lab-on-a-chip diagnostic systems. Therefore, how to integrate sensors and transducers with 3D printing microfluidic structures have become a major challenge and is yet to be resolved.

1.3.2 MEMS Technology for Biomolecular Characterization

MEMS technology has various advantages in terms of functions compared with their macroscopic counterparts: higher sensitivities in sensors, small amount of samples required, fast response. It also offers the advantages of the batch fabrication of many devices and can integrate multiple functional units in a small area. Furthermore, MEMS devices are easily integrated with microfluidic handling of well-defined liquid-phase samples and more importantly, well-controlled micro- or nanoscale environments in which biomolecules are effectively manipulated and analyzed. Therefore, MEMS technology tailored to biomedical

applications holds great potential in facilitating characterization of biomolecular interactions.

MEMS technologies have successfully been implemented in methodologies including fluorescence microarray technology [26, 27], Microfluidic based SPR [28-30], quartz crystal microbalance (QCM) [31, 32], and Microcantilevers [33, 34]. For example, Cretich et al., demonstrated the detection of allergen specific immunoglobulin E (IgE) using electrode microarray coupled to microfluidics, which enables the binding between the allergen and IgE by ensuring an efficient mixing of the samples on the surface of the microarray [27]. Luo et al., used a microfluidic device containing an array of antigens or antibodies attached gold surfaces to monitor and characterize the antibody-antigen binding events [29]. In addition, Godber et al., developed a microfluidic QCM immunosensor with an entirely electronic construction for the quantification of myoglobin interactions kinetics and the ranking of enzyme-cofactor specificities in microchannels. Finally, Etayash et al., used a suspended microchannel resonator, where a sample reagent incorporating channel was embedded inside a microcantilever for use in the real-time detection of bacteria and their response to binding with antibiotics [34]. However, MEMS devices based on the above-mentioned methods lacked the ability to characterize the thermodynamic properties of biomolecules or biomolecular activities to establish a connection between temperature and specific physical properties of substances [21].

1.3.3 MEMS Technology for Biocalorimetry

To fill the void, several types of MEMS calorimeters have been developed. MEMS technology was first adopted in calorimeters that targeted solid or thin film samples. For example, Denlinger et al., developed a microcalorimeter that uses a platinum thin film

resistor for characterizing heat capacity of metallic samples up to 800 K [35]. For the same purpose, Lai et al., used an ultrathin silicon nitride (SiN) membrane based microcalorimeter to support nickel (Ni) heating element as well as to enhance the thermal isolation [36]. The same calorimeter was also used to determine the thermodynamic properties of tin (Sn) nanostructures [37]. For thin film thermodynamic properties measurement, Fominaya et al., presented a nanocalorimeter that specifically targets in the temperature range of 1.5 – 20 K for the study of metal heat capacity [38]. Zhang et al., first employed the method of differential measurement to study the melting behavior of nanometer indium films [39]. Jaeggi et al., first reported a miniaturized AC calorimetric sensor based thermoelectric sensing principle by using a polysilicon/aluminum thermopile realized by complementary metal–oxide–semiconductor (CMOS) IC technology [40]. Besides characterizing thin film properties, microcalorimeter were also used for gas detection. Cavicchi et al. presented a MEMS calorimeter with polysilicon/metal thermoelectric junctions suspended on a diaphragm for combustible gas detection in a differential setup [41]. Guidi et al., reported a thick film microcalorimeter fabricated by screen printing that were suitable for gas sensing applications. However, none of these devices were designed nor optimized for processing liquid samples for characterizing biomolecules.

Efforts have also been made in developing solution based MEMS calorimeters as well. Chancellor et al., developed a droplet based micromachined calorimeters that measuring enthalpies in chemical or biological reactions in picoliter volume [42]. Moreover, Lerchner et al., published a series of articles based on a microfluidic segment flow technology [43] to study a variety of biological applications such as the aggregation of biological samples [44],

degradation of the soil organic matter [45] as well as the infection related heat profile [46]. Similarly, Hany et., developed differential based continuous in-channel delivery method, which was used to calculate the enthalpy change during a reaction [47]. Also, Recht et al., measured the reaction heat of biomolecular binding event in real time by merging sequential injection of small droplets of the ligand into the receptor in a 96-well array format [48]. However, MEMS devices that offer ITC capabilities do not yet allow proper control of reaction conditions for thermodynamic characterization of biomolecular reaction systems. In particular, flow-through based MEMS calorimetric devices have limited sensitivity due to poor thermal isolation. In addition, devices that use droplet-based reactions generally do not allow for well-defined reaction volumes and are further complicated by evaporation-induced noise and volume change. Hence, such devices are not well suited to quantitative measurement of thermodynamic reaction parameters.

In attempt to address these issues, our lab developed MEMS-based DSC and ITC devices using silicon-based microfabrication techniques. Measuring by a differential scheme, the calorimeters consist a sample and a reference measurement chamber, as well as microfluidic handling, miniature environment control, and thermoelectric transduction functionalities for biomolecular characterization that include the study of biomolecule thermodynamic properties or binding parameters associated with its interactions with a target. Its potential, however, for practical applications was hindered for the following reasons. First, the devices were silicon-based. While this allowed for established microfabrication techniques, the high thermal conductivity of silicon necessitated the use of freestanding structures to increase the thermal isolation of the measurement samples. This increased the complexity of the

fabrication process, reduced its yield, and along with the relatively high cost of silicon, made the devices rather expensive. In addition, the fragility of the freestanding structures caused significant reliability issues during the devices' operation, especially at elevated temperatures. Second, the initially demonstrated the silicon-based devices were operating without any characteristic analysis, so that factors such as volume mismatch, reaction volume information, evaporation of reactants might influence both the sensitivity and accuracy of the calorimetric measurements. Finally, the previously demonstrate devices all used PDMS-based microfluidic structures. As stated above, the use of PDMS can significantly bias the result of experiments with inconsistent reagent concentration, and volume information to impact the measurement accuracy.

1.4 Contributions and Significance of This Thesis

This thesis addressed the above limitations of prior MEMS calorimetric devices by implementing polymer-based MEMS calorimetric devices for characterizing biomolecular interactions with reduced sample consumption, and high operational throughput. The work incorporated in this thesis can be divided into four major categories: the development of the polymer-based MEMS thermoelectric transducer; the development of MEMS DSC for the characterization of temperature dependent thermodynamic properties of the biomolecules in solution, and the characterization of thermodynamic properties of the binding between a target and a receptor using MEMS-ITC, as well as the integration of 3D printed microfluidic structures with polymer-based MEMS transduces for the characterization of biomolecular interactions.

The major contributions of this thesis are summarized as follows.

This thesis develops MEMS calorimetric devices for quantitative thermodynamic characterization of biomolecular interactions with improved throughput, reduced sample consumption and device response time. To quantitively characterize thermodynamic properties of biomolecular interactions, this thesis developed MEMS calorimetric devices that offered real-time, in-situ temperature control to biomolecules with well-defined miniature volumes that combined with the improved sensitivity to reduce consumption of material. In addition, the sample volume reduction in combination with the device miniaturization also lead to substantially reduced thermal mass of the measurement system for a rapid response time and improved throughput than those used in conventional calorimeters.

This thesis develops polymer-based calorimetric devices that enhance sensitivity, reduce the device cost, improve the device yield and reliability. Existing MEMS calorimeters were not yet adequate for practical applications. This thesis addressed the limitations of prior MEMS calorimetric devices (in particular those of our previous silicon-based devices) with polymer-based MEMS calorimetric devices. The polymer-based calorimetric device design eliminated the use of silicon, and exploited the low thermal conductivity of the polymer substrate to achieve thermal isolation of reaction samples in the absence of any complex or fragile freestanding structures. The use of inexpensive polymers and the elimination of the freestanding structures simplified the fabrication process, increased the fabrication yield, reduced the device cost, and improved the device reliability.

This thesis demonstrates both polymer-based MEMS DSC and ITC measurement approaches, which are the two most important and commonly used calorimetry measurement modes. The utility of the polymer-based MEMS devices was implemented in both DSC and

ITC measurement approaches, which were the two most important and commonly used calorimetry measurement modes. Specifically, the DSC characterization of protein unfolding had led to the characterization of the specific heat capacity, molar enthalpy change, and melting temperature of the protein. The utility of the device was demonstrated by DSC measurements of the unfolding of lysozyme in a small volume, and at practically useful protein concentrations. In addition, the ITC characterization of biomolecular interactions had led to determination of the stoichiometry, equilibrium binding constant, and enthalpy change for the model reaction system of 18-Crown-6 and barium chloride in an overall 40-time regent consumption reduction compared with the existing devices, making the devices practically applicable. Therefore, the polymer-based devices presented in the thesis can potentially replace the conventional methods with accurate, sensitive measurement with reduced sample consumption, device response time, and the overall experimental duration.

This thesis contributes to the development of fabrication technologies for MEMS calorimetry: (a) A universally applicable photolithographical process for MEMS devices fabrication; (b) the first demonstration of a miniaturized 3D-printed LOC platform that integrates a polymeric MEMS-based measurement approach for quantitative ITC characterization of biomolecular interactions. Due to film retention issue during lift-off, conventional photolithography process was largely incompatible with polymer-based MEMS devices. In this thesis, a thick-film polymer-based MEMS device fabrication technique using an innovative thermally assisted lift-off process was developed. The thermally assisted process facilitated the sacrificial removal of the photoresist, thereby resolving the incompatibility issue, and enabled the fabrication of a thick-film polymer-based MEMS

devices that allowed low-noise, high-efficiency measurements built on a mechanically robust, and inexpensive, commercially available polymer substrate.

Due to its surface property and gas permeability, PDMS can significantly bias the result of calorimetric experiments with inconsistent reagent concentration information and impact the device reusability. To address this, this thesis presented the first demonstration of a miniaturized 3D-printed LOC platform that integrates a polymeric MEMS-based measurement approach for quantitative ITC characterization of biomolecular interactions. The platform replaced PDMS in calorimetric analysis with non-permeable, biocompatible materials, thereby facilitating device operation and maintenance, making the device reusable. In addition, exploiting the topographical flexibility offered by 3D printing, the platform consisted structures that were unavailable to the conventional means of microfabrication, such as cantilever-like structures that both enhanced thermal isolation and reduced device thermal mass, thereby enhancing the measurement sensitivity and reducing the platform response time.

1.5 Thesis Outline

In Chapter 2, polymer-based MEMS thermoelectric sensors fabricated using an innovative low-temperature thermally assisted lift-off process is described [49]. During the process, thick metal or semiconductor films experience controlled breakup due to thermal reflow of the underlying lithographically defined photoresist patterns, and facilitating the sacrificial removal of the photoresist. The process is then used to fabricate polymer-based MEMS thermoelectric sensors consisting of a 60 junction Bi-Sb thermopile. The experimental results of the sensors showed a bulk material comparable thermoelectric, and

electric performances, thus enable the fabricated MEMS sensor to be used in low-noise, high-efficiency thermoelectric measurements.

In Chapter 3, the fabrication method presented in Chapter 2 is used to develop a polymer-based MEMS DSC device [72, 73] for studying the temperature-dependent thermodynamic properties of biomolecules. The device consists of identical serpentine microfluidic sample and reference flow channels and a 200-junction thin-film Sb–Bi thermopile that is situated on a polymer substrate. The temperature induced differential power between the sample and reference measurement channels is measured to determine the temperature dependent thermodynamic properties of the biomolecules. The utility of this MEMS calorimeter is demonstrated by measuring the unfolding of lysozyme in a small volume (0.8 μL), and at practically useful protein concentrations (5 mg/ml)

Chapter 4 describes a quantitative ITC measurement approach implementing in a polymer-based MEMS microdevice. The polymer-based ITC device design eliminates the use of silicon, and exploits the low thermal conductivity of the polymer substrate to achieve thermal isolation of reaction samples in the absence of any complex or fragile freestanding structures, thereby simplifying the fabrication process, increasing the fabrication yield, reducing the device cost, and improving the device reliability. During the ITC device operation, reactants and reference solutions are introduced to their respective measurement chambers, and the reaction-induced differential thermal power is measured and used to compute the thermodynamic binding parameters associated with the reaction. The potential utility of the device has been demonstrated with quantitative ITC measurements of a model reaction system in which the ligand $BaCl_2$ is titrated into the receptor 18-C-6 at a

concentration of 2 mM.

Chapter 5 presents an improved ITC microdevice based on the systematic characterization of the factors that affect both the sensitivity and accuracy of the ITC measurements [111]. Thus, a 3D chaotic mixing-titration ITC design approach is used based on insights gained from these characterizations. The design features 3D mixing-titration channels that integrates the functionalities of reagents mixing, titration, and thermoelectric transducing. This integration eliminates heat loss during mixing, minimize flow-induced measurement noise while maintains a distinctive device response time to allow thermodynamic characterization of reaction systems with fast kinetics. The potential utility of the device has been demonstrated with quantitative ITC measurements of a model reaction system in which the ligand barium chloride is titrated into the receptor 18-Crown-6 at a practically useful limit-of-detection level of 25 nW, and a receptor consumption of 50 ng.

Chapters 6 presents a 3D printing-based ITC LOC platform that integrates with the polymer-based MEMS sensor chip for characterization of biomolecular interactions. In this chapter, the use of PDMS microfluidic structures is eliminated entirely, and the LOC platform exploits the topographical flexibility offered by 3D printing and features fully isolated cantilever-like calorimetric measurement structures in a differential setup. This design layout improves thermal isolation and reduces overall platform thermal mass, thereby enhancing the measurement sensitivity and reducing the platform response time. The utility of the platform is demonstrated by quantitative ITC measurements of the binding of RNase A with 2’CMP at low cost, using practically relevant reagent concentrations (0.2 mM). These results demonstrate the potential of our approach for efficient quantitative ITC characterization of

biomolecular interactions in biomedical applications.

This thesis will conclude with a summary and a discussion of future work in Chapter 7.

Chapter 2 A Thick-Film MEMS Thermoelectric Sensor Fabricated Using a Thermally Assisted Lift-Off Process

In order to develop MEMS calorimeters that are economical, robust, and highly sensitive, one potential approach is to eliminate the use of silicon due to its fragility, relatively high thermal conductivity and manufacturing cost. The promising replacement for silicon is polymeric materials as they possess properties such as robustness, transparency, low thermal conductivity and electrochemical resistance, ideal for thermodynamic characterization of biomolecular interactions. However, the conventional photolithography process is largely incompatible with polymeric materials, and there is a pressing need to develop a suitable photolithographical process for polymeric materials.

This chapter presents a thick-film polymeric MEMS thermoelectric sensor fabricated by an innovative low-temperature thermally assisted lift-off process. During the process, thick metal or semiconductor films experience controlled breakup due to thermal reflow of the underlying lithographically defined photoresist patterns, thereby facilitating the sacrificial removal of the photoresist. This enables rapid and reliable patterning of thick films on polymer substrates that can otherwise be difficult to achieve by conventional processes. Experimental results with a sensor consisting of a 60-junction thick-film antimony-bismuth thermopile demonstrate an electric conductivity of 5.44×10^6 S/m and a Seebeck coefficient of 114 μV/K per junction, which are comparable to those obtained from bulk materials. Thus, the thick-film sensor can potentially allow low-noise, high-efficiency thermoelectric measurements.

2.1 Introduction

Microfabricated thermoelectric sensors that consist of thin-film of two dissimilar metals or

semiconductors, with their patterned junctions at different temperatures to produce a differential voltage, are widely used in microelectromechanical systems (MEMS) [50-53]. However, the sensitivity of existing microfabricated thermoelectric sensors are limited by reduced electric conductivity of metallic materials in thin-film form than in bulk due to scattering of electrons on film surfaces [54], which increases thermal noise [55] as well and decreases the thermoelectric efficiency [56]. Since this issue can be alleviated by using thin films of relatively large thicknesses (hereafter referred to as thick films), there is a need for new methods that allow the deposition and patterning of such films.

Lift-off, an essential fabrication method for thin-film technology, generates patterned material (e.g., metal) films through the deposition of one or more pattern-defining layers of sacrificial photoresists on a substrate [57-62]. However, conventional lift-off techniques are currently limited by the retention of undissolved photoresist in thick-film applications (*i.e.*, unwanted film patterns that remain on the substrate without being lifted off) [63, 64]. In addition, recent research in achieving reliable thick-film lift-off requires specialized materials/instruments [65], multiple processing steps [66], and most significantly, long etching times to increase the undercut depth which may lead to pattern erosion [67, 68]. These issues make it rather difficult to pattern thick films and can also complicate downstream micromachining processes, in particular for flexible substrates. As a result, existing thermoelectric sensors are forced to be fabricated with limited sensitivity and a relatively low yield.

This chapter presents a thick-film MEMS thermoelectric sensor fabricated using an innovative thermally assisted lift-off process. In this process, thick metal or semiconductor

films experience controlled breakup due to thermal reflow of the underlying lithographically defined patterns. This facilitates the sacrificial removal of the photoresist and formation of a thermoelectric sensor consisting of a thick-film, multi-junction thermopile on a flexible substrate. The sensor offers an improved sensitivity by using thick films to alleviate the reduction in the thermal noise and increase in the thermoelectric efficiency. Meanwhile, the sensor can fabricate with a higher yield and less processing time, as thermally induced reflow of photoresist facilitates sacrificial removal of the resist for the patterning of thick metal or semiconductor films. For thick films of a given thickness, the thermal reflow-based technique also allows the use of thinner sacrificial photoresist (by ~60%) compared to that in conventional processes, resulting in the minimization of feature erosion in the sensor. Experimental results with a sensor using a 60-junction thick-film antimony-bismuth thermopile demonstrate an electric conductivity of 5.44×10^6 S/m and a Seebeck coefficient of 114 μV/K per junction, which are comparable to those of bulk material-based thermopiles. Thus, the sensor can potentially be useful in low-noise, high-efficiency thermoelectric measurements.

2.2 Material and Methods

The low-temperature, thermally assisted lift-off fabrication process is applicable to both bilayer and single-layer lift-off processes. The bilayer process (Figure 2-1a-d) involves heating of the lift-off structure after a target material (e.g., metal) has been deposited on top of the bilayer photoresists structure to induce thermal softening and rounding (reflow). Due to the different reflow temperature required, (*e.g.* LOR > 250 ^{o}C, S1811 < 200 ^{o}C) the bottom photoresist undercut layer remains undeformed while the top layer deforms. The strain

generated during the deformation causes the

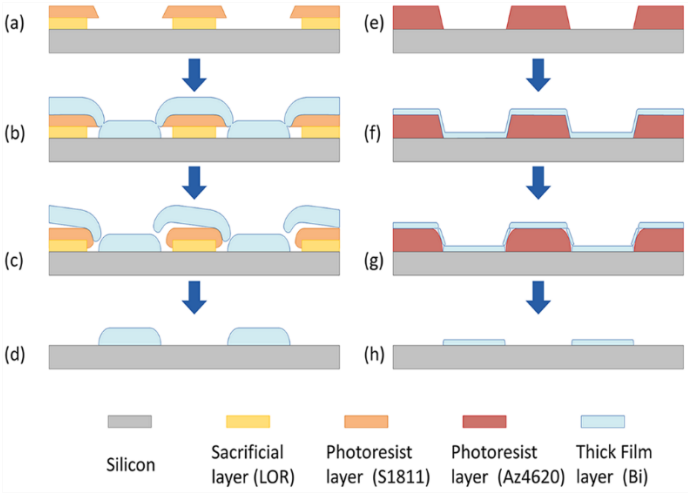

Figure 2-1. Principle of thermally assisted lift-off method: (a-d) bilayer; (e-h) single-layer.

thick-film to conform to the shape of the deformed photoresist, introducing gaps where the deposited thick-film is thinnest due to the poor step coverage of film coating (Figure 2-1c). These gaps allow stripper solution to access the photoresists previously covered by the thick-film, and thus complete the lift-off process. This reflow principle also applies to the single-layer lift-off process (Figure 2-1e-h). However, while conceptually simpler, the single-layer process is more challenging as without the support of a bilayer structure (*i.e.* the undercut profile), the metal or semiconductor film step coverage on the sidewall is much thicker and more difficult to break as compared to the bilayer process (Fig. 1g). Therefore, the positive photoresist AZ 4620 is specifically chosen as its reflow properties have been extensively studied [69].

The thermally assisted lift-off process was first tested for the lift-off of Bi film on a silicon wafer. The bilayer lift-off began with the spin-coating and patterning of 1.2 μm thick layer of LOR 10A and 1 μm of S1811. ~2 μm of Bi was then thermally evaporated, after which the wafer was diced. Half of samples was heat-treated on a hot plate at 170 °C for 2 min to allow

photoresist reflow. This temperature was chosen to match the soft bake temperature of the LOR while being greater than the baking temperature of S811 (115 °C), thus inducing S1811 reflow. The remaining samples was kept at room temperature. The samples were then submerged in remover PG at room temperature to complete the lift-off. Similarly, the single-layer method began with the spin-coating and patterning of 5 μm thick AZ 4620 on another silicon wafer, followed by the thermal evaporation of 0.5 μm Bi. The silicon wafer was again diced and divided to a half so that samples would serve the same purpose as described above. A heat treatment of 115 ºC for 10 mins was used for AZ 4620 photoresist reflow in the single-layer lift-off process.

The lift-off process was then used to fabricate a MEMS thermoelectric sensor on a flexible polyimide film substrate. Both single-layer and bilayer processes were used to fabricate a thermopile that consists of 60 Bi-Sb thermoelectric junctions. The bilayer process began with the reversible bonding of a polyimide film (Kapton® 50HN) to a silicon carrier wafer using spin-coated poly (dimethylsiloxane) (PDMS) as an adhesion layer. A 2 μm layer of Bi was then lifted-off using bilayer process described above, followed by an identical process to lift-off 1 μm thick Sb. Next, a layer of polyimide (PI-2610) with a thickness of 2 μm was spin-coated cured, and served as a passivation layer. Subsequently, a layer of chromium/gold (7/100 nm) was evaporated and patterned as on-chip heaters and sensors for device characterization purposes. Finally, the polyimide film was mechanically released from the carrier wafer completing the fabrication process.

For the single-layer lift-off process, a 0.5 μm layer of Bi was thermally evaporated onto the polyimide film followed by heating to allow the photoresists reflow using the above mentioned

parameters. The Bi film was next submerged in acetone at room temperature to complete the lift-off. Next, 0.5 μm Sb was lifted-off using the same process. This was again followed by the fabrication of on-chip heaters and sensors as well as the mechanical release of the polyimide substrate.

The electrical as well as the thermoelectric performance of the fabricated flexible thermoelectric sensor were assessed. In order to calculate the electrical conductivity of the thermopile junctions, flexible thermoelectric sensors were placed inside an environmental chamber (Test Equity model 115). The temperature of the sensor was determined by the on-chip resistive temperature sensor, whose resistance, along with the resistance of the patterned Bi and Sb films, was measured by a digital multimeter (Agilent 34410A). After the determination of the electrical conductivity, the sensor was placed inside a thermal enclosure to calculate the overall Seebeck coefficient of the thermoelectric materials per junction. The on-chip micro-heaters were driven by a power supply (Agilent E3631A) to generate a differential power input. This resulted in a temperature increase at the hot junctions of the thermopile, which was measured using the temperature sensor. The corresponding thermopile output voltage was measured by a nanovoltmeter (Agilent 34420A). These thermoelectric and resistive measurements were automated using a LabVIEW program.

2.3 Results and Discussion

In order to fully understand the effects of heating on the thick films, the surface morphology of the diced Bi samples from both single and bilayer processes were studied using both optical microscopy and scanning electron microscopy (SEM). Optical microscopes were used to observe and compare before and after the heat treatment for both processes. For the

bilayer process, after placing the sensor on a hotplate at 170 ^{o}C for 2 min the photoresist deformed as shown as a black-colored features (Figure 2-2) located between the patterned thermopile junctions. This was consistent with our expectation that the thermopile junctions (shown as white lines in between black pattern on Figure 2-2b) would not be affected by the film deformation.

SEM (Hitachi S-4700 Scanning Electron Microscope) samples were first tilted at a 70^{o} angle to observe the metal topography under the effect of photoresist reflow. Figure 2-3a showed before heating induced reflow, the Bi film was uniformly coated onto the bilayer photoresist structure. After heating (Figure 2-3b), the Bi film conformed to a dome-shaped profile to break up the film coverage on the photoresist sidewall as we described in Fig. 1 due to the melting and reflow of the photoresist. Next, both the sideview and topview of the Bi thermoelectric junctions were observed using the SEM micrograph confirmed that the Bi film coverage (Figure 2-4a) was indeed broken up (Figure 2-4b) by photoresist reflow. Also, it is important to note that the S1811 photoresist deformed within 10 s upon heating; however, it was not enough to break-up the Bi metal coverage on the photoresist sidewall. In addition, increasing the heating time beyond 2 minutes had no effect on the lift-off photoresist removal time and was avoided because it caused photoresists to stick to the substrate and fail to dissolve in the stripping solution.

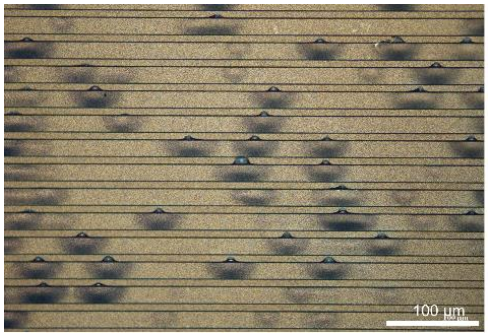

Figure 2-2. Optical micrograph of Bi after heating at 170 °C for 2 min. Black color indicates photoresist deformation.

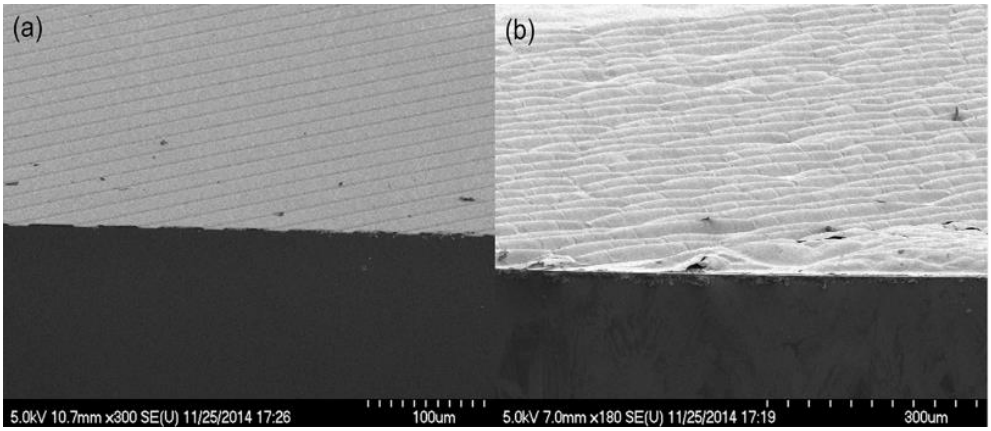

Figure 2-3. SEM micrographs before (a) and after (b) heating induced photoresist reflow.

Specifically, before heating, the deposited Bi film (~2 μm) was thicker than the LOR undercut depth (~1.2 μm), and therefore completely covered the bilayer photoresists. This blocked (Figure 2-4c) the stripping solution (Remover PG) and caused the failure of the lift-off. As a result, 90% of unwanted Bi still remained after submerging in Remover PG for 8 hours at room temperature and an additional 4 hours at 70 °C (Figure 2-5b). On the contrary, after heat treatment (Figure 2-4d), due to the releasing of residual stress, unbound Bi film formed large wavy gaps along the line edges, which allowed remover PG to access the sacrificial photoresist rapidly, thereby enabling total lift-off of 2 μm thick Bi within 4 hours with a minimum feature size of 10 μm and smooth edges at room temperature (Figure 2-5a). This thermally assisted method is also applicable to the simpler single-layer lift-off. Under optical microscope, before heating, (Figure 2-6a) the Bi film exhibited a uniform coating on

the patterned

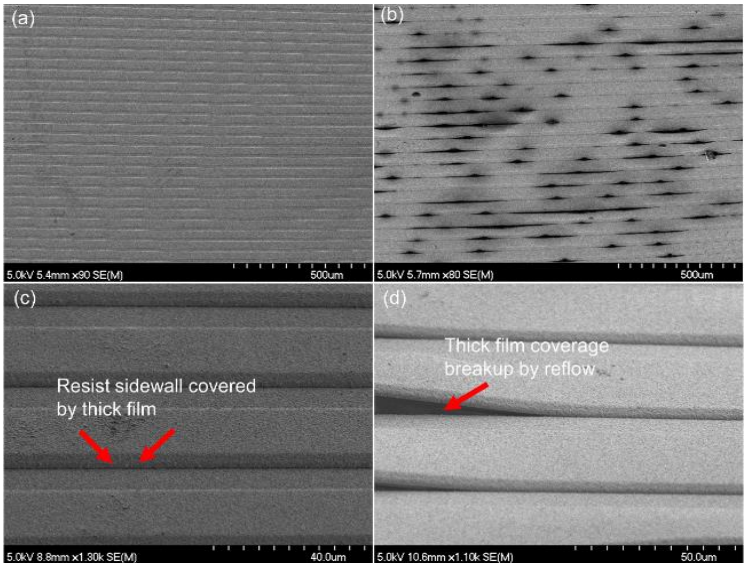

Figure 2-4. (a) SEM micrograph of Bi without heating; (b) SEM micrograph of Bi after heating at 170 °C for 2 min; (c) SEM micrograph of Bi film covering the sidewall; (d) Zoomed in micrograph of the gaps created by heating.

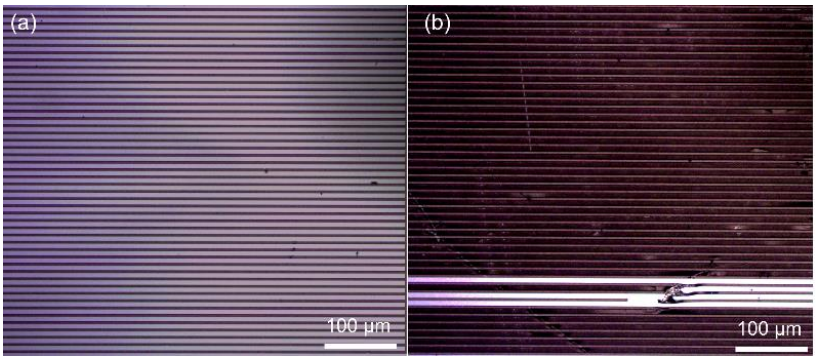

Figure 2-5. (a) A clean Bi lift-off after submerging in Remover PG for 4 hours at room temperature; (b) 90% of unwanted Bi still remained after submerging in Remover PG for 12 hours without prior heat treatment.

photoresist. However, after heating (Figure 2-6b) the Bi film did not exhibit black features as in the bilayer process, instead, the reflow of the AZ 4620 caused the rounding of the photoresist that lead to an increase of the feature width (indicated by arrows). This is expected for the reflow of AZ 4620 [17]. Also, the edge of the photoresist sidewall showed the potential discontinuities of the deposited Bi (black edges) after heating.

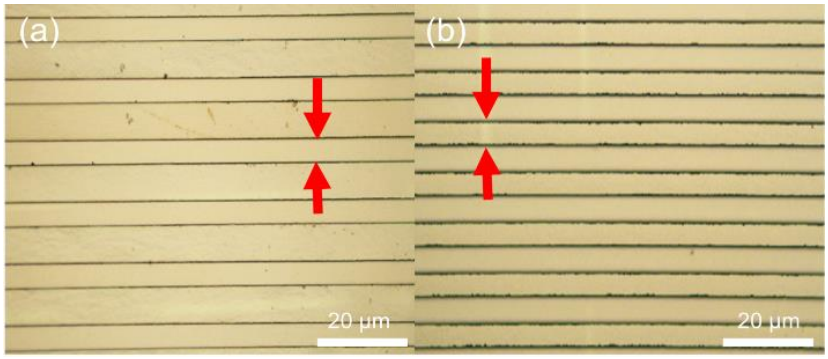

Figure 2-6. (a) Optical micrograph of Bi without heating; (b) optical micrograph of Bi after heating at 110 °C for 10 min.

SEM was then used to confirm the existence of the metal discontinuities on the photoresist sidewall. Without heating (Figure 2-7a, c), the deposited Bi formed a continuous metal cover on the photoresist AZ4620, which prevented the access of the photoresist stripper (acetone) and caused lift-off to fail. We found a 95% of unwanted Bi film still remaining after submerging in acetone for 8 hours at room temperature and an additional 4 hours in acetone at 60 °C. On the contrary, after heating, the reflow of AZ 4620 introduced cracks along the line edges (both on top and bottom), as well as discontinuities on the sidewall (Figure 2-7b, d), so that acetone was able to interact with the AZ4620 and dissolve it. Heat treatment at a higher temperature or for a longer time would cause potential undesirable changes in the AZ4620 photoresist preventing its dissolution in a stripper solution.

The heating of the lift-off structures enabled complete lift-off of 0.5 µm thick Sb and Bi within 8 hours of submerging in acetone at room temperature, or within 4 hours of submerging in acetone at 60 °C (Figure 2-8a, b). The resulting thermoelectric junctions had a minimum feature size of 10 µm and smooth edges. The longer lift-off time compared with the bilayer process was expected, as the cracks and discontinuities were much smaller than the large gaps created by the film break-up using the bilayer process as the metal or semiconductor film covering on the photoresist sidewall is much thicker and more difficult to

break compared to the bilayer process (Figure 2-1g). To sum up, although both processes offer reliable thick-film lift-off, the single-layer process offers simplicity while the bilayer process enables the lift-off of same thick-film thickness while using a much thinner undercut resist layer and is more suitable for applications that benefited from having a thicker film. In addition, the yield of this process is related to the deposited film thickness as well as the sacrificial resist thickness used. Using the same resist thickness, the yield will gradually decrease as the deposited film thickness increases. This is expected as it will be more difficult to break the metal or semiconductor film coverage of the underlying lithographically defined patterns. However, at the testing condition the yield is close to 90%.

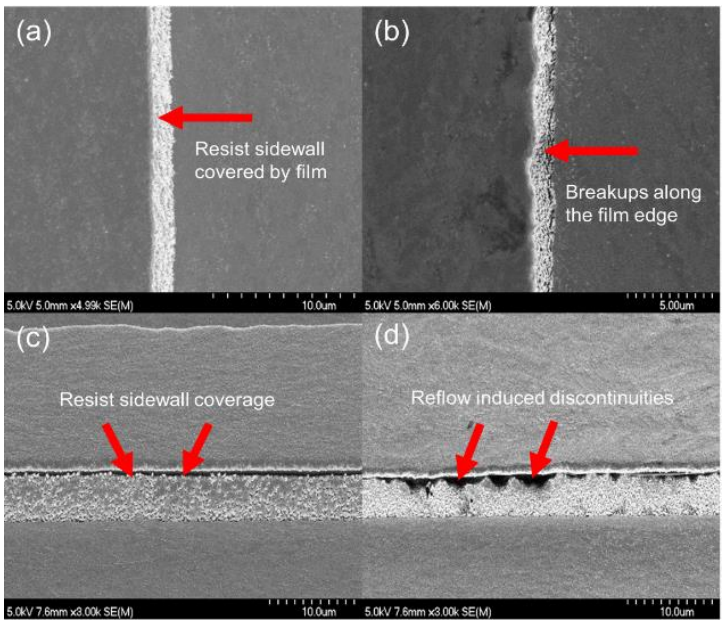

Figure 2-7. SEM micrographs of Bi (a) top-view before heating; (b) top view after heating, showing cracks on the bottom of the sidewall; (c) side view before heating; (d) side view after heating, showing cracks on the top of the sidewall, as well as small.

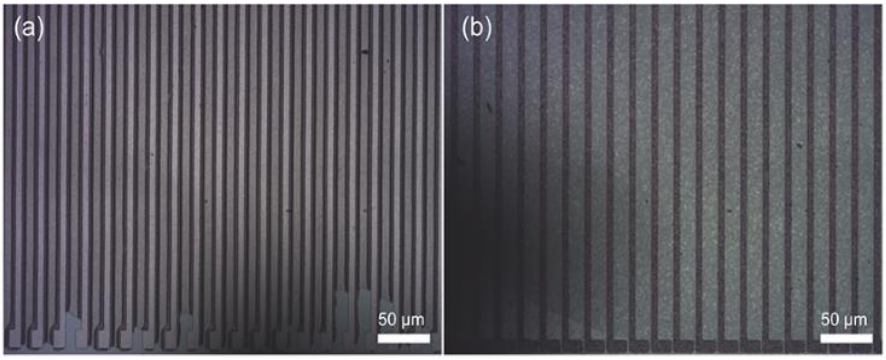

Figure 2-8. (a) 90% of unwanted Bi still remained after submerging in acetone for 12 hours without prior heat treatment; (b) a clean Bi lift-off after submerging in acetone for 8 hours at room temperature. Black shades are a result of microscope artifact.

The bilayer process was then used to fabricate flexible thermoelectric sensors with a minimum feature solution of 10 µm (Figure 2-9c). Higher spatial resolutions are achievable using this method with the use of higher-resolution photomasks as patterned thermoelectric junctions were not damaged by the heating induced film breakup and thus would not limit the feature resolution. The average electrical conductivity of the Bi and Sb was calculated and plotted using the measured resistance for both materials at different temperatures (Figure 2-9a), which were measured using the calibrated on chip temperature sensor. At room temperature, the average electrical conductivity per Bi-Sb junction was obtained as 5.44×10^6 S/m. The electrical conductivity was comparable to that of the bulk material [70], and was due to the use of thick films. In addition, using the sensor shown in Figure 2-9c, the average Seebeck coefficient of the Bi-Sb thermopile per junction was also found to be 114 µV/K (Figure 2-9b). This is within 5% of the Seebeck coefficient for bulk Sb-Bi material at room temperature (119µV/K) [71]. The obtained electric and thermoelectric performance of Bi-Sb thermopile junctions demonstrate there is little effect of heating on the film properties due to the use of low temperature.

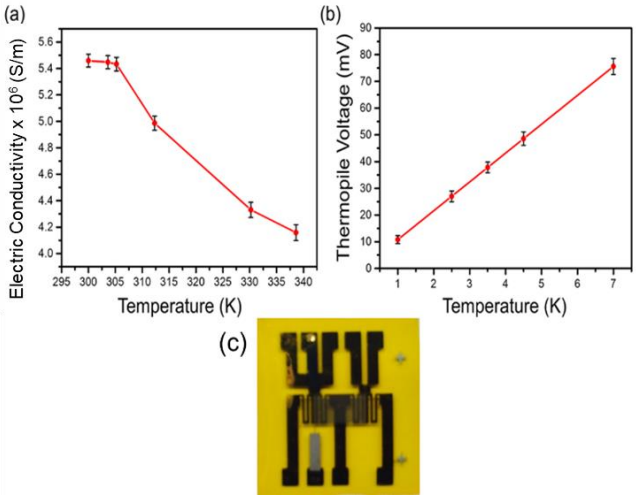

Figure 2-9. Electric and thermoelectric performance of the flexible thermoelectric sensor: (a) electrical conductivities of Bi-Sb (per junction) with as a function of temperature. Error bar was obtained from the resistance measurements of three different devices.

2.4 Conclusion

This chapter has presented a thick-film flexible thermoelectric sensor fabricated using a low-temperature thermally assisted lift-off process. In this process, low-temperature heating induced photoresist reflow causes the breakup of the metal or semiconductor film coverage on lithographically patterned photoresist, thereby facilitating the sacrificial removal of the photoresist, as well as rapid and reliable formation of patterns in the thick films. Both single-layer and bilayer lift-off processes were used to fabricate the sensor. Optical microscopy and SEM methods were used to characterize the topography of the thick-film before and after the reflow process.

This method was then demonstrated by the fabrication of the thermoelectric sensor on flexible substrates. Metal films up to 2 μm thick were patterned within 4 hours at room temperature to produce 60 Bi-Sb thermoelectric junctions with a minimum feature size of 10 μm. Testing of the sensor at room temperature yielded an average electrical conductivity of 5.44×10^6 S/m per Bi-Sb junction. The Seebeck coefficient per Bi-Sb junction was 114 μV/K.

These properties are within 5% of that of those of bulk materials, allowing the thick-film sensor to be of potential utility in low-noise, high-efficiency thermoelectric measurements. Therefore, the method for fabricating polymer-based MEMS thermoelectric sensors was used in the following chapters for characterizing biomolecular activities.

Chapter 3 A Polymer-Based MEMS Differential Scanning Calorimeter

After successfully fabricated the MEMS sensor capable of detecting differential heating power, this chapter adopts the measurement principle and presents a polymer-based MEMS DSC device. The device integrates highly sensitive thermoelectric sensing, real-time temperature monitoring and microfluidic sample and reagent handling for the thermodynamic characterization of biomolecules with minimized sample consumption. The device, based on an inexpensive, commercially available polymer substrate, consists of a pair of calorimetric microchannels that are integrated with resistive temperature sensors and heaters as well as an antimony–bismuth (Sb–Bi) thermopile. For DSC measurements, the two channels are filled respectively with a biomolecular sample and a reference solution, whose temperatures, measured in situ using the resistive temperature sensors, are varied at a constant rate using closed-loop temperature control. The difference in the thermal power between the sample and reference induces a temperature difference, which is measured using the thermopile for thermodynamic characterization of the biomolecules. We demonstrate the utility of this MEMS DSC device by measuring the unfolding of lysozyme in a small volume (1 μL), and at practically useful protein concentrations (5 mg/mL). Thermodynamic properties of lysozyme, such as the molar enthalpy change and melting temperature at different lysozyme concentrations, have been obtained and found to agree with published data.

3.1 Introduction

DSC is a thermal analysis technique which has been used to measure the temperatures and heat flows associated with transitions or thermally active processes in materials as the temperature of the sample is varied [74].

When applied to characterizing biomolecular interactions and conformational transitions [75], DSC allows universally applicable, direct, label-free (i.e., the biomolecules is not labeled by florescent, enzymatic or radioactive material) detection [76], and is widely used in determining the thermodynamic properties of biomolecular interactions and conformational transitions [20, 77]. However, the practical use of conventional DSC instruments is impeded by low throughput, large sample consumption and complicate construction [78]. While MEMS techniques can potentially address the aforementioned issues with improved throughput as well as reduced thermal mass and sample volume, previously-reported MEMS-based DSCs are still limited by drawbacks such as an inability to process liquid samples of well-defined volume, as most of the current MEMS calorimeters are only designed for solid, gas-phase detection [79, 80]. Also the lack of precise environmental control [42] or use of droplet detection [81] can potentially hinder the accuracy of the detection as such devices are prone to environmental noise and miscalculation of the volume-specific information.

We have previously demonstrated a silicon-based MEMS DSC device [82] that integrated microfluidic calorimetric channels and an antimony–bismuth (Sb–Bi) thermopile on a single chip, thereby allowing sensitive measurements with well-defined sample volumes (1 μL) with minimized evaporation. However, its utility was limited by expensive and time consuming silicon-based fabrication processes. Furthermore, the device's robustness was limited by the use of freestanding microstructures, which, at elevated DSC measurement temperatures, were prone to failure.

This chapter aims to address these limitations by presenting a polymeric MEMS DSC

device. The device incorporates microfluidic channels, temperature sensors and heaters, and Sb–Bi thermopile junctions all on an inexpensive, commercially available polymeric substrate. The low intrinsic stress and the elimination of the fragile freestanding structures in the polymeric device lead to significantly improved device robustness and fabrication yield. The low thermal conductivity of the polymeric substrate and the use of air-gaps surrounding the microfluidic channels provide enhanced thermal isolation of samples and reagents for improved measurement sensitivity. The mechanical flexibility of the substrate also accommodates the deformation of the substrate and allows the device to conform to non-planar surfaces that can potentially be useful in applications with geometries with curvature. Moreover, by the use of polymeric materials, the device can be low cost and hence be potentially used in a disposable manner, eliminating cross contamination between samples in different experiments. We demonstrate the utility of this polymeric MEMS DSC device through measurements of the unfolding of the protein lysozyme at 5 mg/mL, a concentration relevant to practical applications.

3.2 Principle and Design

3.2.1 Principle

The polymeric MEMS DSC device monitors voltage differences between hot and cold junctions of a thermopile, induced by heat generation during biomolecular interactions. A sample solution containing target molecules and a reference buffer solution are thermally scanned at a pre-specified rate, and the resulting thermopile voltage is then used to determine the differential power (i.e., the difference in the thermal power) between the sample and reference channels.

The differential power generated (*i.e.*, the difference between the power generated by the sample and reference) can be represented as $\Delta P = P_{mol} - P_{solv}$, where P_{mol} and P_{solv} are the thermal power generated in the sample and reference materials (buffer) respectively. Let the heat capacities of the sample and reference be $C_{mol}(T)$ and $C_{solv}(T)$, respectively. The differential heat capacity between the sample and reference, ΔC, can be then calculated by [83]:

$$\Delta C = \frac{\Delta P}{\dot{T}} = \frac{\Delta U}{K\dot{T}} \tag{1}$$

where ΔU is the measured thermopile output voltage, $\dot{T}$ is the scanning rate, i.e., the rate at which the sample and reference temperatures are varied in time within a range of interest. The device responsivity K, or the thermopile output voltage per unit differential power between the chambers, is determined via calibration experiments (below). Eq. 1 can be used to obtain [83]

$$c_{\mathrm{mol}}(T) = c_{\mathrm{solv}}(T)\left(\frac{v_{\mathrm{mol}}(T)}{v_{\mathrm{solv}}(T)}\right) + \frac{\Delta C(T)}{m_{\mathrm{mol}}(T)} \tag{2}$$

where $v_{mol}(T)$ and $v_{solv}(T)$ are the partial specific volumes of the sample and the buffer respectively, $m_{mol}(T)$ is the mass of the biomolecule in the sample channel. Integrating the sample partial heat capacity over a temperature range of interest allows the determination of the total enthalpy change per mole of biomolecules associated with the biomolecular interaction:

$$\Delta H(T) = \int_{T_0}^{T} c_{\mathrm{mol}}(T)\,dT \tag{3}$$

3.2.2 Design and Fabrication

The polymeric MEMS DSC device (Figure 3-1) consists of two serpentine microfluidic

sample and reference channels that are identical in shape and dimensions and are surrounded by air-gaps to enhance thermal isolation. Polyimide is used as the device substrate because of its excellent mechanical properties (Young's modulus >2 GPa) and thermal stability (glass transition temperature >673 K). 200 thin-film Sb–Bi thermopile junctions is situated on the polymer substrate, each having their hot and cold junctions located under the sample or reference channels, respectively. Sb and Bi are chosen as thermopile material for their high thermoelectric transduction performance and ease of fabrication. A thin-film resistive temperature sensor, which also functions as a microheater as needed for device characterization

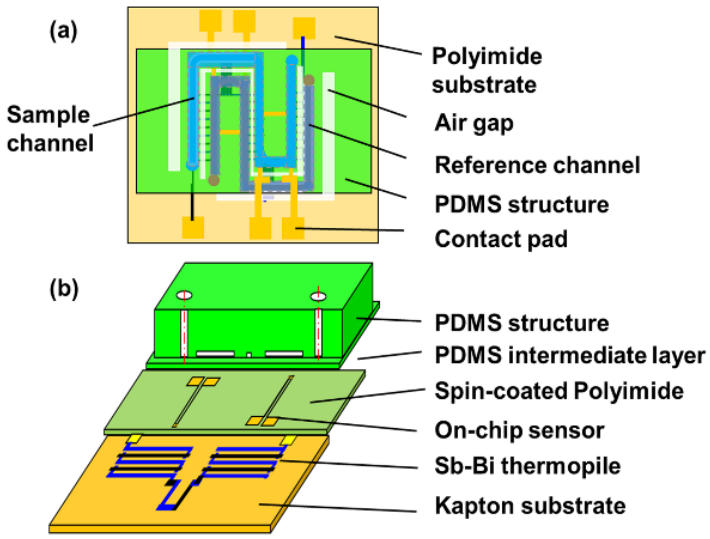

Figure 3-1. Schematic of polymer MEMS DSC device: (a) top and (b) isometric.

purposes, is integrated with each of the sample or reference channels, located on the substrate centrally underneath the region defined by the envelope of the channels (Figure 3-2).

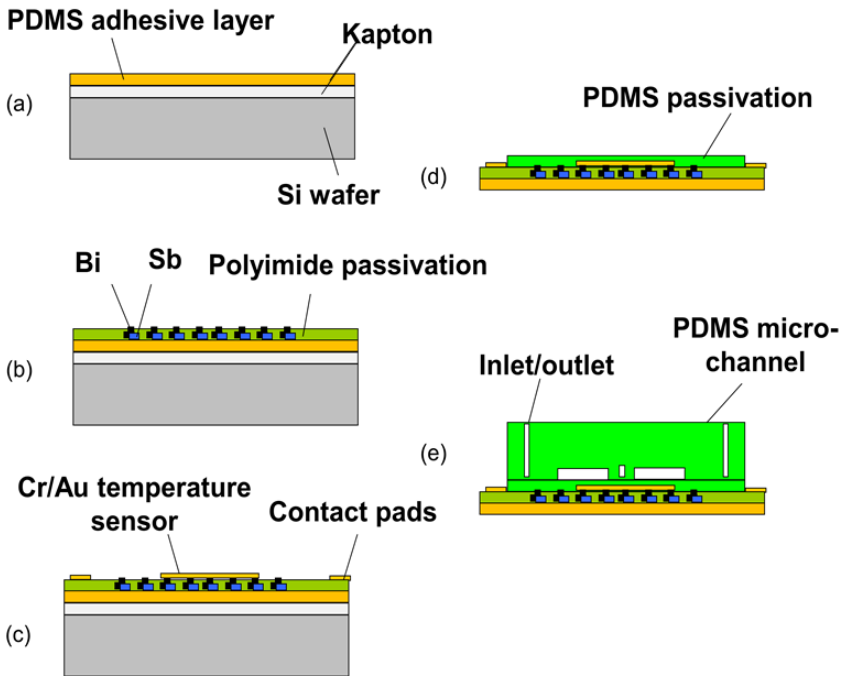

Figure 3-2. Fabrication process of the polymer MEMS DSC device. (a) Reversible bonding of Kapton film to carrier wafer. (b) Fabrication and passivation of Sb-Bi thermopile. (c) Fabrication of temperature sensor (Cr-Au). (d) Mechanical release of Kapton film from carrier wafer.

A polyimide film purchased from DuPont™ (Kapton® 50HN,12.5 μm thick) was used as the substrate, which was initially bonded to a carrier silicon wafer via reversible adhesion provided by a spin coated poly(dimethylsiloxane) (PDMS) layer (20 μm). Sb and Bi (40 μm wide, 2 mm long, 0.5 and 1 μm thick, respectively) thin-films were thermally evaporated and patterned on the substrate using a lift-off process to form a 200-junction thermopile (Figure 3-3c), and then passivated with a spin coated polyimide layer (1.5 μm). Subsequently, a chromium/gold thin film (5/150 nm) was deposited and patterned to define the on-chip temperature sensors and heaters (nominal resistance of 55 Ω), which were passivated with a layer of polyimide-PDMS blend (5% PDMS, 79% polyimide and 16% N-methyl-2-pyrrolidone (NMP) by weight) approximately 2 μm in thickness. This blend also served as a adhesion layer of the PDMS microfluidic structure [84]. The processed Kapton® sheet was mechanically released from the carrier silicon wafer using tweezers (Figure 3-3a).

In parallel, serpentine microfluidic channels (width: 200 μm, height: 200 μm, and length: 25 mm; volume:1 μL) were fabricated of PDMS via soft lithography. The Kapton® sheet was then bonded to the PDMS sheet following oxygen plasma treatment of the contacting surfaces (100 W for 7 s) to complete the fabrication process. The device was finally packaged by soldering conducting wires to the contact pads as well as inserting Teflon tubes (Tygon®E-3603) into the inlet and outlet of the microfluidic channels. Epoxy (Gorilla® Epoxy) was used to secure the solder to the contact pads and the Teflon tubes to the inlet and outlet (Figure 3-3b).

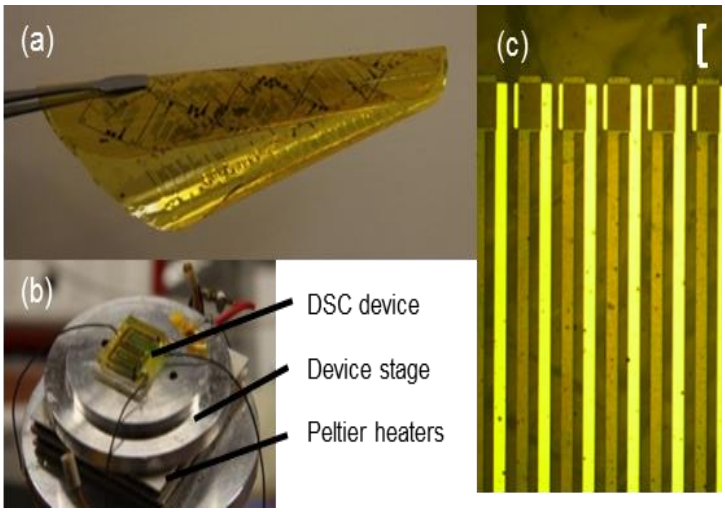

Figure 3-3. Device overlook and thermopile junctions' structure: (a) wafer-level polymer MEMS DSC after peeling off from the silicon wafer (b) polymer MEMS DSC device (c)thermopile junctions, white scale bar indicates a length of 50 μm.

3.3 Experimental Methods

3.3.1 Materials

Lysozyme, used as the targeted sample biomolecule, was purchased from Sigma Aldrich (lyophilized powder, protein ≥90 %) and dissolved in 0.1-M glycine-HCL buffer (pH 2.5). The sample solutions and buffer were degassed overnight in a vacuum chamber built in-house, metered with Micropipettes, and introduced by a syringe pump (New Era Pump

Systems, Inc., NE-1000) before the DSC measurements.

3.3.2 Experimental Setup and Procedure

The experimental setup is shown in Figure 3-4a. The packaged polymeric MEMS DSC device (Figure 3-4b) was placed in a custom-built thermal enclosure consisting of a metal enclosure cap surrounding an aluminum stage on which the device was placed (Figure 3-3b). The thermal enclosure offers additional thermal isolation of the DSC devices from ambient, and ensuring the sample solutions are kept at a constant temperature during measurements as well as minimizing environmental noises. Multiple Peltier devices (Melcor UT15-12-40-F2) were located underneath the aluminum stage to impart heat to or remove heat from the device while the temperature was scanned (i.e., varied at a constant, prespecified rate) with a temperature controller (Lakeshore Model 311). on-chip temperature sensors, calibrated before use, were measured by a digital multimeter (Agilent 34410A), and provided in situ temperature monitoring of the biomolecular samples. The thermopile voltage was measured by a nano-voltmeter (Agilent 34420A). The digital multimeter and nano-voltmeter were connected to a computer such that experimental data collection was automated with LabVIEW (National Instruments, Austin, TX).

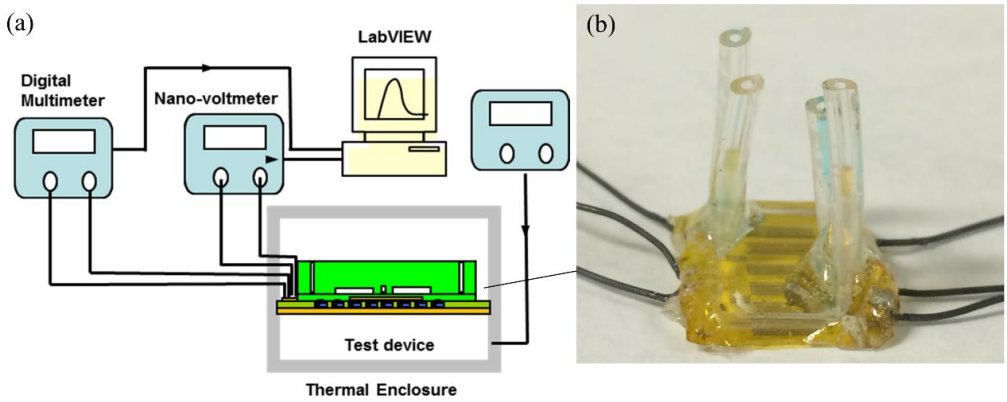

Figure 3-4. (a) Polymer MEMS DSC device test set-up. (b) Image of a packaged device (epoxy was used to secure the electrical connection and the tubing).

The polymeric MEMS DSC device was calibrated using liquids to determine its responsivity, using the procedure described by Cerdeirina et al. [85] The device was first placed inside the thermal enclosure and the temperature of the device was scanned with both of the calorimetric channels empty (298–343 K). The device was then scanned in the same temperature range (298–343 K) with the sample channel filled with water, while the reference channel remained empty. Finally, the device was scanned again with glycerol filling the sample channel and water filling the reference channel. After calibration, the device was thoroughly washed with buffer and deionized water.

3.4 Results and Discussion

3.4.1 Heat Transfer Simulation

We have conducted numerical analysis of heat transfer in the polymeric MEMS DSC device to assess the temperature uniformity and verify the responsivity of the device. Using COMSOL Multiphysics® (Burlington, MA), the three-dimensional model which includes water filled polymeric microstructures, thermopile junctions, Kapton® substrate, passivation layers and the polyimide-PDMS blend adhesive layer in between, accounts for the heat conduction inside the device and convection from the device's outer surfaces to the ambient. The model assumes steady state transfer at each temperature during the temperature ramping process, which occurs at a low rate (5 K/min).

Natural convection inside the microchannels is neglected in the simulation. Natural convection in the water can be characterized by the Rayleigh number [89], $Ra_H = \frac{g\beta\Delta T_{\max} H^3}{\alpha\nu}$ where H is the height of the channels, α thermal diffusivity, β the coefficient of volumetric thermal expansion, ν kinematic viscosity of water, g the gravitational acceleration, and ΔT_{max}

the maximum temperature difference between ambient and device layer of interest. For the condition where a constant temperature boundary condition is applied, natural convection can be considered negligible if $Ra_H \leq 1708$ [86]. For the geometry and operating conditions (ΔTmax up to 70 K) of the device, it is estimated that $Ra_H \sim$ 1.6E-06. It follows that the neglect of the natural convection in the channels is justified.

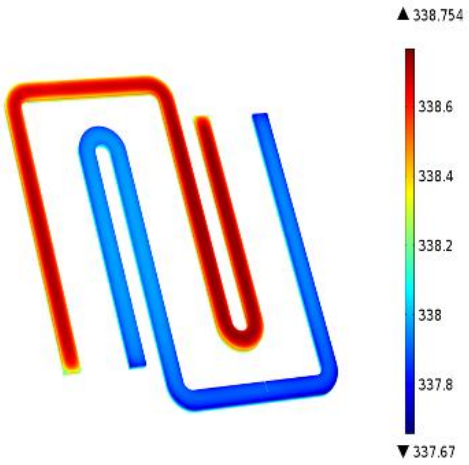

Figure 3-5. Temperature distribution in the device when the substrate was at a Prescribed uniform temperature of 338 k. (estimated heat transfer coefficient: h = 11.57 w/(m^2.k). Normal thermal conductivity: k = 24.4, 7.97, 0.12, 0.15, and 0.13 w/(m.k), for antimony, bismuth, Kapton, PDMS, Polyimide-PDMS blend, respectively).

The model uses the following boundary conditions. Neglecting the thermal contact resistance at the interface of the substrate and the underlying Peltier heater, temperature at the back side of the Kapton substrate is taken to be that of the heater surface. The convection coefficient *h*, representing the natural convection from the outer surfaces of the device to the ambient, is obtained using a correlation in the Nusselt number, which is defined by $Nu = hL/k$ and represents the relative significance of convection to conduction. Here, *k* is the thermal conductivity of the air, *L* the characteristic length (height of the PDMS). For natural convection above a flat isothermal plate, the Nusselt number is given by the correlation $Nu = 0.59 * Ra_{\text{air}}^{0.25}$ [87], where Ra_{air} is the Rayleigh number for air. Finally, a power generation

of 3 mW is applied to the entire sample channel to represent the biological heat generation during the experiments. The thermal conductivity, specific heat capacities and mass densities of the fluids are temperature dependent and are accounted for in the COMSOL simulations.

The temperature distribution within the microfluidic channels is shown in Figure 3-5. It can be seen that the maximum temperature difference between the sample and reference channels is approximately 1.1 K when the substrate temperature was prescribed to 338 K (close to T_m of lysozyme), indicating the excellent thermal insulation of the polymeric DSC device. Also, to estimate the device responsivity, the average temperature difference across the hot and cold thermopile junctions was obtained first from simulation results (0.59 K). Given the 3 mW power generation, the thermal resistance was calculated to be 197 K/W. Using a constant Seebeck coefficient of 122 μV/K (the thermopile voltage per unit temperature difference between its hot and cold junctions), the device responsivity was then calculated to be 4.07 mV/mW. The thermal resistance of the device has been found to differ by no more than 5 % at different substrate temperatures ranging from 298 to 368 K.

3.4.2 Device Calibration

The polymeric DSC device was calibrated to determine its responsivity. The temperature of a device with both channels empty was first scanned, in the range of 298-343 K and the thermopile voltage was used as a calibration baseline and was subtracted from the subsequent calibration scan output to account for errors such as the effect of calorimetric channels volume mismatches. Next, the temperature of the device was scanned at 3 K/min with the sample channel and reference channel filled with water and air, respectively. Known values of material properties (heat capacity, specific volume and molecular weight) of air, water [88,

89], and Eq. (1), the device responsivity was determined to be K = 4.78 mV/mW, which is consistent with the numerically obtained value of 4.07 mV/mW, with the deviation attributable to variations in sensor geometries and material properties that are commonly process-dependent. This responsivity is related to the Seebeck coefficient (S) and the thermal resistance (R), or the temperature difference between the sample and reference channels produced by unit differential power, by $K = SR$. The Seebeck coefficient of antimony bismuth thermopile junctions have been found to be a constant (122 μV/K) in a temperature range of 298-343 K, and thermal resistance of the device, as shown in our simulation above, does not vary significantly with temperature. Thus, the responsivity of the device was approximately constant, and the device was considered to operate linearly within this temperature range.

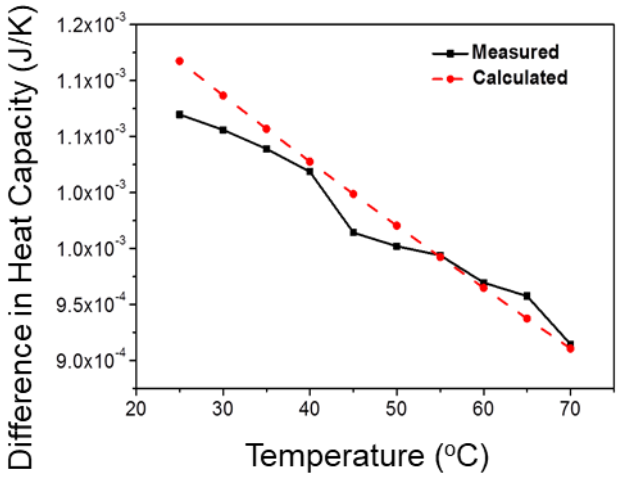

Figure 3-6. Comparison of measured (baseline-subtracted) and calculated differences in heat capacity between water and glycerol.

Finally, the validity of the polymer MEMS DSC device was verified by comparing the experimentally determined and calculated difference in heat capacity of water and glycerol. The temperature of the device was again scanned in the same temperature range after one chamber of the device was filled with glycerol and the other was filled with water. Knowing the device responsivity, the difference in heat capacity between the two fluids during the

temperature scan can be experimentally determined using Eq. (1). This difference in heat capacity as a function of temperature was found to agree with calculation using data reported in the literature (Figure 3-6) [15]. This confirmed that the experimentally determined device responsivity was valid.

3.4.3 Measurement Characteristics

We investigated the device characteristics that are important to DSC measurements, including the baseline stability, measurement noise and thermal time response. The baseline in the device output, i.e., the thermopile voltage in the absence of a differential power input in the temperature range of interest, was measured with both of the calorimetric channels filled with buffer solution. To test the stability of this baseline, the sample and reference calorimetric channels were both filled with Glycine-HCL buffer (0.1 M, pH 2.5) while the temperature of the device was scanned at a constant rate of 5 K/min. After the scan was completed, the device was allowed to cool to room temperature and a subsequent experiment under identical conditions was performed to test the stability of the baseline. As shown in Figure 3-7, there was minimal fluctuation between the two baselines. It is also observed that a non-zero slope appeared at elevated temperatures, possibly as a result of the volumetric mismatch between the reference and sample channels. Also, it was important to note that baseline scan 2 generated much more thermal noise. This could possibly be explained by the acidic HCL based buffer, which was known to be able to etch Bi slowly.

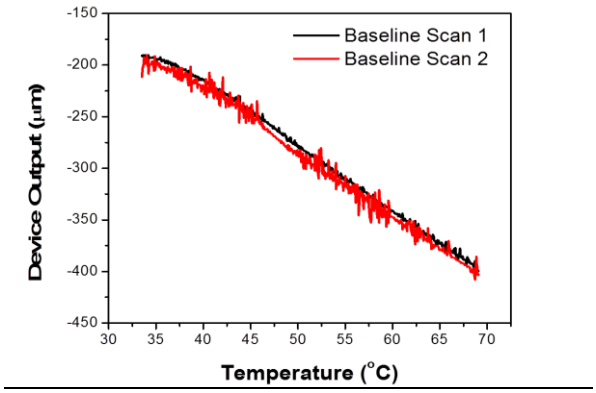

Figure 3-7. Baseline measurements of glycine-HCL buffer (pH 2.5) (temperature scan rate: 5 K/min).

Noise in the output from the DSC measurement systems was observed to be on the level of 100 nV. Using the device responsivity described above, noise levels in the measurement of the differential power between the sample and reference chambers were determined to be 21 nW.

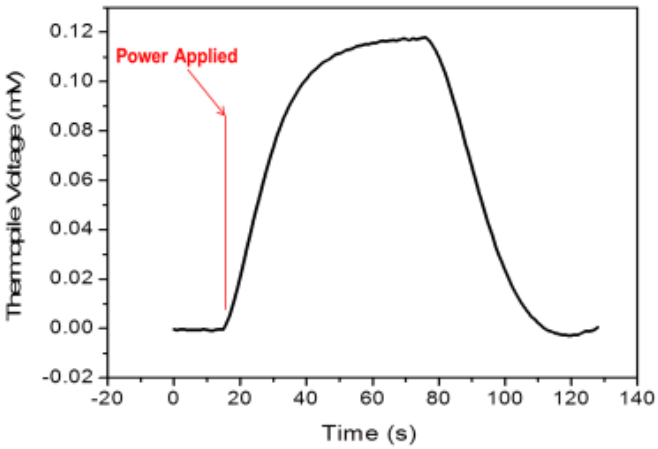

Figure 3-8. Polymer MEMS DSC time responses to a differential power of 150 μW.

To characterize the thermal time response of the MEMS DSC device, a differential power of 150 μW was initially applied to the center region of the sample channel using a microheater. The corresponding thermopile voltage was found to exponentially grow with time upon the application of the differential power (Figure 3-8). After the device output reached steady state, the differential power was removed and the sample channel was then allowed to return to room temperature. Correspondingly, the thermopile voltage decreased to the value before the differential power was applied. Assuming that the time dependence of the

thermopile voltage can be represented by a first-order exponential function, the time constant was determined to be approximately 2.6 s for both the application and removal of the differential power. Thus, the device is considered appropriate for characterizing biomolecular interactions and reactions with kinetics that are sufficiently slow compared with this thermal response time.

3.4.4 Measurement of Protein Unfolding

The calibrated polymeric MEMS DSC device was then used to characterize unfolding of the protein lysozyme. The sample channel was introduced with lysozyme in 0.1 M Glycine-HCL buffer (pH 2.5) while the reference channel remained filled with buffer. The characterization of the unfolding of lysozyme was carried out under identical experimental conditions used in the baseline determination (Section 4.3) that preceded the DSC measurements. The thermopile voltage as a function of temperature, corrected by baseline subtraction, was measured at varying concentrations within a temperature range of 298-348 K (Figure 3-9). The thermopile voltage exhibited a valley in a narrow temperature range of 323-333 K at all lysozyme concentrations, which is consistent with the endothermic thermodynamic

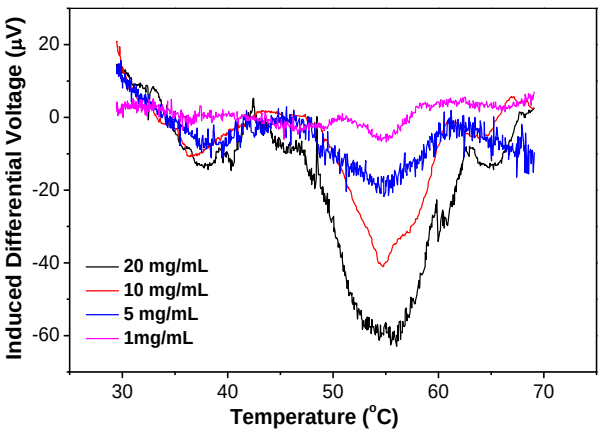

Figure 3-9. Baseline-subtracted differential voltage as a function of temperature for lysozyme unfolding at different concentrations.

nature of a protein unfolding process. Furthermore, ΔC_p of lysozyme and buffer as a function of temperature was calculated from the thermopile voltage by Eq. (1) using the determined device responsivity. The partial heat capacity of the sample as a function of temperature was determined using Eq. (2) and material properties of lysozyme and Glycine-HCL buffer. The partial heat capacity was then used to obtain the thermodynamic properties of lysozyme associated with the conformational transition, such as the molar enthalpy change (ΔH) and melting temperature (T_m, the temperature at which the enthalpy change achieves 50% of ΔH).

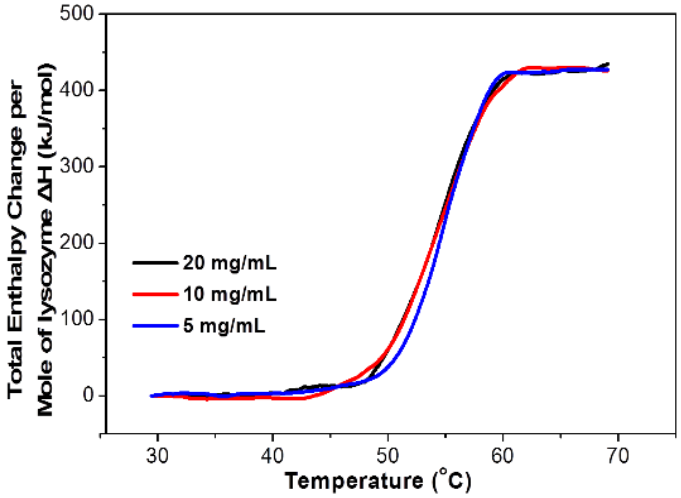

Figure 3-10. Total enthalpy changes per mole of lysozyme during lysozyme unfolding as a function of temperature at different lysozyme concentration.

The molar enthalpy change ΔH and melting temperature T_m were determined using Eq. (3) (carried out numerically) for all lysozyme concentrations but 1 mg/mL, which, while showing a detectable signal from the protein unfolding, was excluded from the quantitative calculations due to the associated low signal-to-noise ratio. As shown in Figure 3-10, ΔH = 419-423 kJ/mol and T_m = 325-327.7 K were obtained consistently at the different protein concentrations. The shape of the enthalpy transition curve of unfolding of lysozyme can be well represented by a two-state model [90], This is consistent with knowledge of proteins. These results agree with the published data (377–439 kJ/mol for the enthalpy change and 328

-331.9 K for the melting temperature), and thus demonstrate the capability of the polymeric MEMS DSC device for highly sensitive detection of biomolecular interactions.

3.5 Conclusioin

This chapter presents a polymeric MEMS device for differential scanning calorimetry (DSC) of biomolecular interactions. The device is based on an inexpensive, commercially available polymer substrate, and consists of a pair of calorimetric microchannels integrated with resistive temperature sensors and heaters as well as an antimony-bismuth (Sb-Bi) thermopile. For DSC measurements, the two channels are filled respectively with a biomolecular sample and a reference solution, whose temperatures, measured *in situ* using the integrated temperature sensors, are varied at a constant rate using closed-loop temperature control. The difference in the thermal power between the sample and reference induces a temperature difference, which is measured using the thermopile for thermodynamic characterization of the biomolecules.

The MEMS DSC device was calibrated using liquids of known heat capacities, allowing the determination of its responsivity (4.78 mV/mW), noise in differential power measurement (21nW) and thermal time constant (2.6 s). The heat transfer behavior in the device was analyzed using finite element simulations, from which the temperature distribution in the sample and reference channels to be uniformly within 1.1 K, and the device responsivity was calculated (4.07 mV/mW) and found in agreement with that determined from calibration experiments. The MEMS device was then applied to the DSC measurement of unfolding of lysozyme, used as a representative protein, in a small sample volume (1 μL) at practically relevant sample concentrations (detectable at 1 mg/mL and quantifiable at 5 mg/mL). The

molar enthalpy change of lysozyme and melting temperature in the lysozyme unfolding process were thus determined to be in the ranges of 419-423 kJ/mol and 325-327.7, respectively, which agree with the reported ranges of 377-439 kJ/mol and 328-331.9 K in the literature.

Chapter 4 Isothermal Titration Calorimetry in A Polymeric Microdevice

In this chapter, the previously developed polymer-based thermoelectric sensor is adopted and used for ITC measurements. ITC is an important biophysical characterization technique for direct thermodynamic characterization of biomolecular reactions, is currently limited by expensive and complicated instrumentation as well as low throughput. Aiming to address this limitation, this chapter present a polymer-based microdevice for quantitative ITC measurements. This microdevice integrates a microfluidic reactor that features efficient passive chaotic mixing as well as thermally isolated, well-defined reaction-reference chambers on a robust polymer-based thermoelectric sensing chip. The microdevice allows biomolecules to mix thoroughly, react with minimal fluid evaporation, real-time monitoring and controlling of the device temperature as well as sensitive differential thermoelectric sensing. During operation, sample and reference solutions are introduced to their respective measurement chambers and the difference in the thermal power from the reaction is measured and used to characterize the complete binding parameters associated with the biomolecular interactions. The utility of the ITC microdevice is demonstrated with ITC measurement of a model reaction system, in which barium chloride ($BaCl_2$) is titrated into 18-Crown-6 (18-C-6) in a 0.85 μL reaction volume. The measurement data were used to calculate the binding parameters of the biochemical reaction, which were found to agree with published results.

4.1 Introduction

Isothermal titration calorimetry (ITC) measures heat either released or absorbed when a ligand solution is titrated or added into a receptor solution of interest under isothermal conditions [93]. ITC is known to be the only technique that can simultaneously determine all reaction associated binding parameters in a single experiment, and is label-free and

solution-based, requiring no molecular labeling or surface immobilization [94]. While widely used in basic biochemical studies, as well as practical applications such as drug discovery and biotherapeutics development, conventional ITC instruments are limited by high cost, complicated design and construction, low throughput, and slow response time.

Microelectromechanical systems (MEMS) technology can enable the integration of ITC measurements on a single chip. However, MEMS devices that offer ITC capabilities do not yet allow proper control of reaction conditions for thermodynamic characterization of biomolecular reaction systems. In particular, flow-through based MEMS calorimetric devices have limited sensitivity due to poor thermal isolation [95]. In addition, devices that use droplet-based reactions generally do not allow for well-defined reaction volumes and are further complicated by evaporation-induced noise and volume change [96-98]. Hence, such devices are not well suited to quantitative measurement of thermodynamic reaction parameters.

To address these issues, our research group previously reported a closed chamber-based MEMS ITC device that featured free-standing microfabricated differential calorimetric sensors, well-defined reaction volumes, and integrated micromixing capabilities [99]. The silicon-based device showed potential for quantitative thermodynamic characterization, although several limitations were observed. First, the high thermal conductivity of silicon necessitated the use of complex, and fragile freestanding structures [100] to enhance device thermal isolation. This reduced yield, caused significant reliability issues during the device's ITC operation and maintenance (e.g., cleaning) and made the device rather expensive to use. Second, the device also neglected the residue fluid flow effects and used a relatively high Reynolds number flow (~23) in the mixing channel. This resulted in significant noise that led to a relatively high limit of detection (650 nW). Hence, ITC measurements required a relatively high receptor concentration (5 mM for 18-C-6), which was not yet adequate for

practical applications.

In this chapter, we aim to address the limitations of existing MEMS ITC devices with polymeric MEMS-based quantitative measurements. The polymer-based ITC device design eliminates the use of silicon, and exploits the low thermal conductivity of the polymer substrate to achieve thermal isolation of reaction samples in the absence of any complex or fragile freestanding structures. The use of inexpensive polymers and the elimination of the freestanding structures simplify the fabrication process, increase the fabrication yield, reduce the device cost, and improve the device reliability. In addition, the closed volume-based MEMS ITC approach, as initially demonstrated by the silicon-based device without further analysis, was systematically characterized in the present work to identify factors such as volume mismatch, reaction volume information, evaporation of reactants, and thermal activity in the mixing and transport of reactants before they enter the calorimetric chamber that influence the sensitivity and accuracy of ITC measurements. These insights are used to generate a polymer-based MEMS ITC design for more sensitive and reliable ITC measurements. The potential utility of the device is demonstrated with quantitative ITC measurements of a model reaction system in which the ligand BaCl2 is titrated into the receptor 18-C-6 at a concentration of 2 mM.

4.2 Principle and Design

In an ITC experiment for the characterization of a ligand-receptor system, the ligand with known concentration and volume is titrated or added into a known concentration of a receptor solution. From measurements during the titrations, the reaction heat is obtained as a function of the ligand concentration. For example, consider a biochemical binding system in which a receptor (M) and a ligand (X) bind in equilibrium and form the complex $M_\alpha X_\beta$:

$$aM + \beta X \Leftrightarrow M_\alpha X_\beta \quad (1)$$

where α, β are the stoichiometric coefficients of the receptor and of the ligand, respectively. The binding parameters of the system, which include the molar enthalpy change of binding (ΔH), the reaction stoichiometry ($N = \beta/\alpha$), as well as the reaction binding constant K_b can thus be determined using the following binding equation, in which biological reaction heat Q is be expressed as [101]:

$$Q = \frac{NM_t \Delta H V_0}{2}\left[1 + \frac{r}{N} + \frac{1}{NK_b M_t} - \sqrt{(1 + \frac{r}{N} + \frac{1}{NK_b M_t})^2 - \frac{4r}{N}}\right] \qquad (2)$$

and is a function of the ligand-receptor concentration ratio for each titration (r). In the equation, M_t is the total concentration of the receptor (both free and bound) in the reaction volume V_0, and X_t is the total concentration of the titrated ligand. The values of N, K_b, and ΔH are then determined by fitting to Eq. (2) using non-linear least-squares analysis [102].

In our approach to ITC measurements, the reaction heat is determined using a differential scheme, where the reaction and reference chambers are used for measuring heat in the presence (ligand-receptor system) and absence of the receptor (ligand-buffer system), respectively. Before entering their respective chamber, a series of liquid segments of different concentration of ligand in a constant volume at a controlled temperature are allowed to react with the same volume of the receptor and a pure buffer, respectively. The differential power generated (i.e., the thermal power difference between the reaction and reference chambers), can be represented as $\Delta P = P_s - P_r$, where P_s and P_r are the thermal power in the reaction and reference chambers, respectively. This differential power can be determined by:

$$\Delta P = \frac{\Delta U}{S} \qquad (3)$$

where ΔU is the output of the thermopile and S is the device's responsivity, i.e., the output electrical voltage generated by unit differential thermal power [82]. The total heat released or absorbed Q_{total} in the calorimetric cell on each injection of reagent is determined by integrating the differential power generated over time. The biochemical reaction heat Q is then obtained by subtracting the non-specific heating contributions obtained from the negative control experiment.

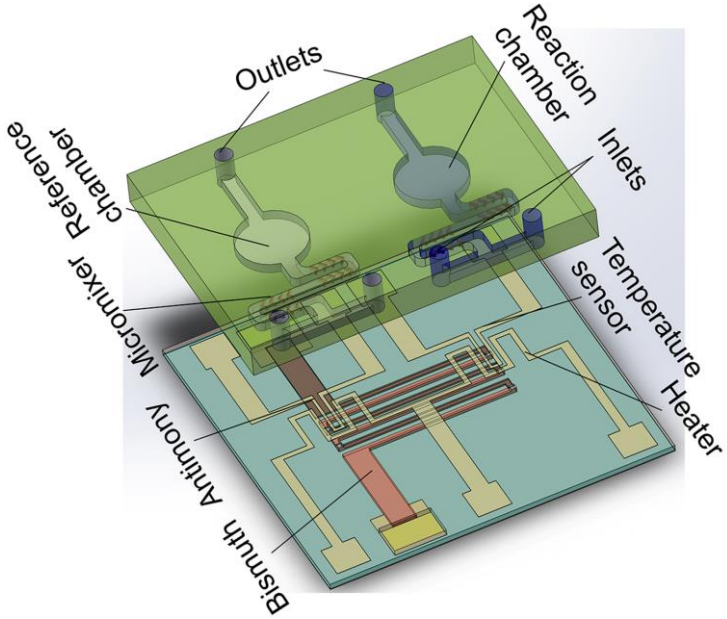

Figure 4-1. The exposed view of the polymeric ITC microdevice. To clearly show the Sb-Bi thermopile, only 5 presentative Sb-Bi thermopile junctions are included in the figure.

Our ITC microdevice (Figure 4-1) consists of two microfluidic chambers that are made from polydimethylsiloxane (PDMS). The chambers contain the binding system and a reference system, respectively. Each of the microchambers is situated on a polymeric substrate and surrounded by air cavities embedded in the sidewalls for effective thermal isolation. The serpentine flow channels connected to the chambers are each integrated with a passive chaotic micro-mixer that uses herringbone-shaped ridges in the ceiling of the channels to generate a chaotic flow pattern that induces mixing of the incoming liquid streams [103]. The length of the flow channels is designed to achieve thorough mixing as

well as to control the reaction time before entering the chamber. An antimony (Sb)-bismuth (Bi) thermopile (60 junctions) is integrated with its hot and cold junctions located beneath the chamber centers. Thin-film resistive micro-temperature sensors and micro-heaters which are used for in-situ monitoring of the chamber temperature, as well as for on-chip device calibration, are integrated, on the substrate beneath the chambers' center.

The microdevice consisted of a polymeric thermal substrate and a microfluidic titration platform. Both components were fabricated individually and bonded together via oxygen plasma at last. The fabrication of the thermal substrate started with reversible bonding of a purchased Kapton film (Kapton®50HN, 12.5 μm thick) to a silicon carrier wafer. Sb and Bi (0.7 and 1.5 μm) as well as chromium/god (7/200 nm) were successfully deposited and patterned successfully, and passivated by a thin polyimide layer (2 μm) to define the thermopile as well as the on-chip temperature heater and sensor. At the same time, the PDMS reagent-handling microfluidic platform was fabricated using soft lithography. It was then bonded to the mechanically released thermal substrate via a layer of polyimide-PDMS mixture.

For microdevice fabrication LOR resists and SU-8 (2000, 2025, and 2075 series) negative photoresist was purchased from Microchem Corp. (Westborough, MA). Polydimethylsiloxane (PDMS) was obtained from Robert McKeown Company (Somerville, NJ). Polyimide (PI-2610 and PI-2611series) was purchased from HD Microsystem (Parlin, NJ). Antimony and bismuth (99.999% in purity) were purchased from Kurt J. Lesker Company (Pittsburgh, PA), and silicon wafers were purchased from Silicon Quest International, Inc. (San Jose, CA). For testing the ITC microdevice, 18-Crown-6 (18-C-6, molecular weight: 264.32 Da,≥ 99.0%

in purity) and barium chloride (BaCl2, molecular weight: 208.23 Da, ≥ 99.999% in purity) were purchased from Sigma (St. Louis, MO), and were diluted with cell culture grade distilled water (Thermo Fisher Scientific, Grand Island, NY) to obtain desired concentrations of 18-C-6 (2 mM) and $BaCl_2$ (0.5 – 10 mM).

4.3 Experimental Procedure

To perform the ITC experiments using our approach buffer and ligand solutions are first introduced into both the reaction and reference chambers, and the resulted differential voltage measured by the thermopile junctions is recorded and used as a baseline, which also serves as a control for the overall ITC measurements. Next, during the ITC measurement of ligand-receptor binding, a known concentration of receptor and different concentrations of ligand, which are typically in pure form and dissolved in well-conditioned buffer, are mixed in the micromixer, and then enter the sample chamber. Simultaneously, the same concentrations of ligand and the buffer are also introduced, becoming mixed before entering the reference chamber. The differential thermal power between the chambers is determined from heat induced differential voltage measured by the Sb-Bi and is used to compute the biochemical reaction heat *Q* at this particular concentration using Eq. (3).

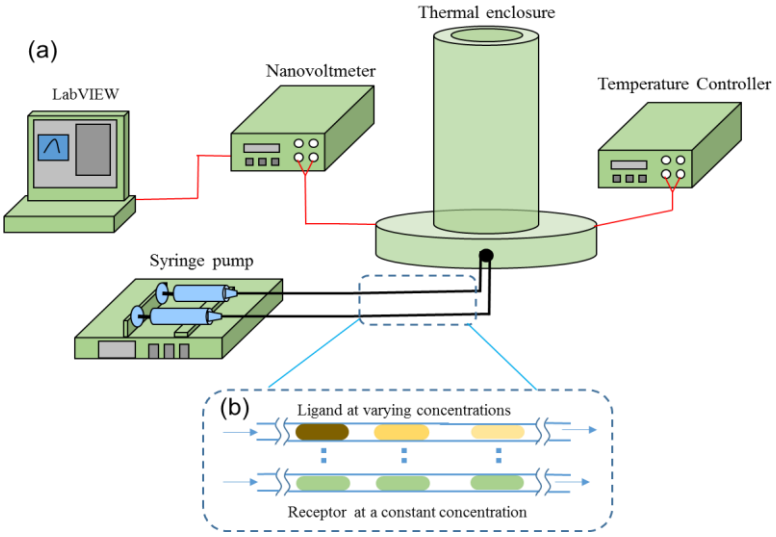

Figure 4-2. Device testing setup (a) thermal enclosure and its connection to measurement instrumentations; (b) microfluidic titration operating principle.

Finally, the titration enabling fluidic delivery was achieved by the following steps. First, air-separated segments of the same concentration of receptor, and different concentrations ligand solutions were each preloaded using a syringe pump into a Teflon access tubing. Titration of the ligand into the receptor (Figure 4-2a, b) was achieved via merging the solutions segments in the micromixer and then delivered into the reaction chamber. The ligand-receptor molar ratio was varied from merging different solutions segments that contain corresponding ligand and receptor concentrations. Similarly, two other identical access tubings were loaded with segments of ligand and buffer solutions, respectively, and were delivered into the reference chamber. Numerical simulations by COMSOL Multiphysics® were used to verify the result of mixing. All access tubings (4 in total) were synchronized by a multiple-injections syringe pump (KD Scientific, KDS 220). Pure buffer solution and sterile water can also be loaded between the reactant segments to clean the chambers.

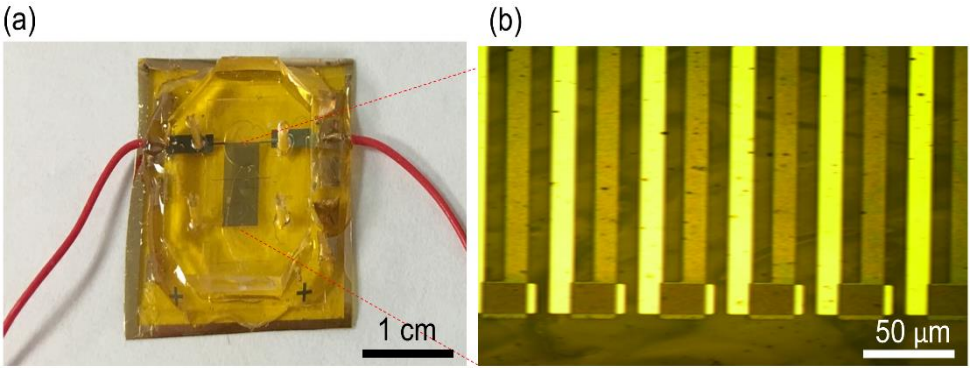

Figure 4-3. (a) The fabricated polymeric ITC microdevice; (b) Sb-Bi thermopile junctions.

4.4 Results and Discussion

The closed chamber-based MEMS ITC approach was systematically characterized in the present work to identify factors such as volume mismatch, reaction volume information, evaporation of reactants, and thermal activity in the mixing and transport of reactants before they enter the calorimetric chamber that influence the sensitivity and accuracy of ITC measurements. First, volume difference between the reaction and reference chambers were experimentally determined, and its effect on the steady state response of the microdevice due to an input thermal power was characterized using numerical simulation. Next, the reaction volume information，the efficiency of the passive chaotic mixers, and the residence time of the reactants in the mixer and connecting channel were also investigated numerically. In addition, the microdevice characteristics including the device responsivity, thermal time response and the device baseline noise, were characterized experimentally. Finally, the fully characterized microdevice (Figure 4-3a, b) was then used in quantitative ITC measurements of $BaCl_2$ reacting with 18-C-6. The ITC microdevice used in the following experiments and simulation model had a 60-junction Sb-Bi thermopile and a reaction and reference chamber with the same radius of 1286 µm and a height of 164, 155 µm, respectively. The center of the chambers was separated by 4.5 mm. The herringbone-shaped ridges integrated micromixers

(width: 200 μm, total length: 15 mm) led the introduced solutions to the measurement chambers while the solutions became well-mixed along the way. The herringbone-shaped ridges were placed on the ceiling of the microchannel, and each of them had a width of 40 μm, a height of 50 μm, a 30 μm separation

4.4.1 Effects of Volume Mismatch

The first potential factor that may affect the sensitivity and accuracy of the microdevice is the volume mismatch between the reaction and reference chambers. To characterize this mismatch, the volume of the SU-8 mold, which was used in soft-lithography to produce the reaction and reference microstructures, was determined to have an average radius of 1287, 1286 μm, and an average chamber thickness of 163, 157 μm with a standard deviation of 5.35, 5.57 μm, respectively. The relatively large thickness standard deviation was expected due to the spinning of highly viscous SU-8 2150 solution, which after baking, was thicker close to the edge of the wafer. Thus, an average of 5.6% volume difference was obtained for reaction and reference chambers.

Using COMSOL Multiphysics, we simulated two cases of the temperature distribution of the microdevice to characterize the effects of the volumetric difference between the calorimetric chambers. The simulation was performed in the absence of liquid flow, as the calorimetric measurements were performed after the liquid flow had been stopped. Also, any residual effect of the liquid flow was addressed by subtracting the baseline (Figure 4-9) from the titration calorimetric measurement data. The first case considered a three-dimensional model of the ITC microdevice that includeded water filled PDMS reaction and reference microstructures, thermopile junctions, Kapton substrate, passivation layers and the

polyimide-PDMS blend adhesive layer in between. The model accounts for the heat conduction inside the device and convection from the device's outer surfaces to the ambient. The thickness of the reference microfluidic structures was intentionally reduced by 5.6% to account for the volume difference due to fabrication tolerances. In addition, because the binding reagents were homogenous, a thermal power of 1.63 μW (obtained based on empirical 18-C-6 and $BaCl_2$ reaction data) was applied uniformly in the reaction chamber to represent typical 18-C-6 and $BaCl_2$ reaction heat generation. From the simulation, an average thermopile differential temperature of 6.38×10^{-4} K (Figure 4-4a) was obtained. Next, the second case considered the same microdevice model, however, in this case, the reaction and reference microstructures had identical dimensions. When the same power was applied to the reaction chamber, an average thermopile differential temperature of 6.31×10^{-4} K was obtained (Figure 4-4b) between the reaction and reference measurement chambers. Thus, the differential temperature from these two models differed by 1.1%, which was considered insignificant so that the effect of volumetric difference on the steady state device response was negligible.

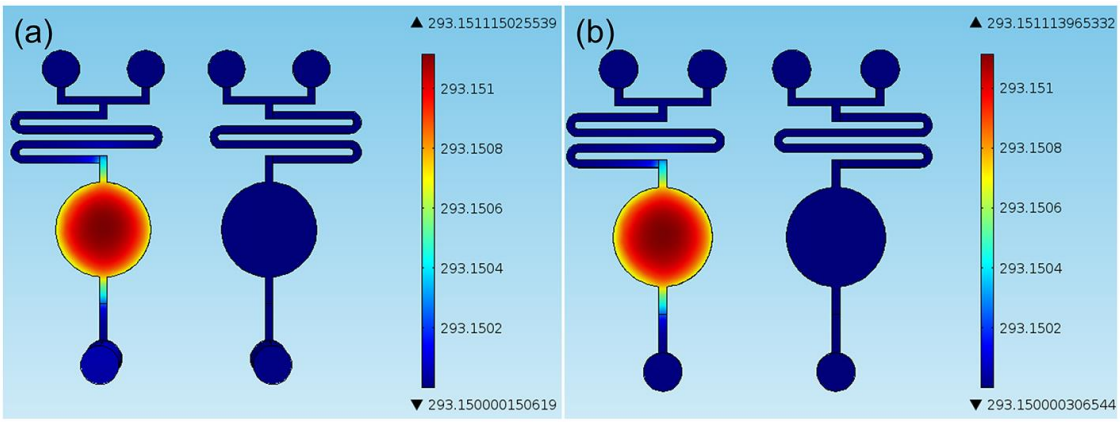

Figure 4-4. Microdevice temperature distribution when a unit power density is applied to the reaction chamber: (a) model with a 5.6 % reaction/reference microfluidic structures volume difference; (b) model with no volume difference.

4.4.2 Determination of the Reaction Volume Information

Another potential source of error in determining the reaction binding parameters was the inaccurate reaction volume information. During ITC measurements, besides the reaction chamber, binding reaction would also have occurred in other microfluidic structures such as the mixing channels, and channel leading into the outlet, contributing to the total heat generation. We used simulation to assess the appropriateness of the reaction chamber volume to be used as the reaction volume in the computation of thermodynamic properties. In the simulation, we first computed the differential temperature when a uniform thermal power was applied to the reaction chamber alone (Figure 4-5a). Then, a uniform thermal power of the same density was applied to the reaction chamber and its associated microfluidic components including the micromixer and the connection channels) to conservative estimate the effects of different choices of the reaction volume (Figure 4-5b). The differential temperature in these two cases differed only by 7%. Thus, it was determined that it was acceptable to use the reaction chamber volume to compute the thermodynamic properties of the reaction system.

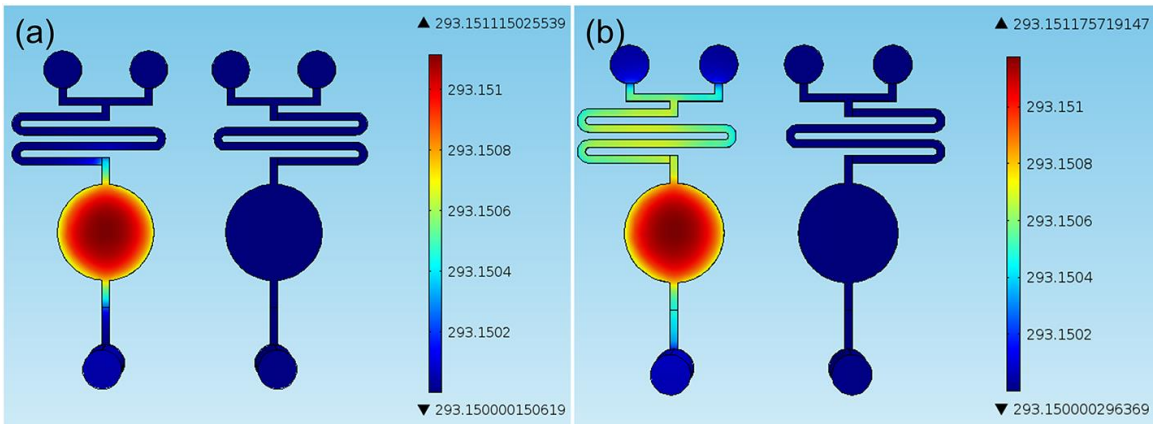

Figure 4-5. The differential temperature between the reaction and reference chambers. (a) A uniform thermal power was applied to the reaction chamber; (b) the uniform thermal power of the same density was applied to chamber and associated microfluidic components.

4.4.3 Characterization of Reagents mixing

Next, to further understand the behavior of the reagents streams passing through the micromixer, and demonstrate the reagents had become fully mixed before entering their perspective measurement chambers, this section presented a numeric simulation of a chaotic micromixer embedded in a serpentine channel that considered the interactions of the fluid flow and the passive chaotic micromixer. The results would yield insight into the design of microchannel dimensions, especially the length of the flow channel. In this model, the flow channels are filled with water, which is treated as an incompressible Newtonian Fluid. Navier-Stokes equation, and the convective-diffusion equation is couple with the flow field to simulate the transport of diluted species. The simulation of the flow channel with and without the chaotic mixer is carried out in the same condition. At the inlet, half of the inlet cross-sectional area is given the solute concentration of 0 mol/m^3; the other half is given the solute concentration of 1 mol/m^3, and the flow rate at the inlet is set to be 50 μL/min for the fluid stream. The density, dynamic viscosity of water is set to be 997 kg/m^3, 100 cP, respectively, and the diffusion coefficient of the solute is set to be 1.0×10^{-11} m^2/s. Additionally, the mixing efficiency at the outlet of the passive-chaotic mixer incorporated channel was determined and compared with the mixing efficiency of a bare PDMS channel. As a result, the distribution of the solute concentration in the channel was shown in Figure 4-6a, b. For the mixer-embedded channel, as the fluid stream flowing through the channel, the solute concentration gradient prescribed by the initial condition gradually decreases, which was evident by the disappearance of the concentration interface at the end of the channel. On the contrary, for the same channel length, a still rather large concentration gradient existed at the outlet of the bare PDMS channel. The solute concentration distribution at the outlet of both channels (Figure 4-6c, d) was used to quantify the mixing uniformity. Calculating using the standard definition [104], a mixing uniformity of 92% and 73% is

obtained for the flow channels of 15 mm in length with and without the chaotic mixer, respectively. In addition, the mixing time was defined as the time required for the reagents to achieve a 90% mixing efficiency, therefore, using a combined flowrate of 50 µL/min, it would take 570 ms for reagents to travel from the beginning to the end of the micromixer. The device was then considered suitable to characterize the thermodynamic binding parameters of a reaction that have a time scale sufficiently slower than the mixing time to avoid heat loss in the micromixer.

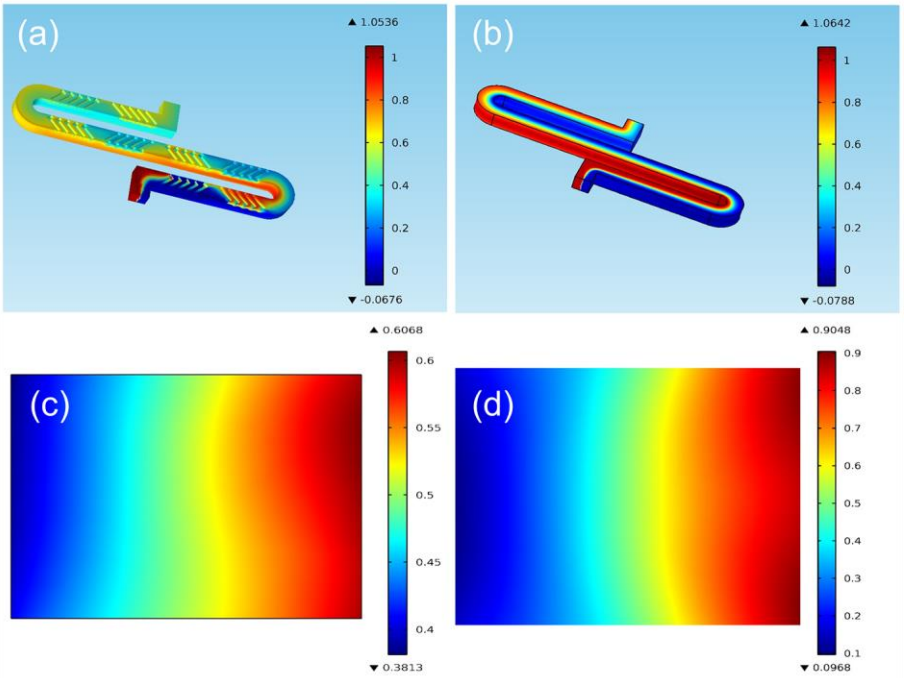

Figure 4-6. The mixing effectiveness of (a) a chaotic mixer integrated channel vs. (b) a straight channel; (c) solute concentration gradient at the outlet of the chaotic mixer integrated channel; (d) solute concentration gradient at the outlet of the straight channel. The simulations presented here were performed in a separate serpentine mixing channels as the mixing was not affected by the rest of the microdevice.

4.4.4 ITC Microdevice Characterization

We next investigated a set of device characteristics that are important to quantitative ITC measurements, including the reagent loss rate through permeation, device responsivity, thermal time response, and stability of the baseline. First, as we employed a closed-chamber

design (compared to the open-volume design of the droplet-based calorimeters), any evaporative reagent loss would occur only through the PDMS walls. Using available empirical data on water permeation through PDMS [105], the reagent loss rate was estimated to be approximately 2% of the reagent volume per hour [106]. Since the entire ITC experiment was completed within 30 min, the reagent loss in our ITC microdevice was negligibly small. Next, the responsivity *S* of each microdevice was calculated by a device steady-state calibration experiment. Driving by the DC voltage source, the on-chip microheater was used to generate a known, constant differential thermal power in one of the two chambers, and the differential voltage measured from the thermopile output was recorded. The device responsivity was then determined by Eq. (3). This same device responsivity was later used in ITC experiments to convert reaction heat induced differential voltage to the differential power. At 298 K, the steady-state response of the ITC device was found to depend on the differential power in a highly linear manner, yielding an approximately constant responsivity of S = 3.7 mV/mW (Figure 4-7) which was sufficient for measuring the heat evolved in our model reaction. We also characterized the device's responsivity at controlled ambient temperatures provided by the thermal enclosure from 20 to 45 °C and found that it remained constant with a relative standard deviation of less than 3%. Therefore, the temperature dependence of the device responsivity could thus be ignored.

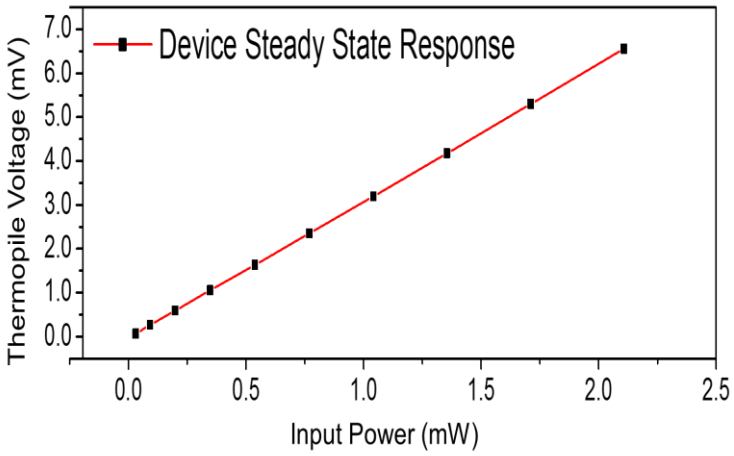

Figure 4-7. Steady state response of the polymer ITC microdevice.

Next, we employed the method that was first described by Mayorga et al [107] to characterize the thermal time response of the ITC microdevice. Specifically, the on-chip heater was used to generate a rectangular electrical calibration pulse (2 mW) to the reaction chamber. The corresponding thermopile voltage was observed to exponentially grow with time upon the application of the differential power. After the device output reached steady state, the differential power was removed and the sample chamber was then allowed to return to room temperature. Correspondingly, the thermopile voltage decreased to the value before the differential power was applied. The decay portion of the instrument response was then fitted to a multiple exponential decay function to determine the time response. However, for our microcalorimeter, the time response could be satisfactorily described by a single exponential function. A device time response of 2.6 s was then determined (Figure 4-8). It was considered appropriate for characterizing biomolecular reaction systems with kinetics that were sufficiently slow compared with this thermal response time.

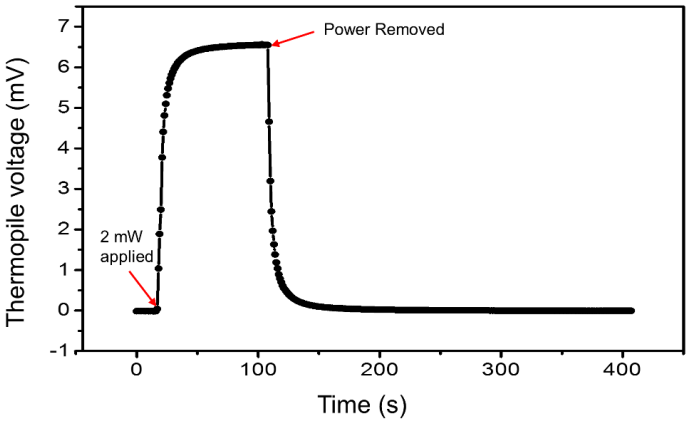

Figure 4-8. Thermodynamic time response of the polymer ITC microdevice.

Finally, the overall baseline of the measurement that also served as the negative control of the ITC experiment was measured by introducing sterile water and 0.4-5 mM $BaCl_2$ to both the reaction chamber and reference chamber simultaneously. To test the stability of this baseline, 5 sequential injections of the reagents were administered, each with a 2-minute interval, and at a combined rate of 50 µL/min. All 5 measurements showed a flow residual non-reaction-specific peaks that were subtracted from the analysis. The baseline noise (~200 nW) also represented the detection limit of our ITC microdevice, which was considered typically adequate for measuring the thermal power generated in biomolecular reaction systems. To compare the baseline noise with the reaction heat induced differential thermal power, 0.8 mM $BaCl_2$ and 2 mM 18-C-6 (each 0.4 µL)was mixed and introduced at the rate of 50 µL/min to the reaction chamber while the reference chamber was introduced with 0.8 mM $BaCl_2$ and water. Contrary to the baseline, the ITC microdevice exhibited a reaction-specific spike attributable to the exothermic nature of the binding between 18-C-6 and $BaCl_2$ (Figure 4-9).

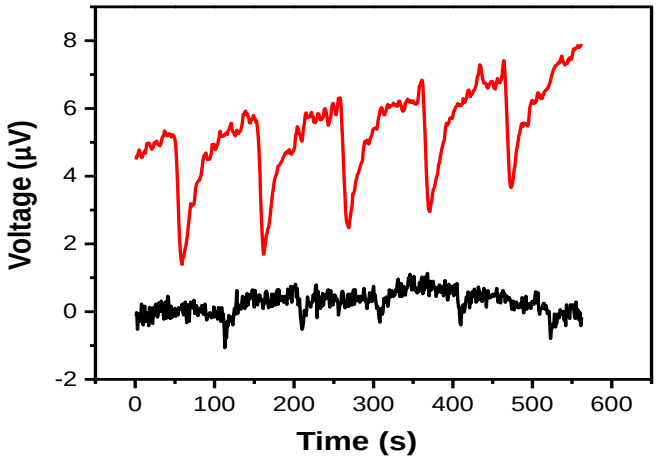

Figure 4-9. Repeatable device output upon introduction of 2 mM 18-C-6 and 2 mM BaCl2 compared with water baseline (baseline is intentionally shifted down).

As a result, a repeatable signal-to-noise ratio of ~5 (appropriate for titration measurements) was observed. Furthermore, it was important to note that the effects of thermal activity in the mixer and the connecting channel from the mixer to the calorimetric measurement chamber (Figure 4-1) were determined by the residence time of the reactants in the mixer and connecting channel (referred to as the mixing and transport time) as compared to the reaction time, i.e., the scale due to reaction kinetics. In our measurements, the mixing and transport time (0.57 sec, estimated based on the combined ligand and receptor carrier flow rate) was short compared to the reaction time (~10 sec, estimated based on consideration of reaction kinetics [108]) for the system of 18-C-6 and $BaCl_2$. Hence, reaction and the associated thermal activity in the mixer and connecting channel can be neglected, and the thermal power measured by the thermopile can be accurately considered to be originated from the reaction of fully mixed reactants in the calorimetric chamber. For other reaction systems with reaction times dominated by the mixing and transport time, the thermal power due to reaction in the mixer and connecting channel cannot be neglected. Fortunately, as this thermal power is rapidly swept into the calorimetric chamber by the imposed fluid flow,

measurements in the calorimetric chamber can still achieve adequate accuracy. For a conservative estimate, we considered the transport of a thermal power uniformly distributed in the channel. Based on convective heat transfer simulation in the mixer and connecting channel using the same flow rate (total of 50 μL/min), it was estimated that approximately 10% of this thermal power would be lost through the walls of the mixer and connecting channel before entering the calorimetric chamber. Thus, the measurement error can still be considered adequately small. More accurate measurements can be achieved by an improved microfluidic design. In particular, the reactants can be mixed and then allow to react in the same location (i.e., by merging the mixer and the calorimetric chamber) to eliminate the unmeasured reaction thermal power, and such a design is being investigated in our ongoing work.

4.4.5 ITC Measurements

The fully characterized microdevice was then used to perform ITC measurements of the titrated reaction of $BaCl_2$ with 18-C-6 to demonstrate its potential for thermodynamic characterization of the biomolecular reaction systems. At the controlled temperature of 298 K, titration reaction used a fixed receptor concentration of 18-C-6 (2 mM) and a series of different ligand concentrations of $BaCl_2$ (in the range of 0.4–5 mM), allowing the molar ratio of $BaCl_2$ to 18-C-6 to be varied from 0.2 to 2.5. Measurement of reaction at each molar ratio occurred in a duration of approximately 4 min (2 min test duration, with 2-minute injection interval) with the entire ITC measurement completed within approximately 28 min. The baseline-subtracted device output (Figure 4-10) exhibited spikes consistent with the titration reactions. Each spike in the device output corresponded to each titration, with a magnitude increasing consistently with titration number. However, no device output increase was

observed between the molar ratio of 2 and 2.5, indicating excessive ligand ($BaCl_2$) concentration at a molar ratio of 2.5 and the reaction was most likely saturated at a molar ratio of 2. This was expected for the reaction system.

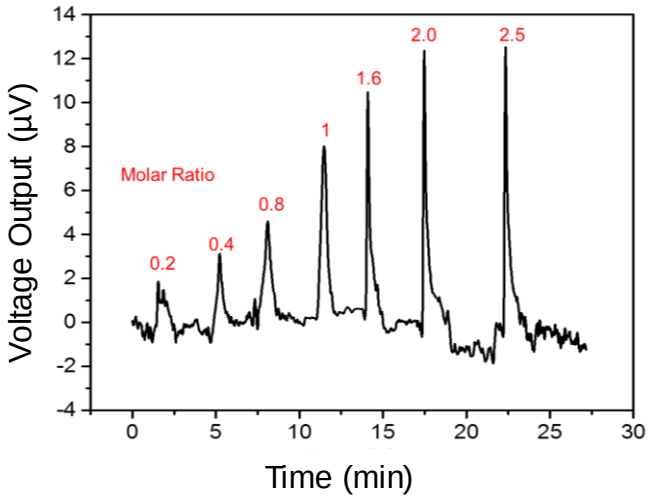

Figure 4-10. Device output of the binding of 2 mM 18-C-6 and BaCl2 at different molar ratios (indicated above each peak) at 298 K.

The Eq. (3) was then used to calculate the differential thermal power that was induced by the titration reaction. The reaction heat at each molar ratio was then determined by integrating the thermal power over the entire period of reaction. A thermodynamic binding isotherm (Figure 4-11) was obtained by plotting the reaction heat as a function of the molar ratio [109]. It could be seen that the reaction heat increased monotonically with the molar ratio until approaching saturation (molar ratio of 2) reflecting that the most binding sites of 18-C-6 were occupied with the addition of $BaCl_2$ until the binding sites were no longer available and excessive $BaCl_2$ became free ligand in solution.

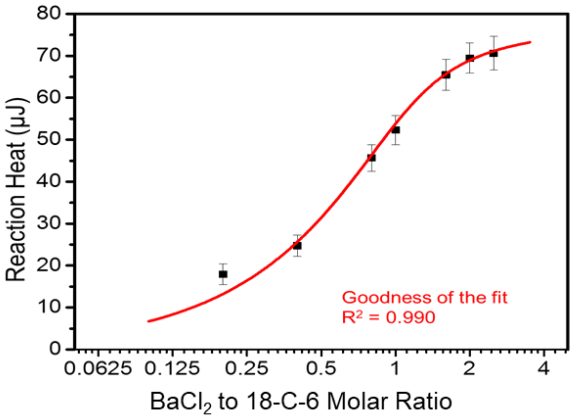

Figure 4-11. Calculated the biochemical heat of 18-C-6 reacting with BaCl2 at different molar ratios, and fitted curve to one binding-site model. Error bars representing the standard deviation calculated from at least three repeated measurements at each molar ratio.

The binding parameters of the reaction system was then determined from the least-square best-fit curve to the binding isotherm. The stoichiometry N, the equilibrium binding constant K_b, and the molar enthalpy change ΔH was determined to be 1.01, 5.5×10^3 M^{-1}, and 32.0 kJ/mol at 298 K, respectively. These properties corresponded to the one to one binding of 18-C-6 and $BaCl_2$, and were within 5% difference with published data using conventional instruments [110].

4.5 Conclusions

This chapter has described a polymeric MEMS-based quantitative measurements approach for the thermodynamic characterization of biomolecular reaction systems. The polymer-based ITC device design eliminates the use of silicon, and exploits the low thermal conductivity of the polymer substrate to achieve thermal isolation of reaction samples in the absence of any complex or fragile freestanding structures. The low-cost availability of polymers and the elimination of the freestanding structures simplify the fabrication process, increase the fabrication yield, reduce the device cost, and improve the device reliability. The ITC microdevice consists of a pair of PDMS microfluidic structures for reactants and

reference solutions to be introduced at a series of molar ratios mixed in a passive chaotic mixer, and fed into the calorimetric measurement chambers at controlled time duration. As the reaction occurs, the resulting differential thermal power between the reaction and reference chambers is measured using a thin-film Sb-Bi thermopile that is embedded in the chamber-supporting polymeric substrate.

The closed volume-based MEMS ITC approach was first systematically characterized in the present work to identify factors such as volume mismatch, reaction volume information, evaporation of reactants, and thermal activity in the mixing and transport of reactants before they entered the calorimetric chamber that influenced the sensitivity and accuracy of ITC measurements. The potential utility of the device was demonstrated with quantitative ITC measurements of a model reaction system in which the ligand $BaCl_2$ is titrated into the receptor 18-C-6 at a reduced concentration of 2 mM. At the controlled temperature of 298 K, the thermodynamic binding parameters of the reaction systems including the stoichiometry, equilibrium binding constant, and enthalpy change, were obtained and found to agree with published data obtained using commercially available ITC instruments. These results demonstrate the potential of the microdevice for quantitative ITC characterization of biomolecular interactions.

Chapter 5 A Sensitive Polymeric MEMS Device Using 3D Chaotic Mixing-titration for Isothermal Titration Calorimetry

In the previous chapter, the polymer based MEMS thermoelectric sensor was integrated with microfluidics for sensitive ITC measurements, however, the sensitivity of the device was limited so that the device was forced to use samples with relatively large concentrations, and thus not yet suitable for practical applications. To address this issue, this chapter presents an alternative microfluidic-based design approach that was guided by the insights of device characterization results in Chapter 4. Featuring integrated 3D diffusive titration, the new device, based on a robust, inexpensive polyimide substrate, incorporates a 450 nL 3D splitting-and-recombination (SAR) passive mixer as the reaction cell, and an antimony-bismuth thermopile for sensitive thermoelectric detection of heat evolved from biomolecular reactions inside the cell. Proof of principle has been obtained by the measurement of 18-Crown-6 (18-C-6, 0.5 mM) reacting with barium chloride ($BaCl_2$, 0.1~1.6 mM) in the microfluidic reaction cell, with a roughly 40 times material consumption reduction than the device presented in chapter 4 and a response time of approximate 800 ms, which are much better suited for studying chemical reactions with fast kinetics. The detection limit was demonstrated to a practically useful level of 25 nW. The calculated thermodynamic binding parameters of the binding system was found to agree with published results.

5.1 Introduction

As introduced in chapter 4, ITC measures biochemical reaction heat rate as a function of reactant concentrations when a ligand solution is titrated into its target receptor solution under isothermal conditions, thereby allowing direct determination of reaction binding parameters for affinity analysis such as the reaction association constant (K_a), enthalpy

change (ΔH), and binding stoichiometry (N) of biochemical reaction systems [112-114]. ITC is well known as the only technique that can simultaneously determine all reactions that are associated with binding parameters in a single experiment. It is label-free and solution-based, which requires no molecular labeling or surface immobilization [115] [116]. Nevertheless, conventional ITC instruments are limited by complicated designs, rather large sample consumption, low throughput as well as relatively slow instrument responses (8-20 s) as a result of their large heat capacity. The slow instrument response time means a significant delay in measuring a sudden heat rate signal, which results in a flat initial rise of the calorimeter response curve, a large elongation during the exponential decay portion, and a shift in the calorimeter baseline. This "dilution" of the curve can bring about an error in the data analysis to affect accuracy in determining reaction binding parameters.

Miniaturized calorimetric devices which are based on the MEMS technology can potentially deal with these issues. However, MEMS devices offering ITC capabilities do not allow suitable control of reaction conditions for thermodynamic characterization of biomolecular reactions systems. Previous devices that used droplet-based reactions also do not allow for well-defined reaction volumes in general and are affected by evaporation-induced noise. Consequently, such devices are not well suited to quantitative measurement of thermodynamic reaction parameters. In addressing these issues, we previously advanced silicon and a polymer based closed volume-based approach for quantitative ITC measurements, featuring micro-fabricated differential calorimetric sensors with micro-fluidic chaotic passive mixing and titration [117]. Nonetheless, these approaches utilized an unfavorable design strategy of having dedicated micro-mixers and thermopile incorporated calorimetric measurement cells. ITC micro-devices made through this design approach were not only vulnerable to heat loss during mixing, which would significantly impair the thermal measurement accuracy, but also needed the utilization of a

high-Reynolds-number flow to accomplish a respectable mixing time. Nonetheless, due to device fabrication limitations, the resulted flow-induced measurement noise lead directly to a relatively high limit of detection (250 nW), which was not yet sufficient for practical applications.

This chapter purposes to concentrate on the limitations of existing MEMS ITC devices with a polymeric MEMS-based 3D chaotic mixing-titration measurement design approach. The design incorporates a bismuth-antimony (Bi-Sb) thermopile with 3D chaotic mixing-titration channels, hence combining the functionalities of micro-mixing, titration, and thermoelectric transducing. By integrating the thermopile with the titration channels, the reaction heat during mixing is now considered, thereby eliminating heat loss in the mixing process. This significantly enhances accuracy of thermal measurement and allows the use of a low-Reynolds-number flow (Re ~ 2) during titration experiments to bring down the flow induced measurement noise, which extremely advances the device's limit-of-detection. Additionally, the integration enables ITC measurements in a well-defined small reaction volume (450 nL) that effectually minimizes the sample heat capacity and causes measurement response time of 700 ms, thus making the technique well-suited for studying reactions with fast kinetics. This approach is then executed in a polymeric MEMS-based microdevice that eliminates the utilization of silicon, and manipulates the low thermal conductivity of the polymer substrate to accomplish thermal isolation of reaction samples in the nonattendance of any complex or fragile freestanding structures, thus making the fabrication process simpler, increasing the fabrication yield, reducing the device cost, and enhancing the device's operational reliability. The micro-device's utility is illustrated through quantitative ITC measurements of 18-Crown-6 (18-C-6 0.5 mM) reacting with barium chloride ($BaCl_2$ 0.1~1.6 mM) at a practically useful device limit-of-detection level of 25 nW. Compared with our formerly reported devices [117], the 3D chaotic mixing-titration design

approach enhances the limit-of-detection by a factor of 10, and minimizes the receptor sample consumption by a factor of 40. The thermodynamic parameters of the reaction system are determined from the ITC measurements and found to agree with the published data, illustrating the efficiency of the design approach.

5.2 Experimental

Again, as mentioned in chapter 4, In an ITC experiment for the thermodynamic characterization of a ligand-receptor reaction system, the ligand with known concentration and volume is titrated or added into a receptor. Thus, the reaction heat is obtained as a function of the ligand-receptor molar ratios. For example, considering a biochemical reaction system in which a receptor (M) and a ligand (X) bind in equilibrium and form the complex $M_\alpha X_\beta$:

$$\alpha M + \beta X \Leftrightarrow M_\alpha X_\beta \qquad (1)$$

where α, β are the stoichiometric coefficients of the receptor and the ligand, respectively. The binding parameters of the system, which include the molar enthalpy change of binding (ΔH), the reaction stoichiometry ($n = \beta / \alpha$), and the reaction association constant K_a can thus be determined by fitting to the equation Chapter 4 Eq. (2).

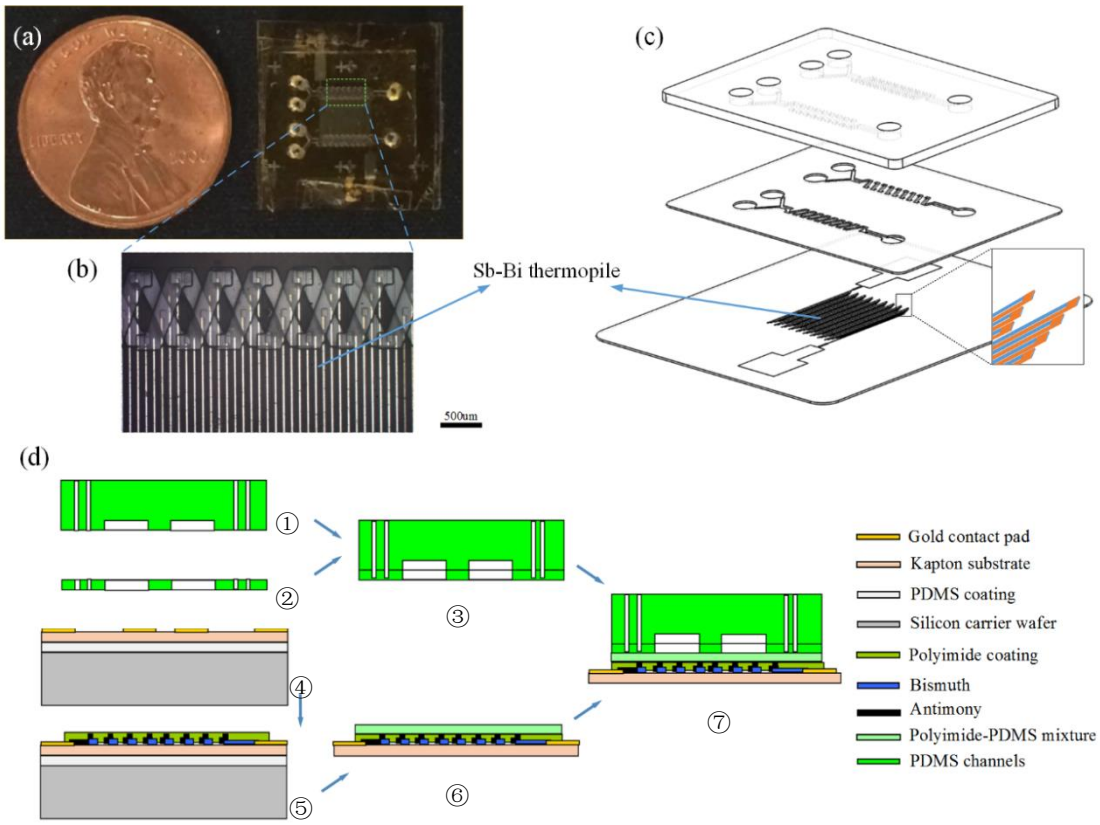

Figure 5-1. Polymer MEMS ITC device: (a) size and top view of the device; (b) Sb-Bi thermopile junctions aligned with the center of the mixer channel; (c) 3-D schematic exploded view; (d) the fabrication process for the designed device: ① top layer of the 3D SAR micromixer; ② bottom layer with through hole channel of the 3D SAR micromixer; ③ channel alignment and bonding; ④ Bonding of polyimide to a carrier wafer; ⑤ Sb-Bi thermopile lift-off; ⑥ mechanical release; ⑦ device bonding and packaging.

The ITC micro-device (shown in Figure 5-1a) has a matching pair of titration channels, based on a 3D splitting-and-recombination (SAR) design, and respectively serves as the measurement cells for the reaction (that is, receptor and ligand) as well as reference solutions. Each of the titration channels is located on a polymeric substrate which is also integrated with an antimony-bismuth (Sb-Bi) thermopile (46 junctions). The hot and cold junctions of the thermopile are aligned under the center of the prospect titration channels (as illustrated in Figure 5-1b, c). The comprehensive fabrication process was described elsewhere [118]. Briefly (as displayed in Figure 5-1d), a polyimide film (Kapton® 50HN, DuPont) was first reversibly attached to a silicon carrier wafer, chromium and gold contact pads, and Sb-Bi thermopile were then lithographically defined. Thereafter, they were lifted-off onto the

Kapton substrate sequentially [119]. Next, a layer of polyimide-PDMS blend was spin-coated onto the substrate to act as a passivation and bonding layer for the micro-fluidic structures. In parallel, soft lithography was utilized in molding two layers of micro-fluidic structures [120]. The bonding of micro-fluidic structures (step ③in Figure 5-1d) and the integration of the ITC micro-device (step ⑦ in Figure 5-1d) were facilitated by the plasma-activated bonding process (RIE 800 SOP, Technics. Power: 50 mW, pressure: 250 mTorr, time: 3 s).

In our approach to ITC measurements, the reaction heat was determined by use of a differential scheme, where two measurement cells are utilized to measure heat in the presence (ligand-receptor system) and absence of the receptor (ligand-buffer system), respectively. In the ligand-buffer system, buffer and ligand solutions are introduced into both the reaction as well as the reference measurement cells. The differential voltage signal output, which is stimulated by the non-specific heating contributions like enthalpy of mixing, is then used as the baseline as well as the negative control for the overall ITC measurements.

In the subsequent ligand-receptor system, a known concentration of receptor and different concentrations of ligand, which are typically in pure form and dissolved in well-conditioned buffer, are mixed and delivered to the reaction cell. At the same time, the same concentrations of ligand and the buffer are also introduced, then fully mixed and delivered to the reference cell. After subtracting the baseline, the ligand-receptor binding induced differential voltage signal output ΔU is then transformed to a differential power ΔP, by the expression $\Delta P = \Delta U/S$, where S is the device's responsivity, that is, the output electrical voltage generated by unit differential thermal power. The total heat evolved Q in binding process can then be determined through integrating this differential power in the due course.

The ITC micro-device is placed in a custom-built thermal enclosure (as illustrated in Figure 2) during measurements. The thermal enclosure includes a metal enclosure cap surrounding a stainless-steel stage. A peltier heater (Marlow Industries, XLT2418) is located underneath the stage, and then attached to a temperature controller (Lakeshore Model 331) so as to modulate the temperature of the micro-device. The thermal enclosure also provides extra thermal isolation of the micro-devices from ambient, and ensures that the sample solutions are kept at isothermal conditions during measurements as well as minimizing environmental noises. The thermoelectric measurements were performed by reading the thermopile differential voltage output using a nanovoltmeter (Agilent 34420A).

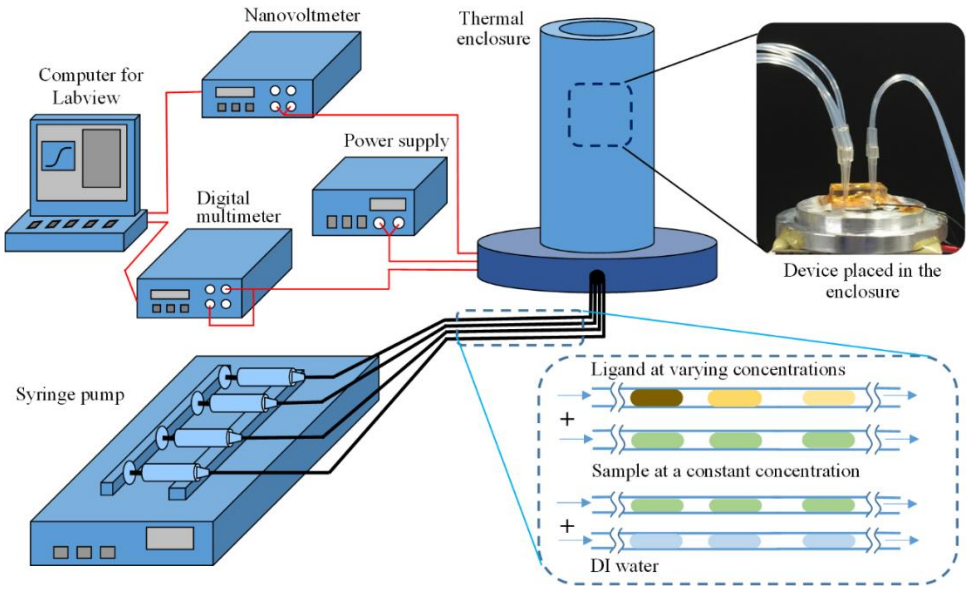

Figure 5-2. setup for the device test.

Before the experiment, in the reaction channel, liquid segments of receptor (18-C-6) with a known concentration as well as ligand solution segments ($BaCl_2$) at predetermined concentrations were preloaded into the two plastic tubing through a multi-channel syringe pump (KD Scientific, KDS 220). The solution segments were then formed through air gaps. In the meantime, in the reference channel, identical liquid segments of ligand and water were also preloaded into the other two tubing (as demonstrated in Figure 5-2). During the

operation, receptor and ligand were introduced and then mixed along the reaction channel whereas ligand and water were under the same manipulation in the reference channel. The heat difference between the sample and the reference channels can be sensed through the thermopile, and utilized in obtaining the thermodynamic properties of the reaction system. The ITC micro-device was placed in a custom built thermal enclosure (as displayed in Figure 5-2) during measurement. The thermal enclosure comprised of a metal enclosure cap surrounding a stainless steel stage. A peltier heater (Marlow Industries, XLT2418) was located underneath the stage, and connected a temperature controller (Lakeshore Model 331) so as to regulate the temperature of the micro-device. The thermal enclosure also provides additional thermal isolation of the micro-devices from ambient, and making sure that the sample solutions are kept at isothermal condition during measurements as well as reducing environmental noises. The thermoelectric measurements were performed through reading the thermopile differential voltage output by use of a nanovoltmeter (Agilent 34420A).

5.3 Results and Discussion

The micro-device was calibrated through measuring its steady-state thermopile output from applied differential thermal power by use of an off-chip temperature heater as well as a sensor setup. At 298K, the steady-state response of the ITC micro-device was realized to be dependent on the differential power in an extremely linear manner, yielding an estimated steady responsivity of S = 3.7 mV/mW. We also characterized the responsivity of the device at controlled micro-device temperature from 20 to 40 °C, and realized that it remained steady with a relative standard deviation of less than 3%. Thus, the temperature dependence of the device responsivity can, therefore, be ignored. Subsequently, a device time response of 800 ms was acquired by use of the ITC micro-device through a method that was initially

explained by Mayorga et al. In particular, the on-chip heater was utilized in generating a rectangular electrical calibration pulse (1 mW) to the reaction cell. The decay portion of the instrument response was then fitted to multiple exponential decay functions so as to establish the time response. Nonetheless, for our ITC micro-device, and based on prior experience, the time response can satisfactorily be explained or described through a single exponential function. The 800 ms response time was regarded suitable for characterizing thermodynamic properties of the biochemical reactions, and for characterizing the reaction kinetics that are suitably slow as compared with this particular response time. It is a 10-time improvement over a commercial unit.

The baseline (negative control) experiment was carried out through introducing sterile water and 0.1-1.6 mM $BaCl_2$ to the reaction and reference cells, respectively. In finding out the optimal experimental stipulation, four injections of the reagents were administered in sequence, each with a 1.5-minute interval, and a flow rate ranging from 10 to 100 µL/min. The increase in the flow rate precisely leads to the baseline noise to intensify monotonically (as illustrated in Figure 5-3a). This can be described by effects like the viscos heating effect from the fluid-solid interactions, as well as enthalpy of mixing. In essence, these effects would be counterbalanced through the use of the differential measurement scheme. Nevertheless, there was an approximate 7% volume difference (primarily in thickness) existing between the reaction and reference measurement cells. It was then expected that these effects would bring about a non-specific differential thermal power (baseline noise) as a result of volume difference during the titration process. Thus, the 10 µL/min flow rate (corresponding to a Reynold's Number of 2) was chosen particularly in optimizing the device signal-to-noise ratio. By use of the flow rate of 10 µL/min, all the baseline experiments demonstrated a similar non-reaction-specific spike noise. This noise was subtracted from the data analysis. In addition, the amplitude of the noise was established to be 25 nW (6 ncal/s),

which was regarded to be sufficient for measuring the thermal power generated in biomolecular reaction systems, and utilized as the detection limit of the ITC micro-device. In comparing the baseline noise with the reaction induced differential thermal power, 4 injections of 0.3 mM $BaCl_2$ and 0.5 mM 18-C-6 (each 0.23 μL) were introduced to the reaction cell whereas the reagents it remained the same in the reference cell. Comparing with the baseline, the micro-device's response to the reaction systems depicted a reaction-specific spike signal that was attributable to the exothermic nature of the binding between 18-C-6 as well as $BaCl_2$ (as illustrated in Figure 5-3b). The amplitude of the signal was 3 times larger than that of the baseline noise, hence illustrating the validity of the ITC experiment.

Subsequently, a fully characterized ITC micro-device was utilized in characterizing the thermodynamic binding parameters of the reaction system, $BaCl_2$ reacting with 18-C-6. Instead of measuring the heat evolved with the titration of $BaCl_2$ to 18-C-6 as in conventional instruments, the ITC micro-device was carried out in a series of measurements at the regulated temperature of 298 K. Each measurement utilized a fixed concentration of 18-C-6 (0.5 mM) as well as a series of concentrations of $BaCl_2$ (in the range of 0.1~1.6 mM), permitting the molar ratio of $BaCl_2$ to 18-C-6 to be varied from 0.2 to 3.2. By varying the molar ratio ($M_{BaCl2}/M_{18\text{-}C\text{-}6}$) from 0.2 to 3.2, the baseline-subtracted device output (as demonstrated in Figure 3c) showed spikes compatible with the titration reactions. Every spike in the device output was consistent with each titration, with a magnitude increasing steadily with the improvement of the molar ratio. This reflected that an increasing larger amount of 18-C-6 participated in the reaction as more $BaCl_2$ molecules were introduced. Nevertheless, no device output improvement was noticed between molar ratio of 2 and 3.2, which indicated excessive ligand ($BaCl_2$) concentration at molar ratio of 3.2. As well, the reaction was most

probably saturated at molar ratio of 2. This was anticipated for the reaction system. It was also noticeable that there was no apparent dilution of the baseline after each binding experiment, enabled by the much reduced micro-device's response time. This holds potential for the micro-device to carry out highly stable ITC measurements as well as enables an accurate thermodynamic data analysis.

Thermopile voltage output measured from the micro-device was then utilized in calculating the differential thermal power. The reaction heat at every molar ratio was quantified through integration of the thermal power over the whole period of reaction time. A thermodynamic binding isotherm (depicted in Figure 3d) was then acquired through plotting the reaction heat as a function of the molar ratio. A least square fitting to Chapter 4. Eq. (2) was used in determining the full thermodynamic binding parameters of the reaction system. Accordingly, the reaction heat increased monotonically with the molar ratio to a point of approaching saturation (molar ratio of 2), which reflected that the more binding sites of 18-C-6 were occupied with the accumulation of $BaCl_2$ until the binding sites were no longer available. Furthermore, and excessive $BaCl_2$ became free ligand in solution. The error bar was as a result of standard deviation between the calculations of the reaction heat for 3 different ITC experiments.

From the least square besting fitting curve (illustrated in Figure 3d), it was noticeable that the stoichiometry was about $n = 0.99$ at 298K, corresponding to the one to one binding of 18-C-6 as well as $BaCl_2$. Additionally, the reaction association constant (K_a) was established to be 6.09×10^3 M^{-1}, whereas the molar enthalpy change (ΔH) was established to be 31.0 kJ/mol at 298 K. These properties are within the 5% difference with published data by use of conventional instruments at the same temperature. This, therefore, demonstrate the utility of

the ITC micro-device, which is enabled by this 3D mixing-titration design approach for precise and sensitive thermodynamic characterization of the binding reactions. In addition, it is significant to note that since the design approach enabled micro-device characteristics, especially in the device response time, it is possible to also attain the kinetic information of the binding reactions by use of this approach. This will be examined for future work.

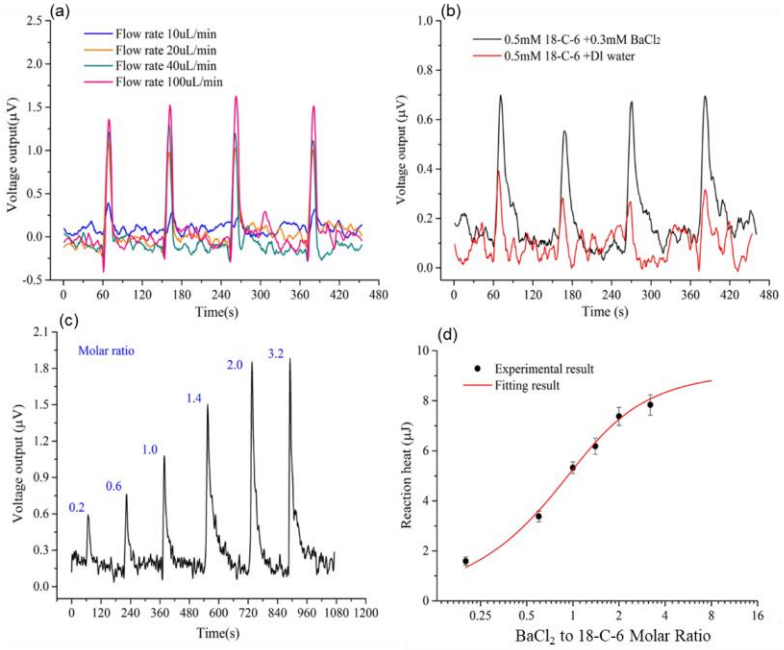

Figure 5-3. (a) the baseline noises under different flow rates; (b) Time-resolved device output upon introduction of sample compared with water baseline as the flow rate is chosen at 10 μL/min; (c) Device voltage output of the 0.5 mM 18-C-6 reacting with $BaCl_2$ at different molar ratios. (d) Non-linear curve fitting of the binding isotherm and the determination of the binding parameters.

5.4 Conclusion

This chapter has discussed a polymeric MEMS-based 3D chaotic mixing-titration design method for the thermodynamic characterization of biomolecular reaction systems. The mixing-titration combines the functionalities of micro-mixing, titration, as well as thermoelectric transducing, thus eliminating heat loss in the mixing process, and enhancing the

device limit-of-detection, further minimizing the micro-device response time, and making the closed volume-based MEMS ITC measurement pertinent for practical usage. The design approach is implemented in an ITC polymeric micro-device that exploits the low thermal conductivity of the polymer substrate to accomplish thermal isolation of reaction samples in the absence of any complex or delicate freestanding structures. This simplifies the fabrication process, thus increasing the fabrication yield, and enhancing the reliability of the device. The ITC micro-device comprises of a pair of bismuth-antimony (Bi-Sb) thermopile incorporated 3D mixing-titration channels which are utilized as both calorimetric measurement cells as well as micro-mixers. During the operation, titration of the ligand into the receptor is accomplished through merging the solutions segments by the reaction cell at regulated time duration. As the reaction takes place, the resulting differential thermal power between the reaction as well as reference cells is quantified by use of a thin-film Sb-Bi thermopile that is implanted in the chamber-supporting polymeric substrate.

The ITC polymeric micro-device was first characterized to have a commercial system similar with 25 nW detection limit, a ten-time enhancement over the earlier shown MEMS ITC devices. The potential utility of the device was illustrated with quantitative ITC measurements of a model reaction system in which the ligand $BaCl_2$ is titrated into the receptor 18-C-6 at a reduced concentration of 0.5 mM. At the regulated temperature of 298 K, the thermodynamic binding parameters of the reaction systems such as the stoichiometry, equilibrium binding constant, and enthalpy change, were acquired and realized to concur with published data that had been obtained by use of commercially available ITC instruments. These results showcased the potential of the microdevice for quantitative ITC

characterization of biomolecular interactions

Chapter 6 Integration of 3D-Printed Micro-fluidic Structures with MEMS Transducers for Isothermal Titration Calorimetry

In the previous chapters, the polymeric MEMS-based measurement approach is integrated with PDMS based microfluidic to enable thermodynamic characterization of biomolecular activities. However, PDMS based microfluidic structures have significant drawbacks that impact measurement sensitivity and accuracy, such as PDMS can both absorb small hydrophobic molecules and adsorb larger biomolecules which can significantly bias the result of experiments with inconsistent reagent concentration information. In addition, due to the high PDMS permeability, water vapor permeation through PDMS can lead to inaccurate reagent volume information and change in reagents molarity, especially at elevated temperature. In this chapter, we eliminate the use of PDMS microfluidic structures entirely, and present a 3D printing-based ITC LOC platform that integrates with the polymeric MEMS-based measurement approach to address these issues. Exploiting topographical flexibility offered by 3D printing, the platform design features fully isolated cantilever-like calorimetric measurement structures in a differential setup. This design layout improves thermal isolation and reduces overall platform thermal mass, thereby enhancing the measurement sensitivity and reducing the platform response time. We demonstrate ITC measurements of the binding of RNase A with 2'CMP completing quantitative ITC measurements at low cost, using practically relevant reagent concentrations (0.2 mM). The binding parameters of the RNase A and 2'CMP binding were again obtained at the controlled temperatures of 298 k, and found in agreement with published data. These results demonstrate the potential of our approach for efficient quantitative ITC characterization of

biomolecular interactions in biomedical applications.

6.1 Introduction

A lab-on-a-chip (LOC) system is a miniaturized platform which integrates one or numerous analyses methods, including DNA sequencing or biochemical detection which are normally carried out in a laboratory, onto a single microchip or nanoscale chip [121]. Being the significant part of the platform, micro-fluidic technology permits fluidic handling as well as manipulation functions within the platform. In the recent past, 3D printing has been believed as being a technology that can have the potential of changing the field of micro-fluidics to excel in many areas aspects and areas. First, it has the capability of fabricating a complete micro-fluidic device in a single step. Second, it enables fabrication in three dimensions. Lastly, it can also enable rapid prototyping [122]. As a result, recent researches that use 3D printing technology in the field of micro-fluidics have flourished [123-127]. Nonetheless, a collection of micro-fluidic structures alone might not enable all the LOC operations since they also need integrated electronics like sensors and transducers to become complete LOC diagnostic systems [128]. Thus, integrating sensors and transducers with 3D printing micro-fluidic structures have become a major challenge which is yet to be determined [129].

One of the bioanalysis techniques, the ITC, has been identified as being possible to benefit from operating in a LOC platform. ITC is a method that measures heat that is either released or absorbed when a ligand solution is titrated or added into a receptor solution of interest under isothermal conditions [93], It is known to be the only technique that can separately establish all reactions associated with binding parameters in a single experiment,

requiring no molecular labeling or surface immobilization [94]. Since operating in a LOC platform potentially permits quantitative ITC measurements with an enhanced device response time, a more efficient sample throughput, and possibly at low cost, micro-fluidics has been utilized together with MEMS transduction to accomplish this. Recently, there have been significant progress in this direction [91, 111, 117, 130], including silicon and polymer based micro-fluidic approach in a closed-chamber design for quantitative ITC measurements. However, these ITC platforms tend to mostly rely on the PDMS-based micro-fluidic structures, which have significant shortcomings in ITC characterization of biomolecular interactions. First, PDMS can both absorb small hydrophobic molecules as well as adsorb larger biomolecules like proteins on its surface. This has been identified as a significant challenge for molecular biological analysis, as the use of PDMS can considerably be unfair to the result of experiments with incompatible reagent concentration information as well as impact the reusability of the device. Furthermore, due to the high PDMS permeability, water vapor permeation through PDMS can lead to achieving of imprecise reagent volume information as well as change in reagents molarity, particularly at increased temperatures. Most significantly, PDMS based micro-fluidics made by soft-lithography methods can only permit the fabrication of two-dimensional (2D) topographical profile per step. Any attempt to enable a high operating efficiency of a 3D micro-fluidic functional structure (such as mixing) would, therefore, require manual and complicated multi-step process integration. These restrict the practical value of the existent ITC micro-devices.

In this chapter, we aspire to focus on addressing these limitations of previous MEMS calorimetric devices by presenting a 3D printing based measurement technique or approach

that attempts to eliminate the utilization of PDMS micro-fluidic structures. Implemented in a LOC platform, this approach permits close volume-based quantitative ITC measurements in a reusable manner. The platform design features fully isolated cantilever-like calorimetric measurement structures in a differential setup in exploiting the topographical flexibility provided by 3D printing. This design layout enhances thermal isolation and minimizes overall platform thermal mass, thus improving the measurement sensitivity as well as reducing the platform response time. This platform, however, is integrated with a polymeric MEMS-based thermoelectric sensor chip that eliminates the utilization of silicon, and makes use of the low thermal conductivity of the polymer substrate to accomplish thermal isolation of reaction samples in the absence of any complex or fragile freestanding structures. Hence, this assists to simplify the fabrication process, increasing the fabrication yield, reducing the device cost, and enhancing the operational reliability of the device. Lastly, the ITC platform can be integrated leak-free in a reversible manner, hence making effective cleaning possible and reducing cross-contamination between ITC measurements, which ultimately enables platform reusability.

Owing to the speedy and automation of 3D printing technology as well as low cost of polymeric materials, the device is economical and holds great commercialization prospect. Measurement data are then used in quantitatively determining the thermodynamic binding parameters, such as the equilibrium binding constant, stoichiometry as well as molar enthalpy change. This is illustrated with the binding of 18-Crown-6 (18-C-6) with barium chloride (BaCl2) together with the binding of ribonuclease A (RNase A) with cytidine 2'-monophosphate (2'CMP), in ~5 μL reaction volumes as well as at concentrations down to

0.1 mM. Thermodynamic binding properties are attained for every system and are noticed to be compatible with the published data. Simultaneously, our research determined a ground work for integrating 3D printing micro-fluidic structures into lab-on-a-chip platforms that can also be extended to other applications.

6.2 Principle and Design

In an ITC experiment of characterizing the binding between a ligand and its receptor, the ligand with known concentration is titrated or added into a known concentration of a receptor solution in a cell with well-defined volumes under isothermal condition. During titration, heat evolved in the ligand-receptor binding system, either endothermic or exothermic, is then measured as a function of the ligand concentration. Specifically, consider a binding system in which a receptor (M) and a ligand (X) bind in equilibrium and form the complex $M_\alpha X_\beta$:

$$\alpha M + \beta X \rightleftarrows M_\alpha X_\beta \quad (1)$$

where α, β are the stoichiometric coefficients of the receptor and ligand, respectively. The binding parameters associated with the system, which include the molar enthalpy change of the binding (ΔH), the reaction stoichiometry ($N = \beta/\alpha$), as well as the binding constant K_b can thus be determined using the binding equation from Chapter 4 Eq. (2):

Our 3D printing based ITC platform (illustrated in Figure 6-1c) comprises of a corresponding pair of 3D printed calorimetric measurement sample/reference chambers, wherein a biomolecular binding system together with a reference are kept, respectively. A series of split-and-recombination micromixers is also printed and situated in the upstream of the measurement chambers. The cantilevers like structures are designed to increase the thermal isolation between the sample and reference chambers. The 3D printed micro-fluidic

structures are then integrated with a polymer based MEMS thermoelectric sensor chip. The sensor chip consists an antimony (Sb)-bismuth (Bi) thermopile (60 junctions), thin-film resistive temperature sensors, and micro-heaters, which are all located on a polymer substrate within the areas occupied by the measurement chambers, as was described in the previous chapter.

The detailed polymeric sensor fabrication process (illustrated in Figure 6-2), which is a polyimide film (Kapton 50HN, 12.5 μm) was first reversely bonded to a silicon carrier wafer. The chromium/gold (Cr/Au) contact pads, temperature sensors/heaters together with Sb-Bi thermopile were lithographically defined and lifted-off onto the Kapton substrate in sequence. After that, a layer of polyimide (2 μm) was spin-coated onto the substrate to act as a passivation layer. During the packaging process, a 5 μm double side tape was applied to the sensor chip, thereby exposing only the contact pads. Then, the micro-fluidic structure was aligned with the sensor ship so that the hot and cold junctions of the thermopile are situated beneath the chamber centers. Lastly, the micro-fluidic structure was mechanically pressed against the sensor chip holder by the cap, and secured by use of screws to conclude the assembly.

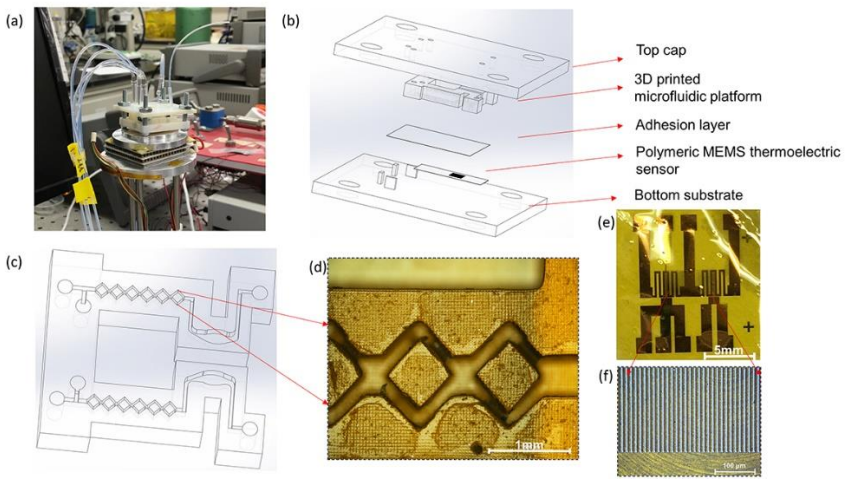

Figure 6-1. *Device photos and schematics; (a) photo of the packaged 3D-printed ITC device; (b) schematic of the packaged device; (c) schematic of the 3Dprinted microfluidic structure; (d) optical micrograph of the 3D-printed planar SAR micromixer. (e) photo of the polymeric thermoelectric sensor; (f) optical micrograph of the Sb-Bi thermopile junctions.*

To perform the ITC experiments, first, ligand and a reference buffer are introduced into both the reaction and reference measurement chambers. The response of the platform under the effect of liquid flow, without the presence of a binding reaction is recorded and used as a baseline. Served as the overall control of the ITC experiment, the baseline experiment eliminates any environmental disturbance and any non-binding specific heating contributions under effect of liquid flow. Next, during the ITC measurement of ligand-receptor binding, air separated reagents liquid plugs, formed by predetermined molar ratios between the ligand and the receptor, which are typically in pure form and dissolved in well-conditioned buffer, are mixed in the micromixer and delivered to the reaction measurement chamber sequentially. Simultaneously, same air separated reference liquid plugs, formed by mixing the ligand and buffer, are delivered to the reference measurement chamber. The binding heat induced temperature change in the measurement chambers is then sensed by the Sb-Bi thermopile, and outputted to a differential voltage signal. The signal is then converted to the differential thermal power using $\Delta P=\Delta U/S$, where S is the device's responsivity, i.e., the output electrical

voltage generated by unit differential thermal power. It is important to note that this differential thermal power includes the contribution from the baseline noise, which will be subtracted during data analysis.

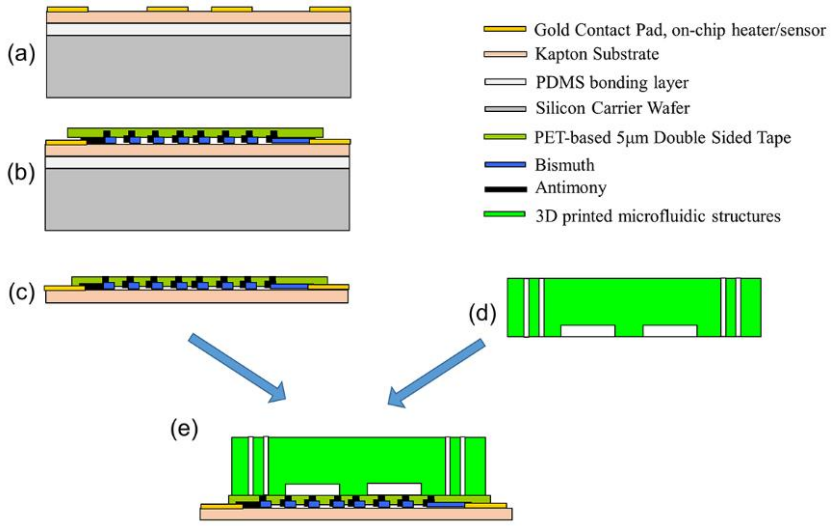

Figure 6-2. *Device fabrication process; (a) reversible bonding of polymer substrate to carrier wafer, and the lift-off of the gold contact pad, on-chip heater/sensors; (b) passivation of Sb-Bi thermopile with a PET-based ultra-thin 5 μm double sided tape; (c) mechan mechanical release of the substrate; (d) 3D printing of the microfluidic structures; (e) reversible packaging of the microfluidic structures to released polymeric thermal chip.*

6.3 Experimental

The micro-fluidic structures were printed by use of the ProJet 3500 HD*Max*® (3D Systems, South Carolina, USA) MultiJet 3D printer, and were made of the VisiJet® M3 (3D Systems, South Carolina, USA) clear UV curable plastic. Hypothetically, the 3D printer has a minimal feature line width of 16 μM together with a minimal wall thickness of 0.5 mm, which are adequate for printing micro-fluidic structures. Nevertheless, it was experimentally established that it can only reliably produce a microstructure with a minimum feature line width of 100 μM or more, together with a minimum wall thickness of 0.6 mm or more.

The test setup for the ITC comprises of a titration-enabling reagent delivery system and platform temperatures control/monitoring systems. The titration was accomplished by the

following steps: First, air-separated segments of the same concentration of receptor, and different concentrations of ligand solutions were each preloaded concurrently into the two Teflon access tubings by use of a multichannel syringe pump. Titration of the ligand into the receptor was realized through merging the solutions segments in the micromixer, and then delivered into the reaction measurement chamber. The ligand-receptor molar ratio was fluctuated from merging various solutions segments containing corresponding ligand as well as receptor concentrations. Similarly, two other identical access tubings were preloaded with segments of ligand and buffer solutions, respectively. They were, then, delivered into the reference chamber. All access tubings (a total of 4) were synchronized by a multiple-injections syringe pump (KD Scientific, KDS 220). Pure buffer solution as well as sterile water can also be loaded between the reactant segments to clean the chambers.

During measurement, the ITC platform was placed in a custom built thermal enclosure, consisting of a metal enclosure cap surrounding a stainless-steel stage. The thermal enclosure provided extra platform thermal isolation from the ambient air, and ascertained that the isothermal condition for platform was satisfied in the ITC measurements process through the use of a closed loop heating method enabled by a peltier heater. Besides, prior to introducing to the ITC platform, the binding reagents were stored in a separate micro-fluidic reservoir so that the reagents would be preheated to the temperature of the platform. The response of the platform is measured by reading the output of the thermopile and through a nanovoltmeter (Agilent 34420A). The calibrated on-chip temperature sensors, whose resistance was read by a digital multimeter (Agilent 34410A) were separately implemented for monitoring of the absolute temperature of both measurement chambers. In addition, the differential power input

utilized for device calibration was produced by the on-chip microheaters that were driven by a DC power supply (Agilent E3631A).

6.4 Results and Discussion

The 3D printed ITC platform utilized in these experiments together with the simulation had a 60-junction Sb-Bi thermopile as well as a sample/reference measurement chamber with a radius of 10 mm and a height of 500 μm, respectively. These constitute 11% difference in chamber volume. The center of the chambers is separated using 4.5 mm. The split-and-recombination micromixer (width: 200 μm, total length: 15 mm) lead the introduced solutions to the measurement chambers whereas the solutions became well-mixed along the way.

6.4.1 Characterization of the LOC ITC Platform

Prior to carrying out the ITC experiments, the device characteristics that are essential to quantitative ITC measurements, such as the efficiency of the micromixer, the platform responsivity, and the baseline noise of the ITC platform at the controlled temperature, were characterized.

First, the mixing efficiency in the last end of the micromixer was established by use of numerical simulation. It considered the whole fluidic part of the ITC platform, as well as the Navier-Stokes equation. On the other side, the convective-diffusion equation was coupled with the flow field to simulate the transport of diluted species. The inlets of the micromixer were then given a 100 μL/min flow rate. Consequently, the distribution of the solute concentration of the whole micromixer, as well as at the micromixer outlet were displayed in Figure 6-3a, b. As the fluid stream flowing through the channel, the solute concentration

gradient prescribed by the initial condition slowly decreased. This is apparent by the disappearance of the concentration interface at the end of the channel. Through calculation using the standard definition, a mixing efficiency of 92% was realized at the outlet of the micromixer. Therefore, the reagents that enter the measurement chamber were then considered well-mixed. As well, the pressured drop across the entire ITC platform was also established to be 1.2 kPa under the prescribed flow rate. By benefitting from this small pressure drop, the ITC platform could then be possibly assembled leak free, and reversibly. Another significant parameter was the residence time of the reactants in the micromixer as well as the connecting channels, which, based on platform dimensions, was established to be 1.2 s. Thus, this initial demonstration of 3D printed ITC platform was well-suited for study biomolecular interactions with a binding time scale much slower than the residence time.

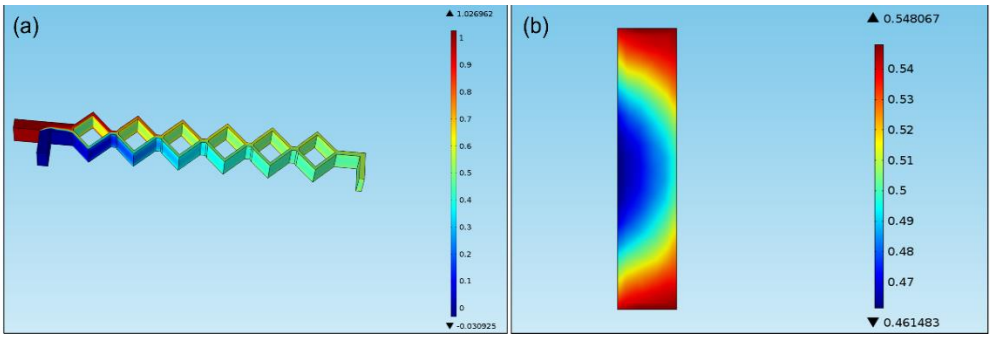

***Figure 6-3**. Solute concentration gradient of (a) the entire micromixer; (d) the outlet of the micromixer.*

After that, the constant state responsivity of the ITC platform was established. Driving by the DC voltage source, the on-chip microheater of the polymeric sensor chip was utilized in generating a known constant differential thermal power in the reaction measurement chambers. The differential voltage measured from the thermopile output was recorded thereafter. The responsivity of the device was then determined by 5.17 mV/mW (as depicted in Figure 6-5a). This responsivity was an enhancement of 40% over the PDMS based

micro-devices described in the previous chapters because of the enhanced thermal isolation permitted through the 3D printed cantilever structure.

At last, the baseline noise of the ITC platform was established by performing the overall control experiment. By mixing, and introducing sterile water as well as a reference buffer to both the measurement chambers concurrently, the liquid flow stimulated baseline noise due to the volume variation from fabrication limitation as was illustrated in Figure 6-6b. Under liquid flow, the response of the platform demonstrated a non-reaction-specific baseline noise with a maximum value of about 1.7 μW. The baseline noise also represented the detection limit of our ITC micro-device, which was sufficient for measuring the thermal power produced in biomolecular interactions. To compare the baseline noise with the binding heat induced differential power, 0.15 mM $BaCl_2$ as well as 0.1 mM 18-C-6 were introduced to the reaction measurement chamber whereas 0.15 mM $BaCl_2$ along with water were introduced to the reference measurement chamber. In contrast to the baseline, the ITC micro-device displayed a reaction-specific spike attributable to the exothermic nature of the binding reaction between 18-C-6 as well as $BaCl_2$ (as illustrated in Figure 6-5b), depicting a repeatable signal-to-noise ratio of ~5 (appropriate for titration measurements). Besides, the repeatability of the baseline prior and subsequent to the ITC experiment was also regarded in the characterization. In doing so, the liquid plugs of binding reagents that were in between the reference solution (separated by air gaps) were preloaded to the tubings. Three separate ITC experiments were then carried out in sequence. As noticeable in Figure 6-5c, the magnitude of the baseline noise remained consistent after the binding experiment. This proposed that the binding reagents had been fully consumed in the reaction, and that there were no

biomolecules attached to the surface of measurement chambers, demonstrating platform reusability.

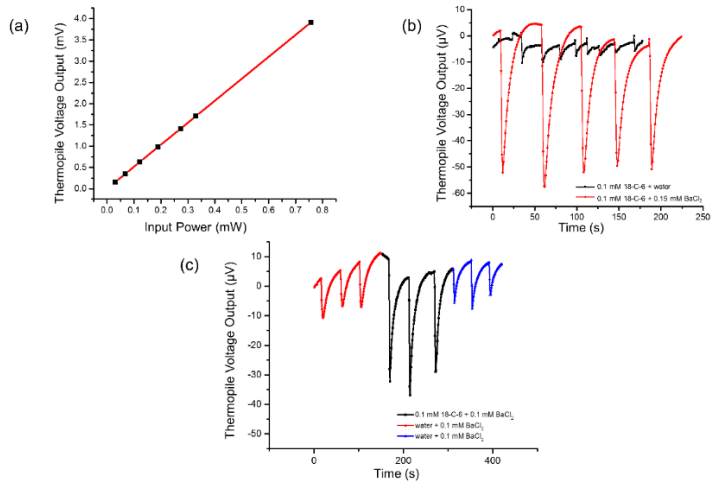

Figure 6-4*. Charaterization of the ITC platform. (a) Steady state platform responsivity calibration; (b) baseline noise calibration; (c) baseline noise repeatbility characterization.*

6.4.2 Quantitative ITC Characterization of Biochemical Reactions

The utility of the 3D printing-based was first illustrated with a model reaction system of 18-C-6 along with $BaCl_2$. The 3D printing-based ITC was carried out in a series of measurements, each with a 90 s interval between experiments, and at a constant temperature of 298 K. Every measurement utilized a fixed concentration of 18-C-6 (0.1 mM) as well as one of a set of concentrations (in the range of 0.02–0.5 mM) of $BaCl_2$. This permitted the molar ratio of $BaCl_2$ to 18-C-6 to be varied from 0.2 to 5. The baseline-subtracted thermopile voltage from the device (as illustrated in Figure 6-5a), in response to each titration exhibited spikes were compatible with the titration reactions, with a magnitude improving steadily with the titration number. This depicts that an increasingly larger amount of 18-C-6 participated in the reaction as more $BaCl_2$ molecules were introduced. Nonetheless, no device output increase was noted between the molar ratio of 2 and 5. This indicated that excessive ligand ($BaCl_2$) concentration and the reactions were most likely saturated at a molar ratio of 2, and

was expected for the reaction system.

The molar ratio-dependent thermopile voltage converted differential thermal power from device responsivity. A binding isotherm was then attained, showing the reaction heat as a function of the molar ratio. It was also used in determining the thermodynamic properties of the binding system by least squares fitting to Eq. (2). The binding isotherm of the reactions of 18-C-6 along with $BaCl_2$, as well as the best fits, have been illustrated in Figure 6-5b. From the binding isotherms at the regulated temperature, the stoichiometry was about n = 0.95, which is in line with the monovalent binding of 18-C-6 as well as $BaCl_2$. In addition, the equilibrium binding constant (K_b) and the molar enthalpy change (ΔH) were determined to be 5700 M^{-1} 35 °C and 29.0 kJ/mol, respectively. These properties correspond with the published data by use of conventional instruments.

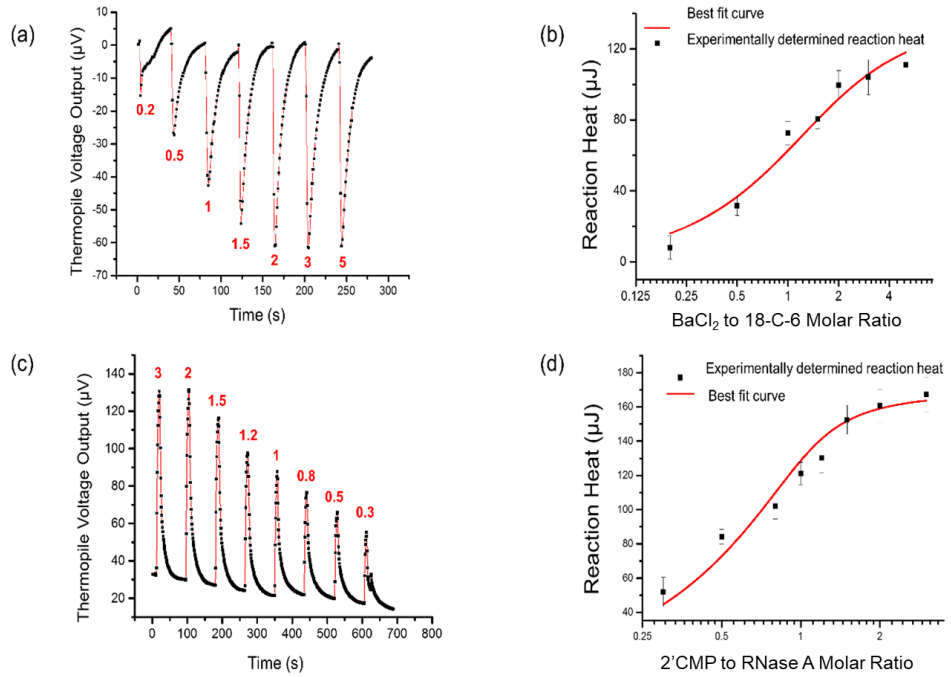

Figure 6-5. *Demonstration of the 3D printing-based ITC platform. (a) Baseline-subtracted device output from the binding of 18-C-6 with $BaCl_2$. Titration numbers corresponded to molar ratios of $BaCl_2$ to 18-C-6 (indicated on the figure; (b) reaction heat as a function of the molar ratio of BaCl2 to 18-C-6; (c) Baseline-subtracted device output from the binding of RNase A with 2'CMP; (d) reaction heat as a function of the molar ratio of 2'CMP to RNase A.*

6.4.3 Quantitative ITC Characterization of Biomolecular Binding

After demonstration of its utility, the ITC platform was then used to characterize biomolecular interactions, by use of RNase A as well as 2'CMP as a representative ligand-protein binding system at regulated temperatures of 298 k. The small molecule 2'CMP is recognized to be a strong inhibitor of substrates that bind to the active site of RNase A. Both reagents were made ready in 50 mM potassium acetate buffer and at pH of 5.5. The concentration of RNase A was then fixed at a practically pertinent level of 0.2 mM, whereas 2'CMP was set up at a series of concentrations in the range of 0.06–0.6 mM to permit 2'CMP-RNase A molar ratio to be varied between 0.3 and 3. The thermopile output of the device exhibited evidently visible spikes in response to the titrations of 2'CMP into RNase A (as illustrated in Figure 6-5c). Besides, it was noted that the spike spanned times for the binding of RNase A and 2' CMP at different molar ratios were about 100 s. Thus, the injection time of 1.8 s was deemed negligible. As the molar ratio of 2'CMP to RNase A improved from 0.06 to 0.6, the spike magnitude also elevated steadily and ultimately became saturated. This showed that as the amount of 2'CMP increases, a larger amount of RNase A participates in the binding until the maximum potential proportion of RNase A-2'CMP complex is formed. The measured molar ratio-dependent thermopile voltage at the regulated temperature was again utilized in computing the differential thermal power (Eq. (3), which was then integrated to attain the reaction heat, thus obtaining a binding isotherm as indicated in Figure 5-6d (error bars again represent standard deviations from triplicate measurements). The reaction heat improved with the molar ratio being the outcome of the increasing amount of 2'CMP presented to RNase A, and slowly approaching a saturation value, which again

reflected that a diminished amount of RNase A molecules was present to react with the added 2'CMP. Additionally, as demonstrated in Figure 5-6d, the binding isotherm was used in determining the thermodynamic properties of the binding system by least squares fitting to Eq. (2). The stoichiometry was established to be about $n = 0.99$, showing monovalent binding between RNase A and 2'CMP. The equilibrium binding constant (K_b) as well as the molar enthalpy change (ΔH) were determined as 8.5×10^4 M^{-1} and 54.0 kJ/mol, respectively. These results are in line with the published data for the 2'CMP and RNase A binding system by use of conventional instruments, supporting the utility of the 3D printing-based ITC platform.

6.5 Conclusions

This chapter has presented an ITC platform that features the integration of 3D printing micro-fluidic with polymeric MEMS-based measurement approach in an attempt to address the practical limitations of the previous PDMS-based ITC micro-devices. By entirely eliminating the use of PDMS micro-fluidic structures, this ITC platform enables close volume-based quantitative ITC measurements in a reusable manner. Besides, through exploiting topographical flexibility offered by 3D printing, the platform permits fully isolated cantilever-like calorimetric measurement structures design that enhance thermal isolation and reduce overall platform thermal mass, thus improves the measurement sensitivity and reduces the platform response time.

This 3D printed ITC platform is also integrated with a polymeric MEMS-based measurement approach consisting of a thermal control as well as a sensing substrate through a reversible mechanical assembly. The 3D printed platform comprises of two calorimetric measurement chambers, each of which is connected to a split-and-recombination micromixer.

On the thermal substrate, the polymeric substrate is integrated with a thin-film Sb-Bi thermopile for differential measurement of thermal power in the chambers. The substrate is also each integrated with a thin-film resistive micro temperature sensor as well as a microheater for *in-situ* temperature monitoring and on-chip device calibration. During the operation, ligand together with receptor solutions are introduced at a given molar ratio, mixed in the micromixer and delivered into the reaction measurement chamber. At the same time, ligand-free buffer as well as receptor solutions are introduced, mixed and delivered into the reference measurement chamber. The differential thermal power in the chambers is then established from the baseline-corrected thermopile voltage. Data from these measurements at a series of ligand-receptor molar ratios are utilized in computing the binding parameters like the stoichiometry, enthalpy of the binding, as well as equilibrium binding.

This chapter has shown ITC measurements of the binding of 18-C-6 with BaCl2, as well as the binding of RNase A with 2'CMP, completing quantitative ITC measurements at low cost, and through the use of practically relevant reagent concentrations. The resulting data are, therefore, used in calculating the binding parameters that are connected with the biomolecular systems, such as the stoichiometry, equilibrium binding constant, as well as the enthalpy change. For the protein-ligand binding system of RNase A together with the 2'CMP, quantitative ITC measurements were carried out with at concentrations that were as low as 0.2 mM. The binding parameters of the RNase A as well as 2'CMP binding were again attained at the regulated temperatures of 298 k, and realized to be consistent with the published data. These results indicate the potential of our approach for efficient quantitative ITC characterization of biomolecular interactions in biomedical applications.

Chapter 7 Concluding Remarks

7.1 Summary of the thesis

This thesis discusses the development of polymer-based MEMS calorimetric devices for thermodynamic characterization of biomolecular interactions. The work presented in the thesis includes the development of a polymer-based thick-film thermoelectric sensor and the integration of the sensor with microfluidic structures, both PDMS-based and 3D printing-based, for temperature-dependent characterization of biomolecular interactions. The significance of the work includes the development of MEMS calorimetric devices for quantitative thermodynamic characterization of biomolecular interactions with improved throughput, reduced sample consumption and response time; the development of polymer-based calorimetric devices that enhance sensitivity, reduce the device cost, improve the device yield and reliability; the demonstration of both DSC and ITC, which are the two most important and commonly used calorimetry measurement modes; the incorporation of polymer-based thermoelectric sensing, real-time temperature control, and microfluidic reagents handling to allow quantitative DSC experiments to be performed with minimized sample consumption; the incorporation of polymer-based thermoelectric sensing, microfluidic passive-chaotic mixing and 3D chaotic mixing to enable accurate, and sensitive close-chambered quantitative ITC measurements with reduced sample consumption; and the development of fabrication technologies for MEMS calorimetry: (a) The universally applicable photolithographical process for the construction of economical, robust polymer-based MEMS devices; (b) the first demonstration of a miniaturized 3D-printed LOC platform that integrates a polymeric MEMS-based measurement approach for quantitative ITC characterization of

biomolecular interactions. The work incorporated in this thesis can be divided into five chapters, each of which is summarized below.

Chapter 2 presents a distinctive low-temperature thermally assisted lift-off method that we used to fabricate a thick-film MEMS thermoelectric sensor. During the fabrication process, thick metal or semiconductor films were subjected to controlled breakup due to thermal reflow of the underlying lithographically defined photoresist patterns, thereby facilitating the sacrificial removal of the photoresist. This technique enables the rapid and reliable patterning of thick films, which can otherwise be difficult to achieve by conventional processes. Using the procedure described, a 60-junction thick-film Sb-Bi thermopile (up to 1.5 μm thick) was successfully patterned on a polymer substrates with various thicknesses. The experimental results demonstrated that the fabricated sensors had an electric conductivity of 5.44×10^6 S/m and a Seebeck coefficient of 114 μV/K per junction, which are comparable to those obtained from bulk materials. Thus, we conclude that this method is useful for the fabrication of sensors, as it allows low-noise, high-efficiency thermoelectric measurements.

In Chapter 3, the fabrication method presented in Chapter 2 was used to develop a polymer-based MEMS DSC device for studying the temperature-dependent thermodynamic properties of biomolecules. The device was integrated with a pair of calorimetric measurement channels, which were filled with a target biomolecule and a reference solution. The device temperature was scanned at a constant rate using closed-loop temperature control. The device was evaluated by the DSC measurement of unfolding of lysozyme at practically relevant sample concentrations (approaching 1 mg/mL). The molar enthalpy change of the lysozyme and melting temperature in the lysozyme unfolding process were thus determined

and found to be consistent with those of previously reported ranges in the literature.

Chapter 4 describes the application of the polymer-based MEMS sensor used in conjunction with PDMS-based microfluidics, which allows accurate quantitative ITC measurements and thermodynamic characterization of biomolecular interactions. By integrating the polymer sensor chip with microfluidic mixing and titration, this integrated approach enables the accurate ITC measurement with considerably reduced analysis times and costs. As the reaction was occurring, the measured differential power between the reaction system and a reference at a series of molar ratios of the reactants was used to determine the binding parameters of the reaction system. In addition, this chapter includes systematic characterizations of factors that influence the sensitivity and accuracy of ITC measurements, such as volume mismatch, reaction volume information, evaporation of reactants, and thermal activity in the mixing and transport of reactants before their entrance into the calorimetric chamber. In addition, the preliminary use of these insights to guide the polymer-based MEMS ITC design, demonstrating ITC measurements at a reduced receptor concentration (2 mM for 18-C-6), is also discussed.

Chapter 5 presents optimization of the polymer-based ITC measurement approach that features an integration of 3D chaotic mixing and microfluidic liquid handling to allow accurate quantitative ITC measurements and thermodynamic characterization of bio-molecular interactions in a sub-microliter volume. This integration eliminates the heat loss during mixing, enables the use of the low-Reynolds-number flow to minimize the flow-induced measurement noise while maintaining a distinctive device response time to allow thermodynamic characterization of the reaction systems with fast kinetics. During the ITC

device operation, reactants and reference solutions were introduced to their respective measurement channels, and the reaction-induced differential thermal power was measured and used to compute the thermodynamic binding parameters associated with the reaction system. The potential utility of the device was demonstrated with quantitative ITC measurements of a model reaction system in which the ligand barium chloride was titrated into the receptor 18-Crown-6 at a practically useful limit-of-detection level of 25 nW and a receptor consumption of 50 ng.

In Chapter 6, the limitations of using PDMS-based microfluidics in ITC characterization of biomolecular interactions are addressed by 3D-printed microfluidic approach. Implemented in a LOC platform, this approach enables close volume-based quantitative ITC measurements in a reusable manner. The exploitation of the topographical flexibility offered by 3D printing allows platform design features that fully isolate the cantilever-like calorimetric measurement structures in a differential setup. This design layout improves the thermal isolation and reduces the overall platform thermal mass, thereby enhancing the measurement sensitivity and reducing the platform response time. This platform was assembled in a leak-free manner with a polymeric MEMS-based thermoelectric sensor in a reversible manner that facilitates the effective cleaning and reduces the cross-contamination between ITC measurements and thus enables platform reusability. The utility of the platform was demonstrated by ITC measurement of the binding of ribonuclease A (RNase A) with cytidine 2'-monophosphate (2'CMP) at concentrations down to 0.1 mM.

7.2 Future work

Although the polymer-based calorimeter presented in this thesis showed commercial

promise, this thesis only demonstrated the viability of the polymer-based approach, and there is still much work that remains to be done for practically employing these devices. The following opportunities might be significant aspects for extending the scope of this thesis as well as paving the way for the commercialization of the device.

7.2.1 Substituting with Organic Thermoelectric Material

Thermoelectric sensing has been proven to be effective in the sensitive calorimetric measurement. However, common thermoelectric materials, such as Bi and Sb, which were used in the experiments conducted for the preparation of this thesis and our previous work as well as bismuth telluride and antimony telluride, are chemicals with different toxicity. Therefore, besides the processing incompatibilities, the mass production of these devices also has environmental safety concerns. Recently, a review by Russ et al. [131] suggested that in certain conditions, organic thermoelectric materials can achieve merits comparable to those of inorganic materials, while also exhibiting unique transport behaviors that are suggestive of optimization pathways and device geometries that were not previously possible. This concept would potentially facilitate the resolution of the above-mentioned issues and theoretically retain the sensitivity of devices. In addition, organic thermoelectric materials can be readily integrated with polymer-based substrates by either inkjet or screen printing method, both of which, once matured, can significantly reduce the cost of device manufacturing by eliminating traditional highly complex vacuum processing routes.

However, the feature resolution of the printing approach is still incomparable to the traditional photolithography method (100 μm vs. 1 μm). Therefore, an opportunity is offered here on potential routes for miniaturization of the printed organic thermoelectric

material-based devices.

7.2.2 Integrating 3D Printed Microfluidics with Polymeric MEMS Sensors

The detection sensitivity and accuracy of thermal biosensors strongly depend also on the thermal isolation of the biomolecular interactions. In our demonstration of the 3D-printed microfluidic devices, the thermal isolation of the device was significantly improved due to the topological flexibility of the 3D-printing technology so that the sample and reference calorimetric measurement chambers can be completely isolated. However, the effectiveness of the methods for integration of the 3D-printed microfluidic structure with polymer-based thermoelectric sensor can still be improved.

In the thesis, we temporarily packaged the device to avoid any leakage by adding a thin double-sided taping layer to promote the adhesion and used a relatively large dimension and a small flow rate to lower the pressure drop across the channels. This approach, however, limited the utility of our device. One potential solution to this problem is to insert the thin polymer thermoelectric sensor in the microfluidic structure during the 3D-printing process. Since the entire polymer-based sensor can be as thin as a few microns, it is possible to print the microfluidic structures direct on the top of the polymer substrate and yet uniformly seals the edge of the polymer substrate to avoid any leakage. This approach has been demonstrated by Aguilera et al. [132] in their experiment of printing a whole motor, integrating bearings, magnets, and speed controller during printing. However, our case is more complicated as we had to align the hot and cold junctions of the thermopile to their respective calorimetric chambers centers, and any offset would potentially induce baseline noise to the measurement. Therefore, an opportunity lies ahead on the ways to reliably integrate 3D-printed microfluidic

structures with Polymer Substrates.

7.2.3 High-Throughput Arrays

An exceedingly important advantage of using the MEMS technology is its ability to perform parallel measurements for biomolecular analysis, enabled by the strategic design and miniaturization employed. The work presented in this thesis established a solid groundwork for the improvement of the throughput through the adoption of polymer-based MEMS sensors. For example, Whiting et al. used an ink paste made from a blend of metal oxide particles and a eutectic alloy to mass-fabricate all-printed thermistors on flexible substrates using screen printing for parallel temperature measurement [133].

In our case, the polymer-based MEMS DSC and ITC devices can also be readily scaled up to form a sensor array on which multiple sets of calorimetric measurement chambers can be aligned and integrated with their perspective sensing unit to characterize biomolecular activities. However, much work is still required for the development of such devices. One prominent issue would be how to handle the fluidic sample delivery and manipulation, especially when there are multiple inlets, and the application requires synchronized sample delivery.

The suggestions listed above are merely a few points that might be worth investigating so that the existing polymer-based device can be improved and becomes practically applicable. The biomolecular activity measurements made by the prospective devices are expected to be accurate, sensitive, and repeatable. Also, the device should enable parallel processing, be economically and environmentally built with many novel features, and functionalities may continuously emerge with the advancement of engineering techniques.

List of Publication Resulting from This Thesis

Refereed Journal Publications

1. Y. Jia, S. Chao, M. He, and Q. Lin, “Integration of 3D-Printed Microfluidic Structures with MEMS Transducers for Isothermal Titration Calorimetry,” in preparation

2. X. Feng, Y. Jia (equal contribution), H. Jiang, Q. Lin, “A Sensitive Polymeric MEMS Device Using 3D Diffusive Titration for Isothermal Titration Calorimetry,” in preparation

3. Y. Jia, Z. Zhang, C. Su, and Q. Lin, "Isothermal titration calorimetry in a polymeric microdevice," Microfluidics and Nanofluidics, vol. 21, p. 90, 2017.

4. Y. Jia, H. Cai, and Q. Lin, "Thick-film MEMS Thermoelectric Sensor Fabricated Using A Thermally Assisted Lift-off Process," *Journal of Micro/Nanolithography, MEMS, and MOEMS,* vol. 15, pp. 024501-024501, 2016.

5. B. Wang, Y. Jia, and Q. Lin, "A Microfabrication-based approach to quantitative isothermal titration calorimetry," *Biosensors & Bioelectronics*, vol. 78, pp. 438-446, Apr 15 2016.

6. Y. Jia, B. Wang, Z. X. Zhang, and Q. Lin, "A Polymer-based MEMS Differential Scanning Calorimeter," *Sensors and Actuators a-Physical,* vol. 231, pp. 1-7, Jul 15 2015.

Refereed Conference Publications

1. Y. Jia, X. Feng, Q. Lin, “A polymeric MEMS Device Using 3d Diffusive Titration for Isothermal Titration Calorimetry”, *The Proceeding of the 19th International Conference on Miniaturized Systems for Chemistry and Life Sciences (MicroTAS 15),* Oct 2015

2. Y. Jia, H. Cai, Q. Lin, “A Heat Induced Bi-Layer Lift-Off Method for Flexible Substrates”, *The Proceeding of the 18th International Conference on Solid-state Sensors, Actuators and Microsystems (Transducers 15),* May 2015

3. Y. Jia, Z. Zhang, B. Wang, Q. Lin, “A Polymer-Based MEMS Isothermal Titration Calorimeter”, *The Proceeding of the 18th International Conference on Miniaturized Systems for Chemistry and Life Sciences (MicroTAS 14),* Oct 2014

4. Y. Jia, B. Wang, Q. Lin, “A Polymer-Based MEMS Differential Scanning Calorimeter”, *The Proceeding of the 27th International Conference on Micro Electro Mechanical Systems (MEMS 14),* Jan 2014

5. B. Wang, Y. Jia, Q. Lin, “A MEMS Isothermal Titration Biocalorimeter” *The Proceeding of the 16th International Conference on Miniaturized Systems for Chemistry and Life Sciences (MicroTAS 12),* Oct 2012

Bibliography

[1] S. Charbonnier, O. Gallego, and A. C. Gavin, "The social network of a cell: Recent advances in interactome mapping," *Biotechnology Annual Review, Vol 14,* vol. 14, pp. 1-28, 2008.

[2] J.-P. Renaud, C.-w. Chung, U. H. Danielson, U. Egner, M. Hennig, R. E. Hubbard*, et al.*, "Biophysics in drug discovery: impact, challenges and opportunities," *Nat Rev Drug Discov,* vol. advance online publication, 08/12/online 2016.

[3] W. Huber and F. Mueller, "Biomolecular interaction analysis in drug discovery using surface plasmon resonance technology," *Current Pharmaceutical Design,* vol. 12, pp. 3999-4021, 2006.

[4] S. S. Sinha, R. K. Mitra, and S. K. Pal, "Temperature-dependent simultaneous ligand binding in human serum albumin," *Journal of Physical Chemistry B,* vol. 112, pp. 4884-4891, Apr 24 2008.

[5] T. Nguyen, R. J. Pei, D. W. Landry, M. N. Stojanovic, and Q. Lin, "Label-free microfluidic characterization of temperature-dependent biomolecular interactions," *Biomicrofluidics,* vol. 5, Sep 2011.

[6] M. Horesh, N. Lidich, S. Yitzchaik, and Y. Hanein, "A Temperature-Differential Affinity Biosensor: Model and D-Optimal Performance Limits," *Ieee Sensors Journal,* vol. 11, pp. 2007-2015, Sep 2011.

[7] T. Nguyen, R. Pei, M. Stojanovic, and Q. Lin, "An aptamer-based microfluidic device for thermally controlled affinity extraction," *Microfluidics and Nanofluidics,* vol. 6, pp. 479-487, Apr 2009.

[8] C. A. Royer and S. F. Scarlata, "Fluorescence Approaches to Quantifying Biomolecular Interactions," *Fluorescence Spectroscopy,* vol. 450, pp. 79-106, 2008.

[9] A. Szabo, L. Stolz, and R. Granzow, "Surface-Plasmon Resonance and Its Use in Biomolecular Interaction Analysis (Bia)," *Current Opinion in Structural Biology,* vol. 5, pp. 699-705, Oct 1995.

[10] P. L. Gentili, F. Ortica, and G. Favaro, "Static and Dynamic Interaction of a Naturally Occurring Photochromic Molecule with Bovine Serum Albumin Studied by UV-Visible Absorption and Fluorescence Spectroscopy," *Journal of Physical Chemistry B,* vol. 112, pp. 16793-16801, Dec 25 2008.

[11] J. R. Krone, R. W. Nelson, D. Dogruel, P. Williams, and R. Granzow, "BIA/MS: Interfacing biomolecular interaction analysis with mass spectrometry," *Analytical Biochemistry,* vol. 244, pp. 124-132, Jan 1 1997.

[12] J. Y. Bao, S. M. Krylova, L. T. Cherney, J. C. Y. LeBlanc, P. Pribil, P. E. Johnson*, et al.*, "Kinetic Size-Exclusion Chromatography with Mass Spectrometry Detection: An Approach for Solution-Based Label-Free Kinetic Analysis of Protein-Small Molecule Interactions," *Analytical Chemistry,* vol. 86, pp. 10016-10020, Oct 21 2014.

[13] M. M. Dinges, K. Solakyildirim, and C. K. Larive, "Affinity capillary electrophoresis for the determination of binding affinities for low molecular weight heparins and antithrombin-III," *Electrophoresis,* vol. 35, pp. 1469-1477, May 2014.

[14] G. Bruylants, J. Wouters, and C. Michaux, "Differential scanning calorimetry in life science: Thermodynamics, stability, molecular recognition and application in drug design," *Current Medicinal Chemistry,* vol. 12, pp. 2011-2020, 2005.

[15] M. Kabiri and L. D. Unsworth, "Application of Isothermal Titration Calorimetry for Characterizing Thermodynamic Parameters of Biomolecular Interactions: Peptide Self-Assembly and Protein Adsorption Case Studies," *Biomacromolecules,* vol. 15, pp. 3463-3473, Oct 2014.

[16] G. Gauglitz and J. Homola, "Direct optical detection," *Analytical and Bioanalytical Chemistry,* vol. 407, pp. 3881-3882, May 2015.

[17] S. G. Patching, "Surface plasmon resonance spectroscopy for characterisation of membrane

protein-ligand interactions and its potential for drug discovery," *Biochimica Et Biophysica Acta-Biomembranes,* vol. 1838, pp. 43-55, Jan 2014.

[18] M. Citartan, S. C. B. Gopinath, J. Tominaga, Y. Chen, and T. H. Tang, "Use of UV-vis-NIR spectroscopy to monitor label-free interaction between molecular recognition elements and erythropoietin on a gold-coated polycarbonate platform," *Talanta,* vol. 126, pp. 103-109, Aug 1 2014.

[19] B. Wang and Q. Lin, "A Mems Differential Scanning Calorimeter for Thermodynamic Characterization of Biomolecules," *2011 Ieee 24th International Conference on Micro Electro Mechanical Systems (Mems),* pp. 821-824, 2011.

[20] P. Gill, T. T. Moghadam, and B. Ranjbar, "Differential scanning calorimetry techniques: applications in biology and nanoscience," *J Biomol Tech,* vol. 21, pp. 167-93, Dec 2010.

[21] A. C. R. Grayson, R. S. Shawgo, A. M. Johnson, N. T. Flynn, Y. W. Li, M. J. Cima*, et al.*, "A BioMEMS review: MEMS technology for physiologically integrated devices," *Proceedings of the Ieee,* vol. 92, pp. 6-21, Jan 2004.

[22] P. S. Dittrich and A. Manz, "Single-molecule fluorescence detection in microfluidic channels - the Holy Grail in mu TAS?," *Analytical and Bioanalytical Chemistry,* vol. 382, pp. 1771-1782, Aug 2005.

[23] H. F. Arata, M. Kumemura, N. Sakaki, and H. Fujita, "Towards single biomolecule handling and characterization by MEMS," *Analytical and Bioanalytical Chemistry,* vol. 391, pp. 2385-2393, Aug 2008.

[24] S. Q. Wang, T. Chinnasamy, M. A. Lifson, F. Inci, and U. Demirci, "Flexible Substrate-Based Devices for Point-of-Care Diagnostics," *Trends in Biotechnology,* vol. 34, pp. 909-921, Nov 2016.

[25] Kenry, J. C. Yeo, and C. T. Lim, "Emerging flexible and wearable physical sensing platforms for healthcare and biomedical applications," *Microsystems & Nanoengineering,* vol. 2, p. 16043, 09/26/online 2016.

[26] B. I. Fall, B. Eberlein-Konig, H. Behrendt, R. Niessner, J. Ring, and M. G. Weller, "Microarrays for the screening of allergen-specific IgE in human serum," *Analytical Chemistry,* vol. 75, pp. 556-562, Feb 1 2003.

[27] M. Cretich, G. Di Carlo, C. Giudici, S. Pokoj, I. Lauer, S. Scheurer*, et al.*, "Detection of allergen specific immunoglobulins by microarrays coupled to microfluidics," *Proteomics,* vol. 9, pp. 2098-2107, Apr 2009.

[28] S. Kim, J. Lee, S. J. Lee, and H. J. Lee, "Ultra-sensitive detection of IgE using biofunctionalized nanoparticle-enhanced SPR," *Talanta,* vol. 81, pp. 1755-1759, Jun 15 2010.

[29] Y. Q. Luo, F. Yu, and R. N. Zare, "Microfluidic device for immunoassays based on surface plasmon resonance imaging," *Lab on a Chip,* vol. 8, pp. 694-700, 2008.

[30] A. Sonato, M. Agostini, G. Ruffato, E. Gazzola, D. Liuni, G. Greco*, et al.*, "A surface acoustic wave (SAW)-enhanced grating-coupling phase-interrogation surface plasmon resonance (SPR) microfluidic biosensor," *Lab on a Chip,* vol. 16, pp. 1224-1233, 2016.

[31] L. E. Agafonova, V. V. Shumyantseva, and A. I. Archakov, "Quartz crystal microbalance for the cardiac markers/antibodies binding kinetic measurements in the plasma samples," *Chemical Physics Letters,* vol. 604, pp. 5-9, Jun 3 2014.

[32] B. Godber, M. Frogley, M. Rehak, A. Sleptsov, K. S. J. Thompson, Y. Uludag*, et al.*, "Profiling of molecular interactions in real time using acoustic detection," *Biosensors & Bioelectronics,* vol. 22, pp. 2382-2386, Apr 15 2007.

[33] B. Wang, F. L. Huang, T. Nguyen, Y. Xu, and Q. Lin, "Microcantilever-based label-free characterization of temperature-dependent biomolecular affinity binding," *Sensors and Actuators B-Chemical,* vol. 176, pp. 653-659, Jan 2013.

[34] H. Etayash, M. F. Khan, K. Kaur, and T. Thundat, "Microfluidic cantilever detects bacteria and measures their susceptibility to antibiotics in small confined volumes," *Nature Communications,* vol. 7, Oct 4 2016.

[35] D. W. Denlinger, E. N. Abarra, K. Allen, P. W. Rooney, M. T. Messer, S. K. Watson*, et al.*, "Thin-Film Microcalorimeter for Heat-Capacity Measurements from 1.5-K to 800-K," *Review of Scientific Instruments,* vol. 65, pp. 946-958, Apr 1994.

[36] S. L. Lai, G. Ramanath, L. H. Allen, P. Infante, and Z. Ma, "High-Speed (10(4)-Degrees-C/S) Scanning Microcalorimetry with Monolayer Sensitivity (J/M(2))," *Applied Physics Letters,* vol. 67, pp. 1229-1231, Aug 28 1995.

[37] L. H. Allen and S. L. Lai, "MEMS-based scanning calorimeter for thermodynamic properties of nanostructures," *Microscale Thermophysical Engineering,* vol. 2, pp. 11-19, Jan-Mar 1998.

[38] F. Fominaya, T. Fournier, P. Gandit, and J. Chaussy, "Nanocalorimeter for high resolution measurements of low temperature heat capacities of thin films and single crystals," *Review of Scientific Instruments,* vol. 68, pp. 4191-4195, Nov 1997.

[39] M. Zhang, M. Y. Efremov, F. Schiettekatte, E. A. Olson, A. T. Kwan, S. L. Lai*, et al.*, "Size-dependent melting point depression of nanostructures: Nanocalorimetric measurements," *Physical Review B,* vol. 62, pp. 10548-10557, Oct 15 2000.

[40] D. Jaeggi, H. Baltes, and D. Moser, "Thermoelectric Ac Power Sensor by Cmos Technology," *Ieee Electron Device Letters,* vol. 13, pp. 366-368, Jul 1992.

[41] R. E. Cavicchi, G. E. Poirier, N. H. Tea, M. Afridi, D. Berning, A. Hefner*, et al.*, "Micro-differential scanning calorimeter for combustible gas sensing," *Sensors and Actuators B: Chemical,* vol. 97, pp. 22-30, 1/1/ 2004.

[42] E. B. Chancellor, J. P. Wikswo, F. Baudenbacher, M. Radparvar, and D. Osterman, "Heat conduction calorimeter for massively parallel high throughput measurements with picoliter sample volumes," *Applied Physics Letters,* vol. 85, pp. 2408-2410, Sep 20 2004.

[43] A. Wolf, T. Hartmann, M. Bertolini, J. Schemberg, A. Grodrian, K. Lemke*, et al.*, "Toward high-throughput chip calorimetry by use of segmented-flow technology," *Thermochimica Acta,* vol. 603, pp. 172-183, Mar 10 2015.

[44] T. Hartmann, N. Barros, A. Wolf, C. Siewert, P. L. O. Volpe, J. Schemberg*, et al.*, "Thermopile chip based calorimeter for the study of aggregated biological samples in segmented flow," *Sensors and Actuators B-Chemical,* vol. 201, pp. 460-468, Oct 2014.

[45] T. Hartmann, M. Muhling, A. Wolf, F. Mariana, T. Maskow, F. Mertens*, et al.*, "A chip-calorimetric approach to the analysis of Ag nanoparticle caused inhibition and inactivation of beads-grown bacterial biofilms," *Journal of Microbiological Methods,* vol. 95, pp. 129-137, Nov 2013.

[46] F. M. Morais, F. Buchholz, T. Hartmann, J. Lerchner, T. R. Neu, B. Kiesel*, et al.*, "Chip-calorimetric monitoring of biofilm eradication with bacteriophages reveals an unexpected infection-related heat profile," *Journal of Thermal Analysis and Calorimetry,* vol. 115, pp. 2203-2210, Mar 2014.

[47] C. Hany, H. Lebrun, C. Pradere, J. Toutain, and J.-C. Batsale, "Thermal analysis of chemical reaction with a continuous microfluidic calorimeter," *Chemical Engineering Journal,* vol. 160, pp. 814-822, 6/15/ 2010.

[48] M. I. Recht, D. D. Bruyker, A. G. Bell, M. V. Wolkin, E. Peeters, G. B. Anderson*, et al.*, "Enthalpy array analysis of enzymatic and binding reactions," *Analytical Biochemistry,* vol. 377, pp. 33-39, 6/1/ 2008.

[49] Y. Jia, H. G. Cai, and Q. Lin, "Thick-film MEMS thermoelectric sensor fabricated using a thermally assisted lift-off process," *Journal of Micro-Nanolithography Mems and Moems,* vol. 15, Apr 2016.

[50] A. van der Horst, D. van der Voort, B. Mimoun, M. Rutten, F. van de Vosse, and R. Dekker, "A Novel Flexible Thermoelectric Sensor for Intravascular Flow Assessment," *Ieee Sensors Journal,* vol. 13, pp. 3883-3891, Oct 2013.

[51] R. Buchner, K. Froehner, C. Sosna, W. Benecke, and W. Lang, "Toward Flexible Thermoelectric Flow Sensors: A New Technological Approach," *Journal of Microelectromechanical Systems,* vol. 17, pp. 1114-1119, Oct 2008.

[52] H. Stachowiak, S. Lassue, A. Dubernard, and E. Gaviot, "A thermoelectric sensor for fluid flow measurement. principles, calibration and solution for self temperature compensation," *Flow Measurement and Instrumentation,* vol. 9, pp. 135-141, Sep 1998.

[53] N. H. Park, T. Akamatsu, T. Itoh, N. Izu, and W. Shin, "Calorimetric Thermoelectric Gas Sensor for the Detection of Hydrogen, Methane and Mixed Gases," *Sensors,* vol. 14, pp. 8350-8362, May 2014.

[54] A. Heiman and V. Halpern, "Electrical Conductivity of Thin Metal-Films at Low-Temperatures," *Thin Solid Films,* vol. 13, pp. 57-&, 1972.

[55] G. Korotcenkov, *Handbook of Gas Sensor Materials- Properties, Advantages and Shortcomings for Applications* vol. 1. New York: Springer, 2013

[56] P. J. Johnson, C. D. Clark, and R. G. C. Artus, "The determination of electrical conductivity by thermal noise measurements," *Journal of Physics D: Applied Physics,* vol. 19, p. 835, 1986.

[57] T. Adrega and S. P. Lacour, "Stretchable gold conductors embedded in PDMS and patterned by photolithography: fabrication and electromechanical characterization," *Journal of Micromechanics and Microengineering,* vol. 20, May 2010.

[58] B. Y. Ahn, E. B. Duoss, M. J. Motala, X. Y. Guo, S. I. Park, Y. J. Xiong*, et al.*, "Omnidirectional Printing of Flexible, Stretchable, and Spanning Silver Microelectrodes," *Science,* vol. 323, pp. 1590-1593, Mar 20 2009.

[59] L. A. Guo and S. P. DeWeerth, "High-Density Stretchable Electronics: Toward an Integrated Multilayer Composite," *Advanced Materials,* vol. 22, pp. 4030-4033, Nov 22 2010.

[60] L. A. Guo, K. W. Meacham, S. Hochman, and S. P. DeWeerth, "A PDMS-Based Conical-Well Microelectrode Array for Surface Stimulation and Recording of Neural Tissues," *Ieee Transactions on Biomedical Engineering,* vol. 57, pp. 2485-2494, Oct 2010.

[61] D. H. Kim, J. H. Ahn, W. M. Choi, H. S. Kim, T. H. Kim, J. Z. Song*, et al.*, "Stretchable and foldable silicon integrated circuits," *Science,* vol. 320, pp. 507-511, Apr 25 2008.

[62] D. H. Kim, J. Viventi, J. J. Amsden, J. L. Xiao, L. Vigeland, Y. S. Kim*, et al.*, "Dissolvable films of silk fibroin for ultrathin conformal bio-integrated electronics," *Nature Materials,* vol. 9, pp. 511-517, Jun 2010.

[63] W. Y. Yin, W. Fillmore, and K. Dempsey, "Optimization of the lithographic performance for lift-off processing," *Microlithography 1999: Advances in Resist Technology and Processing Xvi, Pts 1 and 2,* vol. 3678, pp. 713-720, 1999.

[64] D. F. Witman, J. M. Shaw, M. Hatzakis, E. D. Babich, J. R. Paraszczak, and K. J. Stewart, "A simple bilayer lift-off process," *Microelectronic Engineering,* vol. 11, pp. 549-552, 1990/04/01 1990.

[65] J. Minter, M. Ross, W. R. Livesay, S. Wong, M. Narcy, and T. Marlowe, "Advanced metal lift-off process using electron beam flood exposure of single layer photoresist," *Microlithography 1999: Advances in Resist Technology and Processing Xvi, Pts 1 and 2,* vol. 3678, pp. 1074-1082, 1999.

[66] V. Passi, A. Lecestre, C. Krzeminski, G. Larrieu, E. Dubois, and J. P. Raskin, "A single layer hydrogen silsesquioxane (HSQ) based lift-off process for germanium and platinum," *Microelectronic Engineering,* vol. 87, pp. 1872-1878, Oct 2010.

[67] J. Golden, H. Millar, D. Nawrocki, J. Ross, "Optimization of bi-layer lift-off resist process,"

http://www.microchem.com.

[68] T. E. Wilson, K. A. Korolev, and N. A. Crow, "Bilayer lift-off process for aluminum metallization," *Journal of Micro-Nanolithography Mems and Moems,* vol. 14, Jan 2015.

[69] J. C. Tsai and Y. S. Hsu, "Profile of Microlens Fabricated by the Thermal Reflow Process," *Ieee Transactions on Magnetics,* vol. 47, pp. 598-601, Mar 2011.

[70] K. Jayachandran, "Electrical, Optical and Structural Studies in Bismuth, Antimony, Bismuth Oxide and Antimony Oixude Thin Films," Ph.D. Thesis, Mahatma Gandhi University, Kerala, 1997.

[71] D. M. Rome, *CRC Handbook of Thermoelectrics*, 1 ed. Boca Raton: CRC Press, 1995.

[72] Y. Jia, B. Wang, Z. X. Zhang, and Q. Lin, "A polymer-based MEMS differential scanning calorimeter," *Sensors and Actuators a-Physical,* vol. 231, pp. 1-7, Jul 15 2015.

[73] Y. Jia, B. Wang, J. Zhu, and Q. Lin, "A Polymer-Based Mems Differential Scanning Calorimeter," *2014 Ieee 27th International Conference on Micro Electro Mechanical Systems (Mems),* pp. 306-309, 2014.

[74] M. E. Brown, *Handbook of Thermal Analysis and Calorimetry*, 1 ed.: Elsevier Science, 1998.

[75] P. S. Gill, S. R. Sauerbrunn, and M. Reading, "Modulated Differential Scanning Calorimetry," *Journal of Thermal Analysis,* vol. 40, pp. 931-939, 1993.

[76] S. Youssef, J. Podlecki, R. Al Asmar, B. Sorli, O. Cyril, and A. Foucaran, "MEMS Scanning Calorimeter With Serpentine-Shaped Platinum Resistors for Characterizations of Microsamples," *Journal of Microelectromechanical Systems,* vol. 18, pp. 414-423, Apr 2009.

[77] J. M. Sturtevant, "Biochemical Applications of Differential Scanning Calorimetry," *Annual Review of Physical Chemistry,* vol. 38, pp. 463-488, 1987.

[78] F. E. Torres, P. Kuhnt, D. De Bruyker, A. G. Bell, M. V. Wolkin, E. Peeters*, et al.*, "Enthalpy arrays," *Proceedings of the National Academy of Sciences of the United States of America,* vol. 101, pp. 9517-9522, Jun 29 2004.

[79] G. Vanden Poel, D. Istrate, A. Magon, and V. Mathot, "Performance and calibration of the Flash DSC 1, a new, MEMS-based fast scanning calorimeter," *Journal of Thermal Analysis and Calorimetry,* vol. 110, pp. 1533-1546, Dec 2012.

[80] D. W. Cooke, K. J. Michel, and F. Hellman, "Thermodynamic measurements of submilligram bulk samples using a membrane-based "calorimeter on a chip"," *Review of Scientific Instruments,* vol. 79, May 2008.

[81] S. Maggiolino, N. Scuor, R. L. Mahajan, and O. Sbaizero, "MEMS_DSC: a new device for microcalorimetric analysis in the biological field," *Microsystem Technologies-Micro-and Nanosystems-Information Storage and Processing Systems,* vol. 16, pp. 967-971, Jun 2010.

[82] B. Wang and Q. Lin, "A MEMS Differential-Scanning-Calorimetric Sensor for Thermodynamic Characterization of Biomolecules," *Journal of Microelectromechanical Systems,* vol. 21, pp. 1165-1171, Oct 2012.

[83] L. Wang, B. Wang, and Q. Lin, "Demonstration of MEMS-based differential scanning calorimetry for determining thermodynamic properties of biomolecules," *Sensors and Actuators B-Chemical,* vol. 134, pp. 953-958, Sep 25 2008.

[84] L. J. Matienzo and F. D. Egitto, "Poly(dimethylsiloxane)-polyimide blends in the formation of thick polyimide films," *Journal of Materials Science,* vol. 42, pp. 239-251, Jan 2007.

[85] C. A. Cerdeirina, J. A. Miguez, E. Carballo, C. T. E. de la Puente, and L. Romani, "Highly precise determination of the heat capacity of liquids by DSC: calibration and measurement," *Thermochimica Acta,* vol. 347, pp. 37-44, Apr 17 2000.

[86] A. Bejan, *Heat Transfer*. Canada: John Wiley & Sons, 1993.

[87] W. H. McAdams, *Heat Transimission*, 3 ed. New York: McGraw-Hill, 1954.

[88] M. C. Righetti, G. Salvetti, and E. Tombari, "Heat capacity of glycerol from 298 to 383 K," *Thermochimica Acta,* vol. 316, pp. 193-195, Jun 22 1998.

[89] D. C. Ginnings and G. T. Furukawa, "Heat Capacity Standards for the Range 14-Degrees-K to 1200-Degrees-K," *Journal of the American Chemical Society,* vol. 75, pp. 522-527, 1953.

[90] H. J. Hinz and F. P. Schwarz, "Measurement and analysis of results obtained on biological substances with d.s.c.," *Journal of Chemical Thermodynamics,* vol. 33, pp. 1511-1525, Nov 2001.

[91] Y. Jia, Z. Zhang, B. Wang, and Q. Lin, "A Polymer-based MEMS Isothermal Titration Calorimeter," in *Int. Conf. on Miniaturized Chemical and Biochemical Analysis Systems* San Antonio, 2014, pp. 2315-2317.

[92] Y. Jia, Z. Zhang, C. Su, and Q. Lin, "Isothermal titration calorimetry in a polymeric microdevice," *Microfluidics and Nanofluidics,* vol. 21, p. 90, 2017.

[93] S. Leavitt and E. Freire, "Direct measurement of protein binding energetics by isothermal titration calorimetry," *Current Opinion in Structural Biology,* vol. 11, pp. 560-566, Oct 2001.

[94] Malvern. (2017). *Isothermal Titration Calorimetry*. Available: http://www.malvern.com

[95] C. Hany, H. Lebrun, C. Pradere, J. Toutain, and J. C. Batsale, "Thermal analysis of chemical reaction with a continuous microfluidic calorimeter," *Chemical Engineering Journal,* vol. 160, pp. 814-822, Jun 2010.

[96] M. I. Recht, D. De Bruyker, A. G. Bell, M. V. Wolkin, E. Peeters, G. B. Anderson*, et al.*, "Enthalpy array analysis of enzymatic and binding reactions," *Analytical Biochemistry,* vol. 377, pp. 33-39, Jun 2008.

[97] B. Lubbers and F. Baudenbacher, "Isothermal Titration Calorimetry in Nanoliter Droplets with Subsecond Time Constants," *Analytical Chemistry,* vol. 83, pp. 7955-7961, Oct 2011.

[98] J. Xu, R. Reiserer, J. Tellinghuisen, J. P. Wikswo, and F. J. Baudenbacher, "A microfabricated nanocalorimeter: Design, characterization, and chemical calibration," *Analytical Chemistry,* vol. 80, pp. 2728-2733, Apr 2008.

[99] B. Wang, Y. Jia, and Q. Lin, "A microfabrication-based approach to quantitative isothermal titration calorimetry," *Biosensors & Bioelectronics,* vol. 78, pp. 438-446, Apr 15 2016.

[100] S. Mouaziz, G. Boero, G. Moresi, C. Degen, Q. Lin, B. Meier*, et al.*, "Combined Al-protection and HF-vapor release process for ultrathin single crystal silicon cantilevers," *Microelectronic Engineering,* vol. 83, pp. 1306-1308, 4// 2006.

[101] MicroCal, "ITC Data Analysis in Origin: Tutorial Guide," 2004.

[102] A. Velazquez-Campoy, S. A. Leavitt, and E. Freire, "Characterization of Protein-Protein Interactions by Isothermal Titration Calorimetry," in *Protein-Protein Interactions: Methods and Applications*, H. Fu, Ed., ed Totowa, NJ: Humana Press, 2004, pp. 35-54.

[103] A. D. Stroock, S. K. W. Dertinger, A. Ajdari, I. Mezić, H. A. Stone, and G. M. Whitesides, "Chaotic Mixer for Microchannels," *Science,* vol. 295, pp. 647-651, 2002.

[104] X. S. Feng, Y. K. Ren, and H. Y. Jiang, "An effective splitting-and-recombination micromixer with self-rotated contact surface for wide Reynolds number range applications," *Biomicrofluidics,* vol. 7, Sep 2013.

[105] SABIC. (2017). *Innovative plastics, oxygen and water permeability* Available: http://www.pod-sabic-ip.com/KBAM/Reflection/Assets/Thumbnail/10620_4.pdf

[106] A. Lamberti, S. L. Marasso, and M. Cocuzza, "PDMS membranes with tunable gas permeability for microfluidic applications," *Rsc Advances,* vol. 4, pp. 61415-61419, 2014.

[107] O. L. Mayorga and E. Freire, "Dynamic Analysis of Differential Scanning Calorimetry Data," *Biophysical Chemistry,* vol. 27, pp. 87-96, Jul 1987.

[108] D. Burnouf, E. Ennifar, S. Guedich, B. Puffer, G. Hoffmann, G. Bec*, et al.*, "kinITC: A New Method for

Obtaining Joint Thermodynamic and Kinetic Data by Isothermal Titration Calorimetry," *Journal of the American Chemical Society,* vol. 134, pp. 559-565, Jan 2012.

[109] T. Wiseman, S. Williston, J. F. Brandts, and L. N. Lin, "Rapid Measurement of Binding Constants and Heats of Binding Using a New Titration Calorimeter," *Analytical Biochemistry,* vol. 179, pp. 131-137, May 1989.

[110] L. S. Mizoue and J. Tellinghuisen, "Calorimetric vs. van't Hoff binding enthalpies from isothermal titration calorimetry: Ba2+-crown ether complexation," *Biophysical Chemistry,* vol. 110, pp. 15-24, Jul 2004.

[111] Y. Jia, X. Feng, H. Jiang, and Q. Lin, "A Polymeric MEMS Device Using 3D Diffusive Titration for Isothermal Titration Calorimetry " in *Int. Conf. on Miniaturized Chemical and Biochemical Analysis Systems* Gyeongju, Korea, 2015, pp. 1259-1262.

[112] D. Chen, M. Yang, N. Zheng, N. Xie, D. Liu, C. Xie*, et al.*, "A novel aptasensor for electrochemical detection of ractopamine, clenbuterol, salbutamol, phenylethanolamine and procaterol," *Biosensors and Bioelectronics,* vol. 80, pp. 525-531, 6/15/ 2016.

[113] B. H. Lee, V. T. Nguyen, and M. B. Gu, "Highly sensitive detection of 25-HydroxyvitaminD3 by using a target-induced displacement of aptamer," *Biosensors and Bioelectronics*.

[114] X. Zhang, Q. Zhou, Z. Shen, Z. Li, R. Fei, Eoon H. Ji*, et al.*, "Quantum dot incorporated Bacillus spore as nanosensor for viral infection," *Biosensors and Bioelectronics,* vol. 74, pp. 575-580, 12/15/ 2015.

[115] J. B. Chaires, "Calorimetry and thermodynamics in drug design," *Annu. Rev. Biophys.,* vol. 37, pp. 135-151, 2008.

[116] M. A. O'Neill and S. Gaisford, "Application and use of isothermal calorimetry in pharmaceutical development," *International journal of pharmaceutics,* vol. 417, pp. 83-93, 2011.

[117] B. Wang, Y. Jia, and Q. Lin, "A microfabrication-based approach to quantitative isothermal titration calorimetry," *Biosensors and Bioelectronics,* vol. 78, pp. 438-446, 4/15/ 2016.

[118] Y. Jia, B. Wang, Z. Zhang, and Q. Lin, "A polymer-based MEMS differential scanning calorimeter," *Sensors and Actuators A: Physical,* vol. 231, pp. 1-7, 7/15/ 2015.

[119] Y. Jia, H. Cai, and Q. Lin, "Thick-film MEMS thermoelectric sensor fabricated using a thermally assisted lift-off process," *Journal of Micro/Nanolithography, MEMS, and MOEMS,* vol. 15, pp. 024501-024501, 2016.

[120] B.-H. Jo, L. M. Van Lerberghe, K. M. Motsegood, and D. J. Beebe, "Three-dimensional micro-channel fabrication in polydimethylsiloxane (PDMS) elastomer," *Journal of microelectromechanical systems,* vol. 9, pp. 76-81, 2000.

[121] L. Y. Yeo, H. C. Chang, P. P. Y. Chan, and J. R. Friend, "Microfluidic Devices for Bioapplications," *Small,* vol. 7, pp. 12-48, Jan 3 2011.

[122] S. Waheed, J. M. Cabot, N. P. Macdonald, T. Lewis, R. M. Guijt, B. Paull*, et al.*, "3D printed microfluidic devices: enablers and barriers," *Lab on a Chip,* vol. 16, pp. 1993-2013, 2016.

[123] C. M. B. Ho, S. H. Ng, K. H. H. Li, and Y. J. Yoon, "3D printed microfluidics for biological applications," *Lab on a Chip,* vol. 15, pp. 3627-3637, 2015.

[124] N. Bhattacharjee, A. Urrios, S. Kanga, and A. Folch, "The upcoming 3D-printing revolution in microfluidics," *Lab on a Chip,* vol. 16, pp. 1720-1742, 2016.

[125] A. J. L. Morgan, L. H. San Jose, W. D. Jamieson, J. M. Wymant, B. Song, P. Stephens*, et al.*, "Simple and Versatile 3D Printed Microfluidics Using Fused Filament Fabrication," *Plos One,* vol. 11, Apr 6 2016.

[126] A. A. Yazdi, A. Popma, W. Wong, T. Nguyen, Y. Y. Pan, and J. Xu, "3D printing: an emerging tool for novel microfluidics and lab-on-a-chip applications," *Microfluidics and Nanofluidics,* vol. 20, Mar 2016.

[127] C. I. Rogers, K. Qaderi, A. T. Woolley, and G. P. Nordin, "3D printed microfluidic devices with integrated valves," *Biomicrofluidics,* vol. 9, Jan 2015.

[128] João P. Conde, N. Madaboosi, Ruben R. Soares, J. T. S. Fernandes, P. Novo, G. Moulas*, et al.*, "Lab-on-chip systems for integrated bioanalyses," *Essays in Biochemistry,* vol. 60, pp. 121-131, 06/30 2016.

[129] Y. He, Y. Wu, J. Z. Fu, Q. Gao, and J. J. Qiu, "Developments of 3D Printing Microfluidics and Applications in Chemistry and Biology: a Review," *Electroanalysis,* vol. 28, pp. 1658-1678, Aug 2016.

[130] W. Lee, W. Fon, B. W. Axelrod, and M. L. Roukes, "High-sensitivity microfluidic calorimeters for biological and chemical applications," *Proceedings of the National Academy of Sciences,* vol. 106, pp. 15225-15230, 2009.

[131] B. Russ, A. Glaudell, J. J. Urban, M. L. Chabinyc, and R. A. Segalman, "Organic thermoelectric materials for energy harvesting and temperature control," *Nature Reviews Materials,* vol. 1, Oct 2016.

[132] E. Aguilera, J. Ramos, D. Espalin, F. Cedillos, D. Muse, R. Wicker*, et al.*, "3D printing of electro mechanical systems," in *Proceedings of the Solid Freeform Fabrication Symposium*, 2013, pp. 950-961.

[133] G. Whiting, J. Daniel, S. Uhland, M. Lundgren, D. Sime, A. Arias*, et al.*, "Mass Production of Flexible Printed Temperature Sensors," in *Spring 2012 Materials Research Society (MRS) Meeting*, San Francisco, CA, USA, 2012.